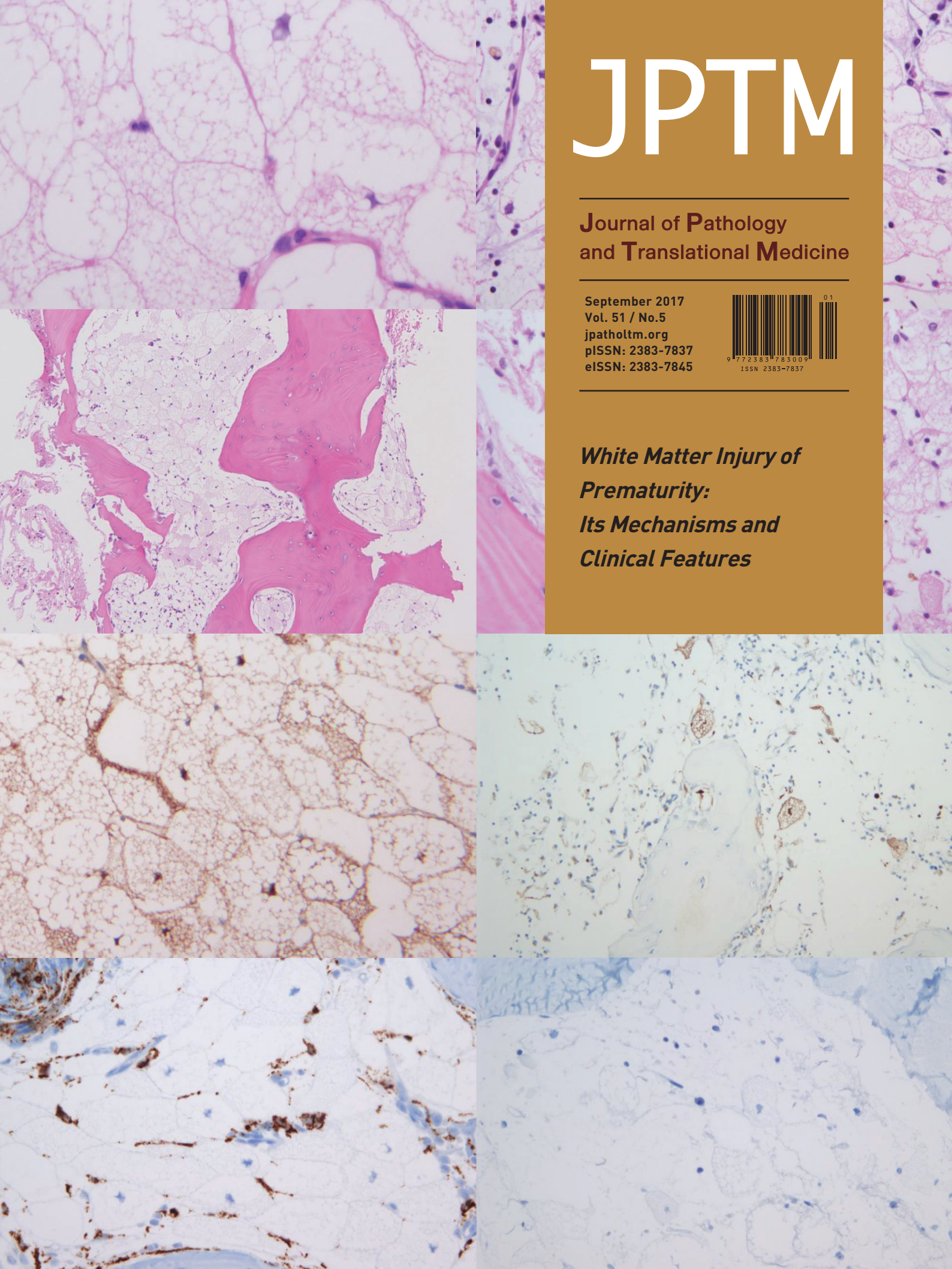

JPTM

Journal of Pathology and Translational Medicine

September 2017
Vol. 51 / No.5
jpatholtm.org
pISSN: 2383-7837
eISSN: 2383-7845

ISSN 2383-7837

White Matter Injury of Prematurity: Its Mechanisms and Clinical Features

Journal of Pathology and Translational Medicine

Volume 51 • Number 5 • September 2017 (bimonthly)
Published since 1967
Printed on 11 September 2017 Published on 15 September 2017

J Pathol Transl Med
pISSN: 2383-7837
eISSN: 2383-7845

Aims & Scope

The Journal of Pathology and Translational Medicine is an open venue for the rapid publication of major achievements in various fields of pathology, cytopathology, and biomedical and translational research. The Journal aims to share new insights into the molecular and cellular mechanisms of human diseases and to report major advances in both experimental and clinical medicine, with a particular emphasis on translational research. The investigations of human cells and tissues using high-dimensional biology techniques such as genomics and proteomics will be given a high priority. Articles on stem cell biology are also welcome. The categories of manuscript include original articles, review and perspective articles, case studies, brief case reports, and letters to the editor.

Subscription Information

To subscribe to this journal, please contact the Korean Society of Pathologists/the Korean Society for Cytopathology. Full text PDF files are also available at the official website (http://jpatholtm.org). *Journal of Pathology and Translational Medicine* is indexed by Emerging Sources Citation Index (ESCI), PubMed, PubMed Central, Scopus, KoreaMed, KoMCI, WPRIM, Directory of Open Access Journals (DOAJ), and CrossRef. Circulation number per issue is 700.

Contact the Korean Society of Pathologists/the Korean Society for Cytopathology

Publishers: Han Kyeom Kim, MD, Hye Kyoung Yoon, MD
Editors-in-Chief: Soon Won Hong, MD, Chong Jai Kim, MD
Published by the Korean Society of Pathologists/the Korean Society for Cytopathology

Editorial Office
Room 1209 Gwanghwamun Officia, 92 Saemunan-ro, Jongno-gu, Seoul 03186, Korea
Tel: +82-2-795-3094 Fax: +82-2-790-6635 E-mail: office@jpatholtm.org

#1508 Renaissancetower, 14 Mallijae-ro, Mapo-gu, Seoul 04195, Korea
Tel: +82-2-593-6943 Fax: +82-2-593-6944 E-mail: office@jpatholtm.org

Printed by iMiS Company Co., Ltd. (JMC)
Jungang Bldg. 18-8 Wonhyo-ro 89-gil, Yongsan-gu, Seoul 04314, Korea
Tel: +82-2-717-5511 Fax: +82-2-717-5515 E-mail: ml@smileml.com

Manuscript Editing by InfoLumi Co.
210-202, 421 Pangyo-ro, Bundang-gu, Seongnam 13522, Korea
Tel: +82-70-8839-8800 E-mail: infolumi.chang@gmail.com

Front cover image: Pathologic and immunohistochemical features of intraosseous hibernoma (Figs. 2 and 3). p502-503.

This journal was supported by the Korean Federation of Science and Technology Societies Grant funded by the Korean Government.

Journal of Pathology and Translational Medicine

J Pathol Transl Med
pISSN: 2383-7837
eISSN: 2383-7845

Volume 51, Number 5, September 2017

CONTENTS

REVIEW

ORIGINAL ARTICLES

CASE REPORTS

CONTENTS CONTINUED

Instructions for Authors for *Journal of Pathology and Translational Medicine* are available at http://jpatholtm.org/authors/authors.php

Journal of Pathology and Translational Medicine 2017; 51: 449-455
https://doi.org/10.4132/jptm.2017.07.25

■ REVIEW ■

White Matter Injury of Prematurity: Its Mechanisms and Clinical Features

Young Ah Lee

Division of Pediatric Neurology, Department of Pediatrics, Beaumont Hospital, Oakland University School of Medicine, Royal Oak, MI, USA

Received: May 2, 2017
Revised: July 19, 2017
Accepted: July 25, 2017

Corresponding Author
Young Ah Lee, MD, PhD
Division of Pediatric Neurology, Department of Pediatrics, Beaumont Hospital, Oakland University School of Medicine, 3555 West 13 Mile Road, Suite N120, Royal Oak, MI 48073, USA
Tel: +1-248-551-7370
Fax: +1-248-551-7373
E-mail: young.lee2@beaumont.org

A developing central nervous system is vulnerable to various insults such as infection and ischemia. While increased understanding of the dynamic nature of brain development allows a deeper insight into the pathophysiology of perinatal brain injury, the precise nature of specific fetal and neonatal brain injuries and their short- and long-term clinical consequences need special attention and further elucidation. The current review will describe the pathophysiological aspects and clinical significance of white matter injury of prematurity, a main form of perinatal brain injury in premature newborns, with a particular emphasis on its potential antenatal components.

Key Words: Prematurity; Injury; White matter; Periventricular leukomalacia

Injuries to the brain can be fatal or lead to catastrophic events regardless of the age of patients, and brain injuries of newborns can be coupled with lifelong intellectual or motor deficits as in cerebral palsy.[1,2] Hypoxia-ischemia (H-I) has long been considered one of the major mechanisms of perinatal brain injuries,[3] and the term hypoxic ischemic encephalopathy (HIE) has been widely used.[4] HIE is defined as an acute encephalopathy caused by intrapartum or late antepartum brain hypoxia and ischemia mostly in term babies.[5] In HIE, compromised oxygen and glucose supply to the brain cells leads to cellular energy failure,[6,7] and a large body of evidence indicates a clear association between HIE and neurodevelopmental problems in surviving infants.[8]

Fetal development is a dynamic process, and the changes in the anatomical constitution and the physiological maturation of the central nervous system with progression of gestation account for the differences between the brain injury patterns of full-term neonates and those of premature neonates.[9] While term newborns with HIE predominantly show diffuse disease, cerebral-deep nuclear disease with prominent involvement of cerebral neocortex, hippocampus, and basal ganglia-thalamus, and deep nuclear-brainstem disease,[10] cerebral white matter is chiefly involved in preterm newborns with HIE.[9,11] This difference in brain injury patterns should be closely related to fetal brain development, as the organization and myelination of fetal brain begin after 6 months of gestation. Myelination of neuronal axons increases conduction speed, and oligodendrocytes are responsible for myelin synthesis in the central nervous system. Oligodendrocytes progenitor cells are formed in the ventricular zone after approximately 20 weeks of gestation, and these cells are vulnerable to oxidative stress. As preterm newborns before 30 weeks of gestation are with deficient myelination, white matter injury of the brain is a main form of brain injury in preterm babies.[12-15]

Diverse pregnancy disorders are associated with preterm birth, which refers to birth before 37 gestational weeks. Spontaneous preterm births are the results of premature labor or preterm premature rupture of membranes, and medically indicated preterm birth is frequently associated with clinical situations where maternal or fetal well-being can be compromised without medical intervention, as in preeclampsia or fetal growth restriction.[16] Premature babies are vulnerable to various perinatal morbidities, and the frequency of short- and long-term complications such as neonatal respiratory distress syndrome and cerebral palsy (CP)

pISSN 2383-7837
eISSN 2383-7845

is significantly increased.[17] This review will summarize the current understanding of white matter injury in premature newborns with special reference to its prenatal components in pathology and clinical significance.

WHITE MATTER INJURY OF PREMATURITY

In immature brains of preterm babies, white matter injuries occur as germinal matrix hemorrhage–intraventricular hemorrhage (GMH-IVH), periventricular leukomalacia (PVL), and diffuse white matter injury.[18] GMH-IVH is a consequence of venous bleeding from thin-walled vessels in the germinal matrix, which easily propagates into the ventricle because of the anatomical relationship with the ventricles. GMH-IVH can evolve into permanent lesions such as porencephalic cyst and hydrocephalus. On the other hand, PVL occurs due to inadequate arterial blood supply to deep white matter, which leads to hypoxia and ischemia in the regions involved (Fig. 1). At the cellular level, PVL is associated with pancellular necrosis and surrounding edema. In diffuse white matter injury, a prominent feature is the loss of oligodendroglia and subsequent decrease in axonal myelination.

CLINICAL FEATURES OF WHITE MATTER INJURY OF PREMATURITY

Several cohort studies have assessed the risk factors of preterm white matter injury.[19-21] Herzog *et al*.[22] examined the impact of putative risk factors of PVL besides prematurity in the Slovenian National Perinatal Information System data and reported that maternal obesity and acute chorioamnionitis increase the risk of PVL more than prematurity does. Gagliardi *et al*.[23] analyzed a prospective singleton infant cohort (n = 2,085) between 23 and 31 weeks of gestational age born in six Italian regions (ACTION study). They looked at the relationships between pregnancy disorders associated with very preterm birth and neonatal outcomes. For the comparisons, the pregnancy disorders were divided into two categories: "disorders of placentation" (hypertensive disorders and fetal growth-restricted [FGR]) and "presumed infection/inflammation" (preterm labor and preterm prelabor rupture of membranes [PPROM]). The risk of mortality, bronchopulmonary dysplasia, and retinopathy of prematurity was higher in FGR infants, and the risk of intraventricular hemorrhage and PVL was lower than in newborns with infection/inflammation disorders when adjusted for gestational age.[23]

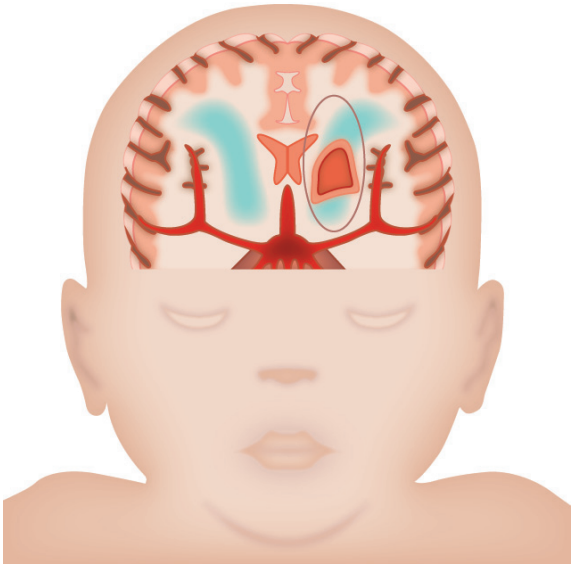

Fig. 1. Schematic representation of diffuse white matter injury (green) and cystic periventricular leukomalacia (circle) in a newborn brain.

An analysis of very preterm infants (n = 753) surviving at least 7 days demonstrated cystic PVL in 9.2%, and the incidence of PVL was highest (16%) in newborns at 28 weeks of gestation. Prenatal inflammation before delivery and the development of PVL showed a strong correlation, and the intrauterine infection and premature rupture of membranes in combination conferred a much higher risk (22%) of PVL. On the other hand, chronic fetal distress such as fetal growth retardation and preeclampsia was seldom followed by PVL (< 2% risk).[24] Another case-control study that analyzed preterm infants with PVL (n = 95) and controls (n = 245) showed an association between PVL and PPROM, gestational age at PPROM, prolonged rupture of membranes ($p < .0001$), administration of tocolytics, and antibiotics. In contrast, preeclampsia, hypertension, FGR, abnormal umbilical artery Doppler, and cesarean delivery in the absence of labor were less frequent. In logistic regression analysis, however, many of these lost statistical significance, while birth weight turned out to be significant. The overall findings suggested that PPROM and prolonged rupture of the membranes affect the neurodevelopmental outcome of the preterm fetus.[25]

RADIOLOGIC FINDINGS OF WHITE MATTER INJURY OF PREMATURITY

Ultrasonography

A developing fetal brain is rapidly changing during pregnancy. However, it is very challenging to monitor this important and rapidly changing fetal organ by conventional transabdominal ultrasonography. In this respect, transvaginal high-resolution

https://doi.org/10.4132/jptm.2017.07.25

ultrasound (US) and three-dimensional (3D) US turned out to be very helpful in the assessment of 3D configuration of fetal brain. 3D US is effective in the prenatal assessment of fetal brain anomalies, vascular malformations, and acquired insults.[26]

US examination has been widely used in the detection of brain lesions in fetuses and newborns. According to a prospective study that examined the frequency of echodensities in the periventricular white matter, basal ganglia, and thalamus of 124 fetuses with risk of preterm birth, echodensities were found in 66% of the cases by transvaginal US examination. The gestational age window of the fetuses was between 26 and 34 weeks, and all mothers were with either hypertensive disorders of pregnancy or preterm labor. The most frequent region was the periventricular area (52%). At least 50% of the periventricular echodensities persisted after delivery. The study showed that echodensities in several areas of the brain are a relatively common finding in high-risk fetuses.[27]

Padilla-Gomes *et al*.[28] compared the frequency of transient periventricular echodensities (TPE), PVL, and hemorrhagic brain lesions in FGR preterm babies and in appropriate-for-gestational-age (AGA) babies. The gestational age of the study population ranged between 24 and 34 weeks, and brain changes were assessed by US at day 3 (US-I), 2 weeks (US-II) after delivery, and term-equivalent age (US-III). They found a higher prevalence of TPE at US-I and PVL at US-II and US-III in FGR neonates. Based on the results, the investigators proposed that fetal growth restriction is associated with an increased prevalence of white matter damage (WMD) in US brain scans of preterm babies.[28]

A series of EPIPAGE cohort of French studies confirmed brain abnormalities in very preterm infants according to clinical parameters such as gestational age, plurality, and fetal growth restriction. Based on cranial US findings, the frequencies of WMD, major WMD, cystic PVL, periventricular hemorrhage, and intraventricular hemorrhage were 21%, 8%, 5%, 3%, and 3%, respectively. The risk of WMD showed an inverse relationship with gestational age, while the incidence of cystic PVL in FGR babies and in AGA babies did not differ.[29] Based on the neonatal US findings, 17% of children with grade III intraventricular hemorrhage and a quarter of children with WMD developed cerebral palsy. In contrast, CP was found in only 4% of children with unremarkable US findings.[30]

Certain placental histopathological findings are associated with fetal and perinatal brain injuries, and brain US findings were shown to be associated with placental histopathological changes consistent with placental underperfusion or inflammation. A prospective analysis of fetuses (n = 77; gestational age, 26 to 34 weeks) demonstrated that moderate brain echogenicity changes such as periventricular echodensity grade IB and intraventricular echodensity grade II and III are found in cases with uteroplacental underperfusion and inflammation. In particular, placental lesions were present in all cases with grade IB periventricular echodensity.[31]

Magnetic resonance imaging

The whole fetal brain structure can also be observed by magnetic resonance imaging (MRI) in the second half of pregnancy.[26] Acute chorioamnionitis is a histological surrogate of intrauterine infection and inflammation and is a component of fetal inflammatory response. This is more commonly found in preterm birth. Anblagan *et al*.[32] examined placental histology and neonatal brain MRI data in a cohort of preterm babies (n = 90) using tract-based spatial statistics to compare fractional anisotropy (FA) data and computational morphometry analysis. The volumes of whole brain, tissue compartments, and cerebrospinal fluid were assessed to determine if acute chorioamnionitis is a risk factor for preterm brain injury. The study decreased FA in the genu, cingulum cingulate gyri, centrum semiovale, inferior longitudinal fasciculi, limbs of the internal capsule, external capsule, and cerebellum in cases with acute chorioamnionitis ($p < .05$, corrected). This suggests that prenatal white matter injury occurs in a substantial proportion of preterm infants.[32]

Banovic *et al*.[33] analyzed the incidence of fetal brain injury by MRI in the cases of preterm labor, preterm prelabor rupture of the membranes, and FGR and compared fetal brain MRI with other antenatal monitoring tools such as US and biophysical profile. They looked at both immediate neonatal outcome and long-term neurodevelopmental handicap at 24 months in 70 cases. While no correlation was found between abnormal MRI and other surveillance tools or immediate neonatal outcome, binary logistic regression showed that fetal brain MRI is the most powerful indicator of long-term neurodevelopmental handicap.[33] A review of prenatal MRI data by Doneda *et al*.[34] also suggested that transient venous hypertension *in utero* is responsible for frontal PVL. The investigators looked for anomalies distributed in the deep medullary vein territory in 78 fetuses with unequivocal cerebral clastic lesions.[34]

Pathophysiology of white matter injury of prematurity

The major reasons for the predominant involvement of cerebral white matter in preterm babies are considered to be the vulnerability of premyelinating oligodendrocytes to reactive oxygen species and cerebral anatomical constitution. Preterm newborns have impaired autoregulation of cerebral blood flow, and there

are vascular end zones and border zones.[35,36] Regarding the etiology of white matter injury of prematurity, accumulated evidence strongly indicates that there are two main pathways involved. One is the ischemic pathway, the other is the inflammatory pathway, and these two pathways can be synergistic.[37-39] The incidence of hypoxic ischemic brain injuries is higher in fetuses exposed to maternal inflammation and infection.[40,41]

Ischemic pathway

The ischemic pathway is mainly related to excitotoxicity and oxidative stress.[42-44] Excitotoxicity is due to depolarization following energy failure of the cells. Depolarization leads to excessive glutamate discharge and calcium influx into the cells, as a result of which nitric oxide synthase is activated. Cellular injury is then induced by increased nitric oxide production. Reperfusion injury following H-I cycles imposes oxidative stress on the cells.[45] Premyelinating oligodendrocytes are more susceptible to oxidative stress than fully differentiated oligodendrocytes are because they lack antioxidant enzymes such as superoxide dismutase and glutathione peroxidase.[38,46]

Inflammatory pathway

A substantial role for inflammatory pathway related to infection and inflammation has been described. Several studies have shown that intra-amniotic infection and inflammation are causative factors of perinatal and long-term complications.[47-49]

Antenatal versus postnatal origin of white matter injury of prematurity

While it is generally considered that perinatal brain injury is a consequence of intrapartum or postpartum events, there is substantial evidence that a certain proportion of brain injuries has antenatal components.[32,50] An examination of 58 stillborn fetuses for the presence of GMH, pontosubicular necrosis (PSN), and PVL revealed at least one lesion in 40% of cases, clearly indicating that GMH and PVL can occur *in utero*. The investigators have also found evidence for the prenatal occurrence of GMH in some cases by US examination and pointed out that PVL and PSN can occur *in utero* as well.[51] Nakamura *et al*.[52] have confirmed cystic brain lesions in two autopsy cases. One was a donor fetus in twin-to-twin transfusion syndrome, and the other was a case of thanatophoric dwarfism. Chronic PVL was found in the second case. The findings observed in these cases imply that cerebral circulatory disturbance is a pathogenetic mechanism of *in utero* brain injuries.[52]

Placental pathology in white matter injury of prematurity

Several studies have documented the importance of placental pathology in white matter injury of prematurity. Chang *et al*.[53] looked at neuropathological findings in 37 third-trimester fetal deaths in conjunction with their placental lesions. There was a correlation between neuronal karyorrhexis or white matter gliosis and severe placental inflammation, and histologically proven PVL was found in two cases.[53] An analysis of 167 preterm babies born between 23 and 34 weeks of gestation revealed a significant association between PVL and chronic deciduitis.[54] In preterm infants, antepartum bleeding of placenta previa is a risk factor for PVL.[55] When Wharton *et al*.[56] performed a case-control study to examine the relationship between PVL and chorioamnionitis in very low-birth-weight infants, severe umbilical cord inflammation was found to be a risk factor of PVL. Kumazaki *et al*.[57] reported massive retroplacental hemorrhage, extensive infarction, and severe perivillous fibrin deposition in preterm infants with ante- or peripartum PVL. The study findings suggest an association between poor placental perfusion and white matter injury of prematurity.

Experimental models

Experimental studies have been done to determine if *in utero* brain injuries are induced in animals. Regarding the consequences of fetal brain injury following *in utero* hypoxia and ischemia, studies have documented both pathological lesions of the brain and the derangement of motor function in rabbits akin to human CP.[58,59] Brain lesions similar to human white matter injury have been easier to reproduce in gyrencephalic animals such as rabbits, dogs, and sheep than in rodents. White matter injuries in models of H-I pathway by hypoperfusion are characterized by more diffuse microglial response, while the experimental simulation of inflammatory pathway using lipopolysaccharide induces lesions with more prominent inflammatory cell infiltration.[60] Rabbits have more traits that can be helpful in studies than other animal species do. Principally, their motor development occurs in the perinatal period, as is the case with humans.[61]

Using a model of placental insufficiency, Buser *et al*.[62] demonstrated selective patterns of gray and white matter injury after global H-I in fetal rabbits. Gray matter injury predominated following H-I at embryonic day 22 (E22), while white matter injury was minimal. They also observed that, following H-I at E25, there was an increased acute white matter injury instead. Consequently, white matter atrophy was detected at E29 in preterm rabbits after H-I at E25, while it was not detected following H-I at E22. As oligodendrocyte progenitors density increases

 https://doi.org/10.4132/jptm.2017.07.25

between E24 and E25 in rabbit forebrain, the investigators proposed that it explains the differences in susceptibility to gray and white matter injury and that this may be the case in white matter injury of preterm newborns.[62]

Derrick *et al*.[63] induced motor deficits in rabbit fetuses using a model of *in utero* placental insufficiency that were akin to motor deficits in human CP in premature and term babies. Surviving preterm rabbit fetuses (67%–70% gestation) subjected to persistent global hypoxia had hypertonia and abnormal motor control. At postnatal day 1, the pups of hypoxic groups had impaired locomotion, motor reflex, sucking, and swallowing. Histological examination revealed acute injury to motor pathways in the subcortical region.[63] In a following study, Derrick *et al*.[61] modeled sustained and repetitive *in utero* H-I resembling placental abruption and labor in the pregnant rabbit. They showed that sustained H-I at E22 and at E25 induces fetal death and other deficits in the surviving animals. Magnetic resonance imaging (MRI) suggested that injury in the internal capsule white matter is responsible for a part of the hypertonia.[61]

The role of intrauterine infection in fetal brain injuries also has been examined in several animal models.[64-66] Field *et al*.[67] introduced *Gardnerella vaginalis* into the pregnant rabbit uterus at E20 or E21 by hysteroscopy to see the effects of intrauterine infection on feto-maternal outcome. Both amnionitis and deciduitis were induced by *G. vaginalis* inoculation, but maternal fever and preterm delivery surprisingly were not. In the fetuses, however, intrauterine infection with *G. vaginalis* decreased the live birth rate, and the fetuses exposed to deciduitis had lower birth weight. In addition, the *G. vaginalis*–inoculated study group had significantly higher frequency of serious brain injury than the control group (60% vs 0%). The study findings indicate that *G. vaginalis* has more pathological impact in the rabbit fetus than in the mother.[67] There is further experimental evidence that intrauterine infection leads to WMD *in utero*. Yoon *et al*.[68] introduced *Escherichia coli* into the pregnant rabbit uterus from E20 to E21, maintained the pregnancy for additional 5 to 6 days by antibiotic treatment, and examined the brains of fetuses and the placentas. Histologically proven white matter pathology was found in 12 fetuses of 10 *E. coli*–inoculated rabbits, but not in the control group ($p < .05$). All of the rabbits with white matter pathology were associated with intrauterine infection.[68] Intrauterine endotoxin administration also induced microstructural changes in the white matter of rabbit newborns, which were detected by diffusion tensor MRI. Term newborn rabbits prenatally exposed to endotoxin at E28 showed decreased FA in periventricular white matter. Brain sections disclosed more frequent activated microglial cells, which may explain the change in diffusivity.[69]

CONCLUSION

Despite the marked improvement in postnatal care during recent decades, there has been no great success in reducing the incidence of white matter injuries in preterm newborns. This indicates that the major targets for prevention of brain injuries are *in utero* events especially in preterm newborns. In this review, I have summarized both the pathophysiological and clinical aspects of white matter injury of prematurity. To prevent and improve the clinical outcome of this potentially catastrophic event, more vigilant prenatal monitoring and further studies to find more powerful prenatal biomarkers of fetal brain white matter injury are urgent.

Conflicts of Interest

No potential conflict of interest relevant to this article was reported.

Acknowledgments

The author is very grateful to Ms. So Won Kim for her excellent assistance in manuscript preparation and editing.

REFERENCES

1. Nelson KB, Ellenberg JH. Neonatal signs as predictors of cerebral palsy. Pediatrics 1979; 64: 225-32.
2. Nelson KB, Ellenberg JH. Apgar scores as predictors of chronic neurologic disability. Pediatrics 1981; 68: 36-44.
3. Graham EM, Ruis KA, Hartman AL, Northington FJ, Fox HE. A systematic review of the role of intrapartum hypoxia-ischemia in the causation of neonatal encephalopathy. Am J Obstet Gynecol 2008; 199: 587-95.
4. Lai MC, Yang SN. Perinatal hypoxic-ischemic encephalopathy. J Biomed Biotechnol 2011; 2011: 609813.
5. Martinez-Biarge M, Diez-Sebastian J, Wusthoff CJ, Mercuri E, Cowan FM. Antepartum and intrapartum factors preceding neonatal hypoxic-ischemic encephalopathy. Pediatrics 2013; 132: e952-9.
6. Blumberg RM, Cady EB, Wigglesworth JS, McKenzie JE, Edwards AD. Relation between delayed impairment of cerebral energy metabolism and infarction following transient focal hypoxia-ischaemia in the developing brain. Exp Brain Res 1997; 113: 130-7.
7. Gilland E, Bona E, Hagberg H. Temporal changes of regional glucose use, blood flow, and microtubule-associated protein 2 immunos-

taining after hypoxia-ischemia in the immature rat brain. J Cereb Blood Flow Metab 1998; 18: 222-8.
8. Ferriero DM. Neonatal brain injury. N Engl J Med 2004; 351: 1985-95.
9. Gopagondanahalli KR, Li J, Fahey MC, *et al*. Preterm hypoxic-ischemic encephalopathy. Front Pediatr 2016; 4: 114.
10. Yokochi K, Fujimoto S. Magnetic resonance imaging in children with neonatal asphyxia: correlation with developmental sequelae. Acta Paediatr 1996; 85: 88-95.
11. Murray AL, Thompson DK, Pascoe L, *et al*. White matter abnormalities and impaired attention abilities in children born very preterm. Neuroimage 2016; 124(Pt A): 75-84.
12. Back SA, Luo NL, Borenstein NS, Levine JM, Volpe JJ, Kinney HC. Late oligodendrocyte progenitors coincide with the developmental window of vulnerability for human perinatal white matter injury. J Neurosci 2001; 21: 1302-12.
13. Back SA, Luo NL, Borenstein NS, Volpe JJ, Kinney HC. Arrested oligodendrocyte lineage progression during human cerebral white matter development: dissociation between the timing of progenitor differentiation and myelinogenesis. J Neuropathol Exp Neurol 2002; 61: 197-211.
14. van Tilborg E, Heijnen CJ, Benders MJ, *et al*. Impaired oligodendrocyte maturation in preterm infants: potential therapeutic targets. Prog Neurobiol 2016; 136: 28-49.
15. Wellmann S, Buhrer C, Schmitz T. Focal necrosis and disturbed myelination in the white matter of newborn infants: a tale of too much or too little oxygen. Front Pediatr 2014; 2: 143.
16. Romero R, Espinoza J, Kusanovic JP, *et al*. The preterm parturition syndrome. BJOG 2006; 113 Suppl 3: 17-42.
17. Marlow N, Wolke D, Bracewell MA, Samara M; EPICure Study Group. Neurologic and developmental disability at six years of age after extremely preterm birth. N Engl J Med 2005; 352: 9-19.
18. Folkerth RD. Neuropathologic substrate of cerebral palsy. J Child Neurol 2005; 20: 940-9.
19. Bolisetty S, Dhawan A, Abdel-Latif M, *et al*. Intraventricular hemorrhage and neurodevelopmental outcomes in extreme preterm infants. Pediatrics 2014; 133: 55-62.
20. Cooper MS, Mackay MT, Fahey M, *et al*. Seizures in children with cerebral palsy and white matter injury. Pediatrics 2017; 139: e20162975.
21. Wagenaar N, Chau V, Groenendaal F, *et al*. Clinical risk factors for punctate white matter lesions on early magnetic resonance imaging in preterm newborns. J Pediatr 2017; 182: 34-40.e1.
22. Herzog M, Cerar LK, Sršen TP, Verdenik I, Lučovnik M. Impact of risk factors other than prematurity on periventricular leukomalacia: a population-based matched case control study. Eur J Obstet Gynecol Reprod Biol 2015; 187: 57-9.
23. Gagliardi L, Rusconi F, Da Frè M, *et al*. Pregnancy disorders leading to very preterm birth influence neonatal outcomes: results of the population-based ACTION cohort study. Pediatr Res 2013; 73: 794-801.
24. Zupan V, Gonzalez P, Lacaze-Masmonteil T, *et al*. Periventricular leukomalacia: risk factors revisited. Dev Med Child Neurol 1996; 38: 1061-7.
25. Bauer M, Fast C, Haas J, Resch B, Lang U, Pertl B. Cystic periventricular leukomalacia in preterm infants: an analysis of obstetric risk factors. Early Hum Dev 2009; 85: 163-9.
26. Pooh RK. Imaging diagnosis of congenital brain anomalies and injuries. Semin Fetal Neonatal Med 2012; 17: 360-76.
27. Rosier-van Dunné FM, van Wezel-Meijler G, Odendaal HJ, van Geijn HP, de Vries JI. Changes in echogenicity in the fetal brain: a prevalence study in fetuses at risk for preterm delivery. Ultrasound Obstet Gynecol 2007; 29: 644-50.
28. Padilla-Gomes NF, Enríquez G, Acosta-Rojas R, Perapoch J, Hernandez-Andrade E, Gratacos E. Prevalence of neonatal ultrasound brain lesions in premature infants with and without intrauterine growth restriction. Acta Paediatr 2007; 96: 1582-7.
29. Larroque B, Marret S, Ancel PY, *et al*. White matter damage and intraventricular hemorrhage in very preterm infants: the EPIPAGE study. J Pediatr 2003; 143: 477-83.
30. Ancel PY, Livinec F, Larroque B, *et al*. Cerebral palsy among very preterm children in relation to gestational age and neonatal ultrasound abnormalities: the EPIPAGE cohort study. Pediatrics 2006; 117: 828-35.
31. Rosier-van Dunné FM, van Wezel-Meijler G, Kaschula RO, Wranz PA, Odendaal HJ, de Vries JI. Placental histology related to fetal brain sonography. Arch Dis Child Fetal Neonatal Ed 2011; 96: F53-8.
32. Anblagan D, Pataky R, Evans MJ, *et al*. Association between preterm brain injury and exposure to chorioamnionitis during fetal life. Sci Rep 2016; 6: 37932.
33. Banović V, Škrablin S, Banović M, Radoš M, Gverić-Ahmetašević S, Babić I. Fetal brain magnetic resonance imaging and long-term neurodevelopmental impairment. Int J Gynaecol Obstet 2014; 125: 237-40.
34. Doneda C, Righini A, Parazzini C, Arrigoni F, Rustico M, Triulzi F. Prenatal MR imaging detection of deep medullary vein involvement in fetal brain damage. AJNR Am J Neuroradiol 2011; 32: E146-9.
35. Alderliesten T, Lemmers PM, Smarius JJ, van de Vosse RE, Baerts W, van Bel F. Cerebral oxygenation, extraction, and autoregulation in very preterm infants who develop peri-intraventricular hemorrhage. J Pediatr 2013; 162: 698-704.e2.
36. Wong FY, Leung TS, Austin T, *et al*. Impaired autoregulation in preterm infants identified by using spatially resolved spectroscopy. Pediatrics 2008; 121: e604-11.
37. Deng W. Neurobiology of injury to the developing brain. Nat Rev

Neurol 2010; 6: 328-36.
38. Khwaja O, Volpe JJ. Pathogenesis of cerebral white matter injury of prematurity. Arch Dis Child Fetal Neonatal Ed 2008; 93: F153-61.
39. Volpe JJ. Brain injury in premature infants: a complex amalgam of destructive and developmental disturbances. Lancet Neurol 2009; 8: 110-24.
40. Rezaie P, Dean A. Periventricular leukomalacia, inflammation and white matter lesions within the developing nervous system. Neuropathology 2002; 22: 106-32.
41. Zhao J, Chen Y, Xu Y, Pi G. Effect of intrauterine infection on brain development and injury. Int J Dev Neurosci 2013; 31: 543-9.
42. Back SA, Rosenberg PA. Pathophysiology of glia in perinatal white matter injury. Glia 2014; 62: 1790-815.
43. Burd I, Welling J, Kannan G, Johnston MV. Excitotoxicity as a common mechanism for fetal neuronal injury with hypoxia and intrauterine inflammation. Adv Pharmacol 2016; 76: 85-101.
44. Perrone S, Tataranno LM, Stazzoni G, Ramenghi L, Buonocore G. Brain susceptibility to oxidative stress in the perinatal period. J Matern Fetal Neonatal Med 2015; 28 Suppl 1: 2291-5.
45. Back SA, Han BH, Luo NL, *et al*. Selective vulnerability of late oligodendrocyte progenitors to hypoxia-ischemia. J Neurosci 2002; 22: 455-63.
46. Back SA, Luo NL, Mallinson RA, *et al*. Selective vulnerability of preterm white matter to oxidative damage defined by F2-isoprostanes. Ann Neurol 2005; 58: 108-20.
47. Boyle AK, Rinaldi SF, Norman JE, Stock SJ. Preterm birth: Inflammation, fetal injury and treatment strategies. J Reprod Immunol 2017; 119: 62-6.
48. Malaeb S, Dammann O. Fetal inflammatory response and brain injury in the preterm newborn. J Child Neurol 2009; 24: 1119-26.
49. Yuan TM, Sun Y, Zhan CY, Yu HM. Intrauterine infection/inflammation and perinatal brain damage: role of glial cells and Toll-like receptor signaling. J Neuroimmunol 2010; 229: 16-25.
50. Murthy V, Kennea NL. Antenatal infection/inflammation and fetal tissue injury. Best Pract Res Clin Obstet Gynaecol 2007; 21: 479-89.
51. Skullerud K, Skjaeraasen J. Clinicopathological study of germinal matrix hemorrhage, pontosubicular necrosis, and periventricular leukomalacia in stillborn. Childs Nerv Syst 1988; 4: 88-91.
52. Nakamura Y, Fujiyoshi Y, Fukuda S, *et al*. Cystic brain lesion *in utero*. Acta Pathol Jpn 1986; 36: 613-20.
53. Chang KT, Keating S, Costa S, Machin G, Kingdom J, Shannon P. Third-trimester stillbirths: correlative neuropathology and placental pathology. Pediatr Dev Pathol 2011; 14: 345-52.
54. Maleki Z, Bailis AJ, Argani CH, Askin FB, Graham EM. Periventricular leukomalacia and placental histopathologic abnormalities. Obstet Gynecol 2009; 114: 1115-20.
55. Oda N, Takeuchi K, Tanaka A, Maruo T. Obstetric risk factors associated with the development of periventricular leukomalacia in preterm infants born to mothers complicated by placenta previa. Fetal Diagn Ther 2008; 24: 345-8.
56. Wharton KN, Pinar H, Stonestreet BS, *et al*. Severe umbilical cord inflammation-a predictor of periventricular leukomalacia in very low birth weight infants. Early Hum Dev 2004; 77: 77-87.
57. Kumazaki K, Nakayama M, Sumida Y, *et al*. Placental features in preterm infants with periventricular leukomalacia. Pediatrics 2002; 109: 650-5.
58. Drobyshevsky A, Derrick M, Luo K, *et al*. Near-term fetal hypoxia-ischemia in rabbits: MRI can predict muscle tone abnormalities and deep brain injury. Stroke 2012; 43: 2757-63.
59. Drobyshevsky A, Luo K, Derrick M, *et al*. Motor deficits are triggered by reperfusion-reoxygenation injury as diagnosed by MRI and by a mechanism involving oxidants. J Neurosci 2012; 32: 5500-9.
60. Hagberg H, Peebles D, Mallard C. Models of white matter injury: comparison of infectious, hypoxic-ischemic, and excitotoxic insults. Ment Retard Dev Disabil Res Rev 2002; 8: 30-8.
61. Derrick M, Drobyshevsky A, Ji X, Tan S. A model of cerebral palsy from fetal hypoxia-ischemia. Stroke 2007; 38(2 Suppl): 731-5.
62. Buser JR, Segovia KN, Dean JM, *et al*. Timing of appearance of late oligodendrocyte progenitors coincides with enhanced susceptibility of preterm rabbit cerebral white matter to hypoxia-ischemia. J Cereb Blood Flow Metab 2010; 30: 1053-65.
63. Derrick M, Luo NL, Bregman JC, *et al*. Preterm fetal hypoxia-ischemia causes hypertonia and motor deficits in the neonatal rabbit: a model for human cerebral palsy? J Neurosci 2004; 24: 24-34.
64. Burd I, Balakrishnan B, Kannan S. Models of fetal brain injury, intrauterine inflammation, and preterm birth. Am J Reprod Immunol 2012; 67: 287-94.
65. Duncan JR, Cock ML, Scheerlinck JP, *et al*. White matter injury after repeated endotoxin exposure in the preterm ovine fetus. Pediatr Res 2002; 52: 941-9.
66. Girard S, Kadhim H, Roy M, *et al*. Role of perinatal inflammation in cerebral palsy. Pediatr Neurol 2009; 40: 168-74.
67. Field NT, Newton ER, Kagan-Hallet K, Peairs WA. Perinatal effects of Gardnerella vaginalis deciduitis in the rabbit. Am J Obstet Gynecol 1993; 168(3 Pt 1): 988-94.
68. Yoon BH, Kim CJ, Romero R, *et al*. Experimentally induced intrauterine infection causes fetal brain white matter lesions in rabbits. Am J Obstet Gynecol 1997; 177: 797-802.
69. Saadani-Makki F, Kannan S, Makki M, *et al*. Intrauterine endotoxin administration leads to white matter diffusivity changes in newborn rabbits. J Child Neurol 2009; 24: 1179-89.

Journal of Pathology and Translational Medicine 2017; 51: 456-462
https://doi.org/10.4132/jptm.2017.07.19

■ ORIGINAL ARTICLE ■

The Potential Roles of MELF-Pattern, Microvessel Density, and VEGF Expression in Survival of Patients with Endometrioid Endometrial Carcinoma: A Morphometrical and Immunohistochemical Analysis of 100 Cases

Dmitry Aleksandrovich Zinovkin
Md Zahidul Islam Pranjol[1]
Daniil Rudolfovich Petrenyov[2]
Eldar Arkadievich Nadyrov[3]
Oleg Gennadievich Savchenko[4]

University Research Laboratory, Gomel State Medical University, Gomel, Belarus; [1]University of Exeter Medical School, Institute of Biomedical and Clinical Science, Exeter, Devon, United Kingdom; [2]Laboratory of Endocrinology and Biochemistry, Institute of Radiobiology National Academy of Sciences, Gomel; [3]Laboratory of Clinical Research, Republican Research Center for Radiation Medicine and Human Ecology, Gomel; [4]Department of Oncology, Gomel State Medical University, Gomel, Belarus

Received: May 14, 2017
Revised: July 6, 2017
Accepted: July 19, 2017

Corresponding Author
Dmitry Aleksandrovich Zinovkin, MD
University Research Laboratory, Gomel State Medical University, Lange Str. 5, Gomel, Belarus
Tel: +375-29-182-7416
Fax: +375-232-77-36-72
E-mail: zinovkin2012@gmail.com

Background: In this study, we hypothesized that microcystic, elongated, fragmented (MELF)-pattern, vascular endothelial growth factor (VEGF) expression by cancer cells and microvessel density of cancer stroma may be associated with progression of endometrioid adenocarcinoma. **Methods:** The study used data from the Belarus Cancer Registry and archival histological material of 100 patients with retrospectively known good (survival) and poor (disease progression and death) outcomes. All cases were immunohistochemically stained for CD34 and VEGF. Two independent samples were compared for the characteristics of signs, and obtained results were analyzed by receiver operating characteristic analysis, Mann-Whitney U test, χ^2 test (Yates correction), and Mantel-Cox test. Multivariate Cox hazard analysis and Spearman correlation test were used. A p-value of less than .05 was considered statistically significant. **Results:** The observed survival rate of patients with endometrioid adenocarcinoma was significantly lower ($p = .002$) in MELF-pattern positive patients when compared with MELF-pattern negative patients. The overall survival rate of patients whose tumors had more than 114 vessels/mm^2 of tissue was significantly low ($p < .001$). Interestingly, a similar observation was found in patients with increased vessel area, evidenced by VEGF expression in the glandular tumor component. **Conclusions:** Our study suggests, for the first time, that these criteria may be used as risk factors of endometrioid adenocarcinoma progression during 5 years after radical surgical treatment. However, a large independent cohort of samples should be considered in the future to validate our findings.

Key Words: Carcinoma, endometrioid; Vascular endothelial growth factor; Prognosis; MELF; Vessel density

The stromal microenvironment of tumors is gradually becoming a main focus in the field of cancer research. It is believed that malignancy is a result of complex molecular and cellular interactions between the elements of tumor microenvironment and surrounding host tissues which induce selection and expansion of the neoplastic cells.[1] In 2005, Zigrino *et al*.[2] reported an interaction of tumor cells with the stromal elements during tumor progression and paid special attention to the ability of the neoplastic cells to modify stroma by changing the adjacent connective tissue and modulating cellular metabolism of the host. In such circumstances, a new stroma is formed in areas of tumor invasion, including the parts of distant metastases, creating favorable conditions for the aggressive potential of tumor cells. This event in the areas of active cancer cell invasion is common in tumor progression.[2]

Murray *et al*.[3] introduced the acronym "MELF" (microcystic, elongated, fragmented) which describes the unusual changes incurred by the endometrioid adenocarcinoma (EA) when invading into the myometrium. These changes are characterized by the formation of microcysts lined with eosinophilic cytoplasm, elon-

pISSN 2383-7837
eISSN 2383-7845

gated glandular structures, and clusters of individual cells.[3] Though earlier it was believed that this fibromyxoid stromal reaction was initially a degenerative process, a number of studies have shown that the MELF pattern can be a specific tumor stroma reaction, similar to the epithelial-mesenchymal interactions observed in other tumors.[4]

Angiogenesis is defined by formation of new blood vessels from preexisting ones, playing a key role in uncontrolled proliferation of cells, survival of localized malignant cells and distant tumor invasion. Increased microvessel density, an indirect marker of intense tumor vascularization, is known to be associated with both evolution of the disease and patient survival. The formation of new vessels depends on the interaction between different hormones/growth factors and microvascular endothelial cells lining the existing microvessels.[5,6] The endometrium expresses several growth factors involved in angiogenesis, including epidermal growth factor, transforming growth factor, and vascular endothelial growth factor (VEGF). VEGF is one of the most common promoters of angiogenesis, expressed even by the normal endometrium. As an angiogenetic factor, VEGF stimulates proliferation of endothelial cells and also increases vascular permeability and protein extravasations.[7-9]

In this study, we hypothesized that MELF-pattern, VEGF expression by cancer cells, and microvessel density may be associated with the progression of EA and survival of patients. Therefore, we investigated the role of vessel and stroma of tumor microenvironment and reported for the first time that these criteria may be used as prognostic factors for EA of the uterine corpus.

MATERIALS AND METHODS

Ethical approval

The study was approved by the Committees for Medical and Health Sciences of Research Ethics of Republican Research Center for Radiation Medicine and Human Ecology and Gomel State Medical University. Dispensation from the requirement of patient consent was granted.

Patient characteristics

This retrospective study involved women with endometrial EA who were treated between January 2010 and December 2012 in the Grodno region, Republic of Belarus. The inclusion criteria for the study were stage I–III (International Federation of Gynecology and Obstetrics [FIGO], 2009), the presence of EA as the main cause of death, progression of the tumor, age between 45 and 80, hysterectomy, and an absence of malignant tumors in other parts of the body. The control subjects were selected cases of EA stage I–III with 5-year survival, age between 45 and 80, and no history of other malignant tumors. The exclusion criteria for the study were as follows: stage IV (FIGO, 2009), death from postoperative complications during the first month after hysterectomy, death from causes not related to EA progression, Lynch syndrome, synchronous and metachronous malignancies, and age less than 45 or more than 80.

A total of 100 out of 156 cases of EA during the study period were determined to be eligible for inclusion in the study. The power analysis demonstrated that the number of patients was sufficient to conduct further research. The study used data from the Belarus Cancer Registry and archival histological material of 100 patients with histopathological diagnosis of EA. Histologic typing was performed according to the histological classification of endometrial cancer by the World Health Organization. Patients were divided into two groups. The first group included 48 subjects who had recurrence or died of EA within 5 years after diagnosis (unfavorable outcome). The second group consisted of 52 subjects who had no recurrence or death within 5 years after diagnosis (favorable outcome). The average age in the group with favorable outcome was 62.7 ± 10.1 years and it was 65.2 ± 9.6 years in the group with an unfavorable outcome. Patient characteristics by FIGO stage and tumor grade are presented in Table 1.

Hematoxylin and eosin staining protocol

Five-micrometer-thick sections were prepared from the archival histological blocks. They were mounted on microscopic slides. Next, the sections were deparaffinized in two portions of xylene and rehydrated in descending concentrations of ethanol. Subsequently, they were stained with hematoxylin and eosin by standard methods. The sections were cleansed in carbolic xylene, dehydrated in ascending alcohol concentrations, dried and mounted under coverslips using Biomount medium (DAKO, Glostrup,

Table 1. Characteristics of the patient groups by FIGO stage (2009) and tumor grade

Characteristic	Unfavorable outcome group (n=48)	Favorable outcome group (n=52)
FIGO		
I	20	23
II	23	23
III	5	6
Grade		
G1	17	16
G2	25	31
G3	6	5

FIGO, International Federation of Gynecology and Obstetrics.

Denmark).

Primary antibodies and detection system

Primary antibodies used in this study include the following: ready-to-use monoclonal rabbit anti-CD34 (clone EP88) and ready-to-use polyclonal rabbit anti-VEGF (Diagnostic Biosystems, Pleasanton, CA, USA). Mouse/Rabbit PolyVue Plus HRP/DAB Detection System (Diagnostic Biosystems) was used for primary antibodies visualization.

Immunohistochemical staining protocol

The 4–5-μm-thick sections of tissue on l-polylysine coated glass slides were deparaffinized and washed with distilled water for 3 minutes. Antigen retrieval was performed using antigen unmasking solutions Tris-EDTA buffer (1 mM, pH 9.0) and citrate buffer (1 mM, pH 6.0), with preheating in the microwave at 800 W for 5 minutes and at 600 W for 10 minutes, respectively. The sections were then allowed to cool in the same solution. Endogenous peroxidase blocking was performed in 5% hydrogen peroxide for 20 minutes, and blocking of nonspecific antibody binding was ensured by incubating the sections in 5% casein in Tris-buffered solution for 1 hour. Following a brief wash in Tris-buffered solution, the sections were incubated in moist chamber at room temperature for 2 hours with corresponding primary antibodies. Tissue sections were then incubated at room temperature for 30 minutes with anti-mouse horseradish peroxidase secondary antibodies. Between each step the sections were washed twice with Tris-buffered solution for 5 minutes each. The reaction product was visualized with 3.3'-diaminobenzidine staining for 5 minutes, followed by Mayer's hematoxylin counter-staining.[10]

Morphometry

Determination of tumor vessels of microvasculature was carried out in the field with the largest number of capillaries (hot spots). The number and the area of vessels per 1 mm^2 were determined by counting the number in 5 fields under the magnification of ×400. These results were converted to 1 mm^2 area of the tumor tissue. The microscope Nikon Eclipse 50i with digital camera DS-F1 and NIS-Elements software (Nikon, Tokyo, Japan) was used for this morphometric work.

Statistical analysis

All data were presented by the median, lower and upper quartiles. A two-tailed Fisher test was used to compare the groups according to the presence or absence of MELF-pattern. Mann-Whitney test and receiver operating characteristic (ROC)-analysis were used for comparing the study groups based on the evaluated criteria. Determining the confidence interval (CI) and the area under the ROC-curve were the compulsory component of the ROC-analysis. The quality prediction model was labelled excellent at area under the curve 0.9–1.0, very good at 0.8–0.9, good at 0.7–0.8, medium at 0.6–0.7, and unsatisfactory at 0.5–0.6. According to the threshold indicator, the patients were divided into two groups for 5-year survival analysis by Mantel-Cox test. A Spearman correlation test was used for groups. A multivariate Cox proportional hazard analysis was developed using stepwise regression (forward selection, enter/remove limits p = .10) to identify independent predictors of outcomes. A p-value of less than .05 was considered statistically significant. R v.3.4.0 free soft was used for statistical analysis.

RESULTS

MELF-pattern

Distinctive changes in the glands that characterized the MELF-pattern were related with fibromyxoid stromal reaction. For instance, invasion of the myometrium by tumor glands showed that there is an absence of fibroblastic reaction (Fig. 1A). Intriguingly, fibromyxoid reaction compressing cancer glands were observed in the MELF pattern as expected (Fig. 1B).

The MELF-pattern was observed in eight cases (16.7%) in the group with favorable outcome. Fibromyxoid changes were typical for the MELF-pattern which was observed in 17 cases (56.7%) of EA in the group with unfavorable outcome. Statistical difference (p = .014) was detected by comparing the number of the MELF-pattern present in the two groups. The observed survival rate of a patient with EA was significantly lower (p = .002) when MELF pattern was present compared with when MELF-pattern was not present (Fig. 2A).

Number of vessels

In the group with favorable outcome of the disease, the vessels were mostly detected in a small or moderate amount, with an oval-shaped lumen. Slight atypia was observed in the endothelium where the basement membrane was visualized throughout the cross-section of the vessels (Fig. 1C). On the contrary, the vessels of the microvasculature within the hot spot areas in cases with unfavorable outcome had mostly irregularly-shaped lumen. They were closely located to each other, often forming a densely branching network. It should be noticed that the endothelium had an irregular shape and an irregular intermittent basement membrane in the unfavorable outcome group (Fig. 1D).

https://doi.org/10.4132/jptm.2017.07.19

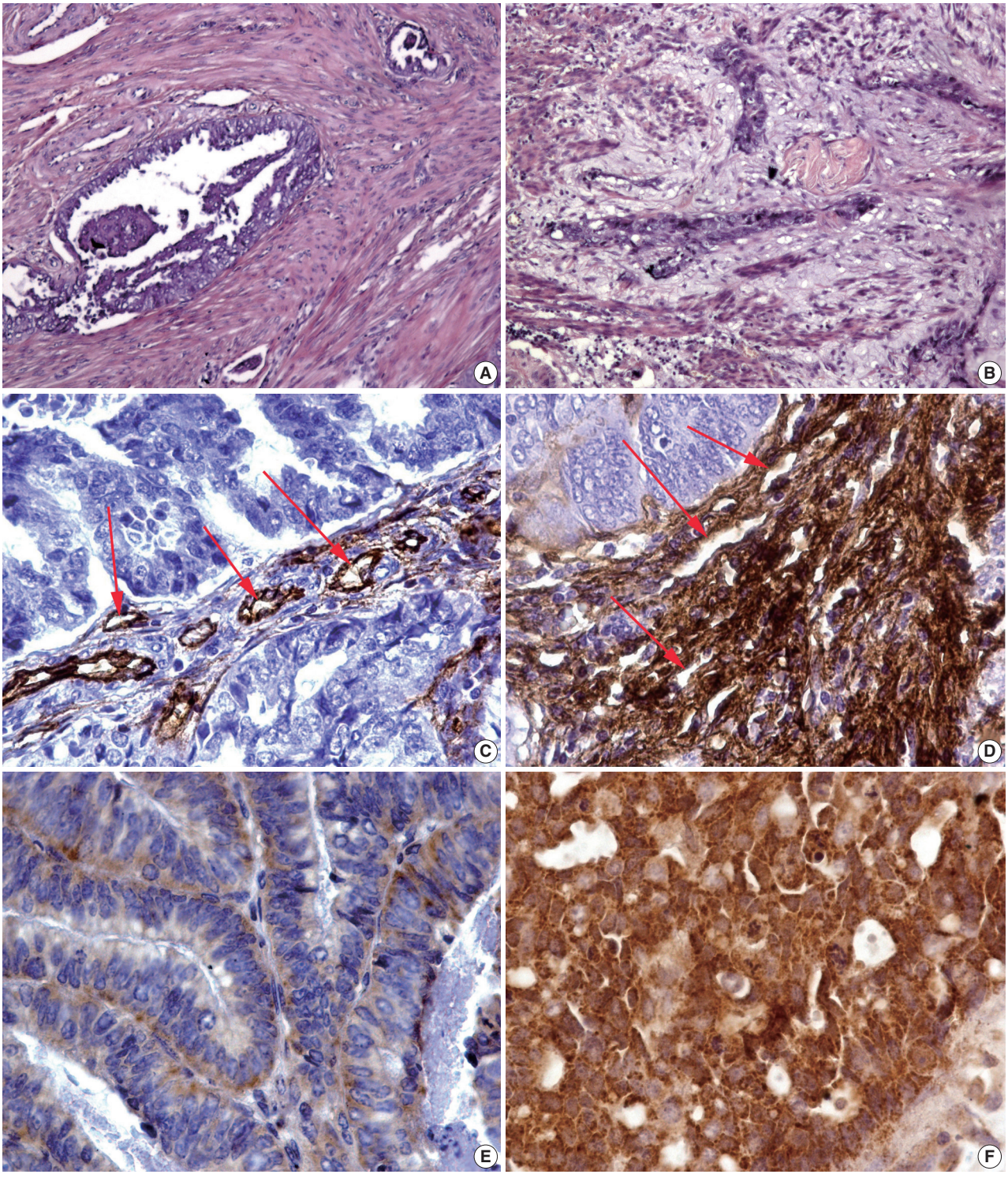

Fig. 1. (A) Stroma without fibroblastic reaction and tumor glands invading the myometrium. (B) MELF-pattern of the stroma with fibromyxoid reaction compressing the cancer glands. (C) Vessels in EA stroma with round lumen in group of patients with favorable outcome (arrows, CD34 immunostaining). (D) A large number of unusual vessels with dilated lumens in group of patients with unfavorable outcome (arrows, CD34 immunostaining). (E) Weak focal expression of VEGF in glands of EA, commonly detectable in patients with good outcome (VEGF immunostaining). (F) Diffuse strong expression of VEGF in glands of EA in cases of unfavorable outcome (VEGF immunostaining). MELF, microcystic, elongated, fragmented; EA, endometrioid adenocarcinoma; VEGF, vascular endothelial growth factor.

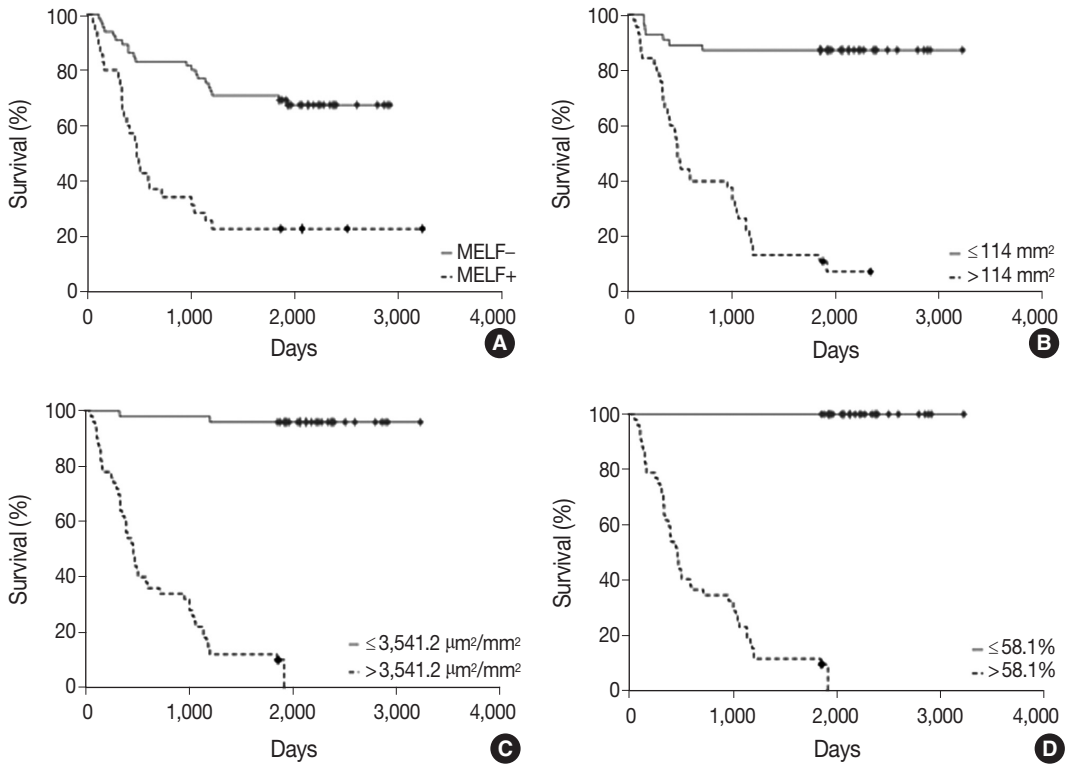

Fig. 2. Cumulative proportion survival. (A) MELF-pattern. (B) Number of vessels per 1 mm^2. (C) Area of vessels per 1 mm^2. (D) VEGF expression by tumor glands. MELF, microcystic, elongated, fragmented; VEGF, vascular endothelial growth factor.

In the group of patients with unfavorable outcome, the median number of vessels in 1 mm^2 of EA tissue was 139.1 (range, 74.1 to 174.6), and in the group with favorable outcome the median was 95.5 (range, 57.0 to 171.0). A significantly increased number of vessels were detected in the group with unfavorable outcome ($p < .001$; $z = 5.625$), compared to favorable outcome group.

The ROC-analysis of this index showed that the area under the ROC-curve was 92.3% (95% CI, 82.5 to 97.6; $p < .001$). The sensitivity was 86.7% (95% CI, 69.3 to 96.2), the specificity was 96.7% (95% CI, 82.8 to 99.9), and the threshold value of the index was 114.0 vessels/mm^2.

After studying the overall survival rate of patients with EA depending on the number of vessels in 1 mm^2 of tumor, it was found that the survival rate was statistically lower ($p < .001$) in patients whose tumors had more than 114.0 vessels/mm^2 of tumor tissue (Fig. 2B).

Area of the vessels

The median of the vessel area in 1 mm^2 of tumor tissue in group 1 was 4,904.1 $\mu m^2/mm^2$ (range, 4,400.1 to 6,245.1 $\mu m^2/mm^2$). The median of this index in the second group was 2,818.9 $\mu m^2/mm^2$ (range 1,348.2 to 5,449.8 $\mu m^2/mm^2$). A significantly larger area of vessels was detected in the unfavorable outcome group ($p < .001$, $z = 6.247$) compared with the favorable outcome group.

After performing ROC-analysis of the vessel area in 1 mm^2 of tumor tissue, it was found that the area under the ROC-curve was 97.0% (95% CI, 89.0 to 99.7; $p < .001$). The sensitivity, specificity, and threshold value of the index were 100% (95% CI, 88.4 to 100.0), 96.7% (95% CI, 82.8 to 99.9), and 3,541.2 $\mu m^2/mm^2$, respectively.

The study of the overall survival rate of patients with EA depending on the vessel area of 1 mm^2 of tumors showed that the survival rate was statistically lower ($p < .001$) in patients whose vascular area in tumors was more than 3,541.2 $\mu m^2/mm^2$ (Fig. 2C).

VEGF

The expression of VEGF, one of the main stimulators of angiogenesis, was observed in all cases of EA. Diffuse expression of this marker was detected in the stroma and glandular component of EA. However, in cases of favorable outcome, a weak staining was observed in the cytoplasm, indicating a lower expression of VEGF (Fig. 1E). In the glandular component of the tumor, VEGF

 https://doi.org/10.4132/jptm.2017.07.19

expression was, however, more evident and uniform. In the group with unfavorable outcome, an opposite result of immunohistochemistry was observed: the VEGF expression was strong, detected as brown staining foci in the cytoplasm of the tumor cells (Fig. 1F).

In cases with unfavorable outcome, the median of VEGF expression was 82.1% (range, 59.1% to 100.0%) and it was statistically higher ($p < .001$; $z = 6.616$) in comparison with the median of cases with favorable outcome, which was 49.0% (range, 20.8% to 62.1%).

The ROC-analysis of VEGF expression showed that the area under the ROC-curve was 99.8% (95% CI, 93.6 to 100.0; $p < .001$). The sensitivity was 100.0% (95% CI, 88.4 to 100.0) and the specificity was 96.7% (95% CI, 82.8 to 99.9). The threshold value of the index was 58.1%. The survival rate was statistically lower ($p < .001$) in patients whose VEGF expression of the glandular tumor component was more than 58.1% (Fig. 2D), as expected.

Correlation analysis

Our study demonstrated a significant correlation between the MELF-pattern and VEGF expression in both groups. For instance, the correlation between the two was $r = .541$ ($p < .001$). This was also observed between VEGF expression and the area of vessels ($r = .762$, $p < .001$) and number of vessels ($r = .648$, $p < .001$). Correlation analysis describes the changes in cancer stroma caused by VEGF expression in cancer cells.

Multivariate Cox's proportional hazard model

A multivariate Cox's regression analysis revealed that MELF-pattern and the area and number of vessels per 1 mm^2 of tumor tissue are independent prognostic factors of 5-year survival of patients with EA (Table 2).

DISCUSSION

Our study shows that the MELF pattern is more frequently observed in cases with unfavorable outcome than in those with favorable outcome, suggesting that the presence of MELF pattern may be a prognostic factor for patient survival. It can be assumed that MELF is a "medium" which enhances the spread of the tumor cells. After aggressive radiation therapy, a similar change of fibromyxoid response in the stoma was observed in squamous cell carcinoma of the vulva, just as MELF pattern in EA.[11] Immunohistochemical and genetic study of MELF pattern in EA disclosed stromal cell separation and disappearance and downregulation of E-cadherin expression.[12] As pointed out by several authors, these changes are probably crucial in increasing the invasive capacity of EA and intensification of its metastatic potential. In the univariate analysis, the presence of stromal fibromyxoid reactions by MELF pattern was associated with an unfavorable prognosis of EA.[8,10,11]

Table 2. Multivariate Cox's proportional hazard model analysis of prognostic factors in patients with endometrioid adenocarcinoma

Factor	p-value	Hazard ratio	95% CI
MELF-pattern	.013	2.20	1.18–4.09
No. of vessels	.009	3.31	1.33–8.16
Area of vessels	<.001	1.03	1.01–1.17

CI, confidence interval; MELF, microcystic, elongated, fragmented.

The number and area of microvessels in our study showed statistically significant difference between the survival rates of patients with favorable outcome and unfavorable outcome. This can be used as a strong potential prognostic factor in the survival of patients with EA. Microvessel density in tumor-invaded tissue is increased by local angiogenesis that results in enhanced cancer cell proliferation during tumor progression. In gynecological cancer, angiogenesis is one of the crucial factors of tumor progression and plays a significant role in the maintenance of the growth of malignancies and their metastatic potential.[13] Some authors suggested that the density of vessels of microvasculature is an indirect marker of the intensity of tumor vascularization, which is known to be associated with the progression of endometrial cancer and 5-year survival rate.[14,15] In such reports, immunohistochemical marker CD34 was proven useful in the detection of these endothelial cells.[16] The immunohistochemical expression of CD34 by endothelial cells allows counting the number and area of tumor vessels, which are prognostic signs that do not depend on other tumor characteristics, such as expressions of proliferation markers and adhesion molecules.[17]

Our study shows VEGF expression as a predictor of survival in patients with EA. For instance, the higher the expression of VEGF in cancer cells, the lower the survival of the patients, as predicted in our study. Nowadays, VEGF is the most frequently studied angiogenic promoter; its expression is observed in the normal endometrium as well as in other uterine malignancies, although it is higher in cancer tissue when compared with normal.[18] VEGF stimulates endothelial cell proliferation, but it also increases vascular permeability, which helps the tumor cells to migrate to metastatic sites.[19-21] Saito *et al*.[22] reported that based on the surgical materials of 85 cases of EA, there was a significant VEGF expression in both highly differentiated and moderately differentiated tumors compared to poorly differentiated ones. In addition, it was reported that estrogen levels decrease the expression of VEGF, which may be an indication of increased survival of patients with EA.[23]

We showed for the first time that there is a significant presence of MELF pattern and an increased number and area of vessels in cases of EA with unfavorable outcome. In our study, VEGF expression correlated with the area and number of vessels, but it did not have any predictive force according to multivariate Cox's proportional hazard analysis. Although our data suggest that these criteria may be used as prognostic factors of EA during the 5 years after radical surgical treatment, a larger independent cohort of samples should be studied to verify these findings.

Conflicts of Interest

No potential conflict of interest relevant to this article was reported.

REFERENCES

1. Gacche RN, Meshram RJ. Targeting tumor micro-environment for design and development of novel anti-angiogenic agents arresting tumor growth. Prog Biophys Mol Biol 2013; 113: 333-54.
2. Zigrino P, Löffek S, Mauch C. Tumor-stroma interactions: their role in the control of tumor cell invasion. Biochimie 2005; 87: 321-8.
3. Murray SK, Young RH, Scully RE. Unusual epithelial and stromal changes in myoinvasive endometrioid adenocarcinoma: a study of their frequency, associated diagnostic problems, and prognostic significance. Int J Gynecol Pathol 2003; 22: 324-33.
4. Dogan Altunpulluk M, Kir G, Topal CS, Cetiner H, Gocmen A. The association of the microcystic, elongated and fragmented (MELF) invasion pattern in endometrial carcinomas with deep myometrial invasion, lymphovascular space invasion and lymph node metastasis. J Obstet Gynaecol 2015; 35: 397-402.
5. Kukreja I, Kapoor P, Deshmukh R, Kulkarni V. VEGF and CD 34: a correlation between tumor angiogenesis and microvessel density-an immunohistochemical study. J Oral Maxillofac Pathol 2013; 17: 367-73.
6. Żyła MM, Kostrzewa M, Litwińska E, Szpakowski A, Wilczyński JR, Stetkiewicz T. The role of angiogenic factors in endometrial cancer. Prz Menopauzalny 2014; 13: 122-6.
7. Stefansson IM, Salvesen HB, Immervoll H, Akslen LA. Prognostic impact of histological grade and vascular invasion compared with tumour cell proliferation in endometrial carcinoma of endometrioid type. Histopathology 2004; 44: 472-9.
8. Stefansson IM, Salvesen HB, Akslen LA. Vascular proliferation is important for clinical progress of endometrial cancer. Cancer Res 2006; 66: 3303-9.
9. Stewart CJ, Crook ML, Manso L. Fascin expression in low-grade uterine endometrioid adenocarcinoma: correlation with microcystic, elongated and fragmented (MELF)-type alteration at the deep invasive margin. Histopathology 2011; 59: 73-80.
10. Bajracharya D, Shrestha B, Kamath A, Menon A, Radhakrishnan R. Immunohistochemical correlation of matrix metalloproteinase-2 and tissue inhibitors of metalloproteinase-2 in tobacco associated epithelial dysplasia. Dis Markers 2014; 2014: 197813.
11. Zaino RJ. Unusual patterns of endometrial carcinoma including MELF and its relation to epithelial mesenchymal transition. Int J Gynecol Pathol 2014; 33: 357-64.
12. Stewart CJ, Crook ML. Galectin-3 expression in uterine endometrioid adenocarcinoma: comparison of staining in conventional tumor glands and in areas of MELF pattern myometrial invasion. Int J Gynecol Pathol 2010; 29: 555-61.
13. Erdem O, Erdem M, Erdem A, Memis L, Akyol G. Expression of vascular endothelial growth factor and assessment of microvascular density with CD 34 and endoglin in proliferative endometrium, endometrial hyperplasia, and endometrial carcinoma. Int J Gynecol Cancer 2007; 17: 1327-32.
14. Aybatli A, Sayin C, Kaplan PB, Varol F, Altaner S, Süt N. The investigation of tumoral angiogenesis with HIF-1 alpha and microvessel density in women with endometrium cancer. J Turk Ger Gynecol Assoc 2012; 13: 37-44.
15. Haldorsen IS, Stefansson I, Grüner R, *et al*. Increased microvascular proliferation is negatively correlated to tumour blood flow and is associated with unfavourable outcome in endometrial carcinomas. Br J Cancer 2014; 110: 107-14.
16. Ozdemir O. Mast cell density, angiogenesis, and their significance in tumor development. Gynecol Oncol 2006; 100: 628-9.
17. Simionescu C, Mărgăritescu C, Stepan A, Pirici D, Ciurea R, Cernea N. Tumor angiogenesis, macrophages and mast cell microdensities in endometrioid endometrial carcinoma. Oncol Lett 2013; 6: 415-20.
18. Nunobiki O, Nakamura M, Taniguchi E, *et al*. Adrenomedullin, Bcl-2 and microvessel density in normal, hyperplastic and neoplastic endometrium. Pathol Int 2009; 59: 530-6.
19. Schmid BC, Oehler MK. Improvements in progression-free and overall survival due to the use of anti-angiogenic agents in gynecologic cancers. Curr Treat Options Oncol 2015; 16: 318.
20. Saarelainen SK, Staff S, Peltonen N, *et al*. Endoglin, VEGF, and its receptors in predicting metastases in endometrial carcinoma. Tumour Biol 2014; 35: 4651-7.
21. Wang J, Taylor A, Showeil R, *et al*. Expression profiling and significance of VEGF-A, VEGFR2, VEGFR3 and related proteins in endometrial carcinoma. Cytokine 2014; 68: 94-100.
22. Saito M, Sato Y, Watanabe J, Kuramoto H, Kaba S, Fukuda T. Angiogenic factors in normal endometrium and endometrial adenocarcinoma. Pathol Int 2007; 57: 140-7.
23. Matias-Guiu X, Davidson B. Prognostic biomarkers in endometrial and ovarian carcinoma. Virchows Arch 2014; 464: 315-31.

Journal of Pathology and Translational Medicine 2017; 51: 463-470
https://doi.org/10.4132/jptm.2017.05.25

■ ORIGINAL ARTICLE ■

The Intraoperative Immunohistochemical Staining of CD56 and CK19 Improves Surgical Decision for Thyroid Follicular Lesions

Ju Yeon Pyo · Sung-eun Choi
Eunah Shin[1] · JaSeung Koo[2]
SoonWon Hong

Department of Pathology, Gangnam Severance Hospital, Yonsei University College of Medicine, Seoul; [1]Department of Pathology, CHA Gangnam Medical Center, CHA University, Seoul; [2]Department of Pathology, Severance Hospital, Yonsei University College of Medicine, Seoul, Korea

Received: February 9, 2017
Revised: May 21, 2017
Accepted: May 25, 2017

Corresponding Author
SoonWon Hong, MD, PhD
Department of Pathology, Gangnam Severance Hospital, Yonsei University College of Medicine, 211 Eonju-ro, Gangnam-gu, Seoul 06273, Korea
Tel: +82-2-2019-3540
Fax: +82-2-3463-2103
E-mail: soonwonh@yuhs.ac

Background: When differential diagnosis is difficult in thyroid follicular lesions with overlapping histological features, the immunohistochemical staining can help confirm the diagnosis. We aimed to evaluate the effectiveness of rapid immunohistochemical stains of CD56 and cytokeratin 19 on frozen sections of thyroid follicular lesion and explore the possible gains and limitations of the practice. **Methods:** Eighty-six nodules of 79 patients whose intraoperative frozen sections were selected as the control group, and 53 nodules of 48 patients whose intraoperative frozen sections were subject to rapid immunohistochemistry were selected as the study group. **Results:** Five nodules (6%) in the control group were diagnosed as follicular neoplasm and six nodules (7%) were deferred. In the study group, six nodules (11%) were follicular neoplasm and none were deferred. Three nodules (4%) in the control group showed diagnostic discrepancy between the frozen and permanent diagnoses, but none in the study group. The average turnaround time for the frozen diagnosis of the control group was 24 minutes, whereas it was 54 minutes for the study group. **Conclusions:** Intraoperative rapid immunohistochemical stains significantly decreased the diagnostic discrepancy in this study. Considering the adverse effects of indefinite frozen diagnosis or discrepancy with permanent diagnoses, the intraoperative rapid immunohistochemical stain can help to accurately diagnose and hence provide guidance to surgical treatment.

Key Words: Thyroid; Follicular patterned lesion; Immunohistochemistry; Frozen; CD56; CK19

Follicular patterned lesions of the thyroid impose not so trivial diagnostic difficulty because the cytological features can be deceiving and the diagnosis of malignancy depends on non-disputable histologic evidence other than morphologic criteria.[1] Thus, unlike other tumors, a limited number of representative sections of the lesion cannot be relied upon for an accurate diagnosis, and the diagnostic accuracy of fine needle aspiration and intraoperative frozen diagnosis are often compromised.[2] Moreover, it is not surprising to find that even thyroid experts have discrepancy in the diagnosis of follicular lesions, harboring the entire spectrum of benign to malignant tumors,[3-6] and yet, an accurate diagnosis is just as important for the follicular patterned lesions as for other tumors because treatment plans totally depend on the pathologic diagnosis. As such, there have been efforts to more actively utilize core biopsy in the diagnosis of thyroid lesions with expectations that immunohistochemical (IHC) stains will aid in more accurate diagnosis.[7-9] However, we must not overlook the fact that IHC stains in follicular patterned lesions can vary from area to area,[10] and so the IHC stain results in the core biopsy can be more often misleading than not. We also should consider the fact that for follicular neoplasm, a key to the diagnosis is the presence or absence of a complete capsule of the entire lesion,[1] which can never be accurately assessed by core biopsy alone, irrespective of the IHC stain results. These limitations in the preoperative diagnosis of the follicular patterned lesions naturally lead to the conclusion that at present, there is no alternative other than assessing the histology of the entire lesion in cases of follicular patterned lesions. However, we propose that if not preoperatively, we can at least aid in making surgical decision intraoperatively by applying IHC stain to frozen section. Even though differential diagnosis of the follicular neoplasm and follicular variant papillary thyroid carcinoma (FVPTC) is difficult on frozen sections, shedding light on the more possible diagnosis between the two is plausible by frozen section and it can be an aid enough for the surgeon. We propose that IHC stains that are ancillary in the differential diagnosis of follicular neoplasm and FVPTC can also be applied

pISSN 2383-7837
eISSN 2383-7845

to the frozen section intraoperatively, and among many that are used in permanent sections, we chose CD56 and cytokeratin 19 (CK19) based on our past experiences. We aimed to evaluate the exact positive yields of the IHC stains on intraoperative frozen sections and explore the possible gains and limitations of the practice.

MATERIALS AND METHODS

Patients and nodules

Eighty-six nodules of 79 patients whose intraoperative frozen sections were not subject to IHC stains at all were selected as the control group (Fig. 1A) and 53 nodules of 48 patients whose intraoperative frozen sections could be subject to IHC stains if necessary were selected as the study group (Fig. 1B). For each group, the study duration was about a month. This study was approved by the Institutional Review Board of Gangnam Severance Hospital with a waiver of informed consent (IRB No. 3-2015-0133).

Rapid IHC stain

Fresh frozen tissue in OCT compound was sectioned with Cryo-cut Microtome (Leica Biosystems, Newcastle Upon Tyne, UK) in 3–4 μm thickness, placed on silane coated slide, and let dry. The slide was then stained for rapid immunohistochemistry in LEICA BOND-III Autostainer using Bond Polymer Refine Detection kit (Leica Biosystems). Briefly, the dry slide was fixed in 4% paraformaldehyde for 1 minute, immersed in peroxide block for 2 minutes to endogenous peroxidase blocking, washed and then applied with primary antibody for 4 minutes. After washing with Bond Wash solution, the slide was sequentially applied with post primary agent for 2 minutes and polymer for 2 minutes with washings in-between. The antibodies used were CK19 (1:80, RCK108, mouse monoclonal, DAKO, Carpinteria, CA, USA) and CD56 (1:50, 123C3, mouse monoclonal, DAKO). They were detected with 3,3'-diaminobenzidine (DAB) chromogen and DAB enhancer and counterstained with hematoxylin. The entire process takes roughly about 30 minutes.

Microscopic evaluation

Nodules of the control group were intraoperatively diagnosed based on the hematoxylin and eosin (H&E) findings alone and the total amount of time spent on the diagnosis, so-called turnaround time, was recorded. Nodules of the study group were subject to IHC stains for CD56 and CK19 only when the diagnosis could not be reached on H&E findings alone. When H&E findings were informative enough for definitive diagnosis, IHC stains were not performed and the turnaround time was recorded. According to El Demellawy *et al.*,[11] membranous staining of follicular epithelial cells for CD56 (≥10% cut-off) was considered positive. As shown in the diagnostic algorithm of Fig. 1B, those lesions showing cytological features suspicious for, but not diagnostic of, papillary thyroid carcinoma (PTC) were subject to IHC stains, and PTC was diagnosed when the suspicious cells were CD56-negative and CK19-positive (Fig. 2A–C). When the suspicious cells were CD56-positive, however, the diagnosis of either follicular neoplasm (Fig. 2D–F) or adenomatous hyperplasia (Fig. 2G–I) was reached.[11-13] These diagnoses were based upon consultation to an experienced thyroid pathologist (S.W. Hong). The turnaround time was recorded after the IHC stains for the study group. For the control group, the frozen diagnoses were deferred when the histological or cytological features of the nodules were equivocal or when the histological features were suspicious of follicular neoplasm (Fig. 1A). The intraoperative diagnoses were classified as benign, malignant, follicular neoplasm, and deferred. The number of lesions showing discrepancy between the frozen diagnosis and permanent diagnosis and the type of discrepancy were evaluated in those that were not deferred in the intraoperative diagnosis. Final diagnoses on the permanent sections of the deferred lesions and those that were reported as follicular neoplasm intraoperatively were also evaluated.

Statistical analysis

The type of intraoperative diagnosis, the number of discrepancy between the frozen diagnosis and the final permanent diagnosis, and the turnaround time in the intraoperative diagnosis of the two groups were analyzed by Student's t test and Fisher exact test. Statistical analysis of data was performed using the SPSS software ver. 17.0 (SPSS Inc., Chicago, IL, USA). The p-value less than .05 were considered statistically significant.

RESULTS

Seventy-nine patients allocated to the control group consisted of 14 men and 65 women. Forty-eight patients in the study group consisted of eight men and 40 women. The clinicopathologic characteristics in two groups were tabulated (Table 1). There was no significant statistical difference in the distribution of gender and age between the two groups. A total of 84 nodules out of 86 in the control group (98%) were diagnosed within 40 minutes and only two nodules (2%) were diagnosed after 40 minutes. The turnaround time of 40 minutes was agreed to be a reasonable cutoff by the departments of pathology and surgery, considering

 https://doi.org/10.4132/jptm.2017.05.25

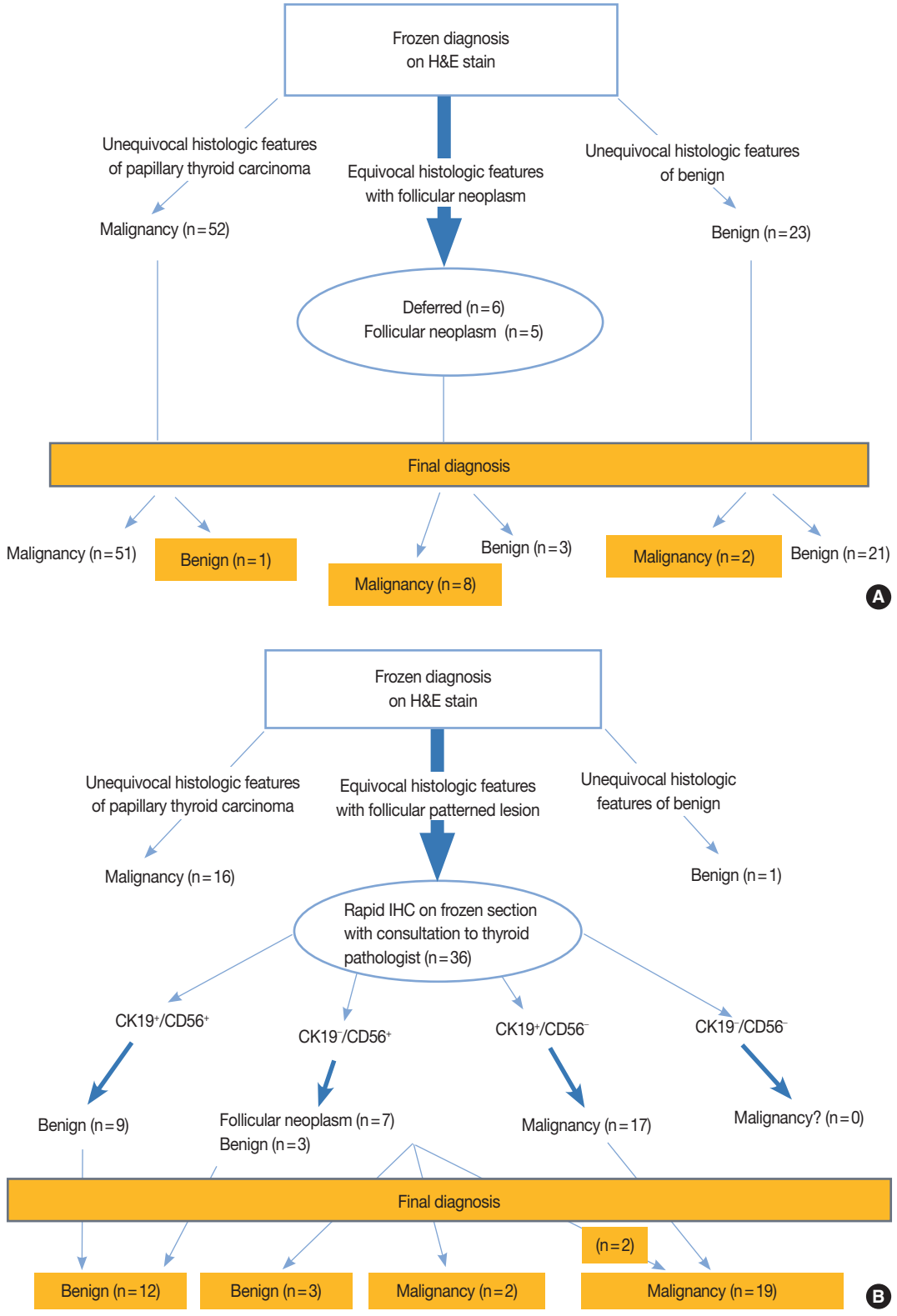

Fig. 1. Diagnostic algorithm of thyroid follicular patterned lesions on frozen section. (A) Control group. (B) Study group. H&E, hematoxylin and eosin; IHC, immunohisteochemisty; CK19, cytokeratin 19.

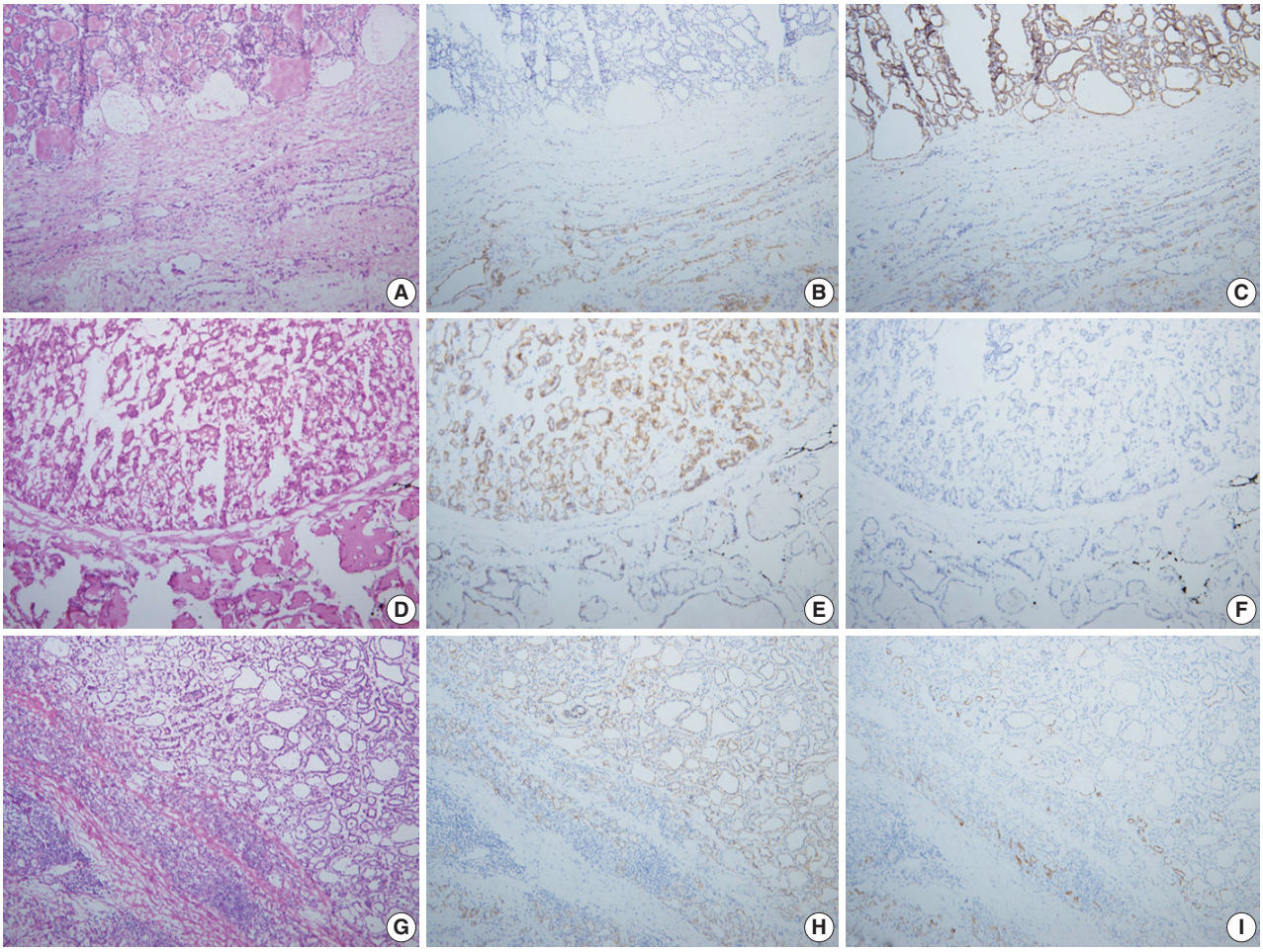

Fig. 2. Histologic and immunohistochemical features of thyroid follicular lesions. (A) Frozen section of follicular patterned lesion reported as follicular variant papillary carcinoma. (B) Immunohistochemical stain for CD56 showing diffuse negative reaction in the tumor cells as opposed to the adjacent normal thyroid tissue. (C) Immunohistochemical stain for cytokeratin 19 (CK19) showing diffuse strong positive reaction in the tumor cells. (D) Frozen section of follicular patterned lesion reported as follicular neoplasm. (E) Immunohistochemical stain for CD56 showing diffuse positive reaction in the tumor cells as opposed to the adjacent normal thyroid tissue. (F) Immunohistochemical stain for CK19 showing diffuse negative reaction. (G) Frozen section of follicular patterned lesion reported as adenomatous hyperplasia. (H) Immunohistochemical stain for CD56 showing multifocal patchy positive reaction in the tumor cells and the adjacent normal thyroid tissue as well. (I) Immunohistochemical stain for CK19 showing positive reaction in the adjacent normal thyroid and also in a few tumor cells though much attenuated.

the time required to construct one block of typical frozen section and the time required for rapid IHC. This is in line with the guidelines recommended by the Joint Commission of International Certification and the guidelines for quality management of the Korean Society of Pathologists. For frozen sections without immunostaining, the turnaround time was kept within 15 minutes to 20 minutes. The average turnaround time to diagnosis was 24 minutes for the control group. For the study group, 17 out of 53 nodules (32%) were diagnosed within 40 minutes and 36 nodules (68%) were diagnosed after 40 minutes ($p < .000$). The average turnaround time for the study group was 57 minutes (Table 1). As for the type of intraoperative frozen diagnosis, in 75 out of 86 nodules of the control group (87%) and 47 out of 53 nodules of the study group (89%), a clear definite diagnosis was possible. Five out of 86 nodules in the control group (6%) were diagnosed as follicular neoplasm, and six nodules (7%) were deferred. In contrast, six nodules out of 53 in the study group (11%) were diagnosed as follicular neoplasm, and none were deferred. There was no significant statistical difference in the distribution of intraoperative frozen diagnosis between the two groups (Table 1).

With respect to the diagnostic discrepancy between frozen diagnosis and permanent diagnosis in the two groups, three nodules out of 75 (4%) in the control group showed discrepancy

https://doi.org/10.4132/jptm.2017.05.25

Table 1. Clinicopathologic features of the control group and the study group

Parameter	Control group	Study group	p-value
Sex (man:woman)[a]	14:65 (18:82)	8:40 (17:83)	1.000[b]
Age, mean (range, yr)[a]	49 (24–75)	45 (24–68)	.258[c]
Man	50 (32–75)	54 (41–68)	
Woman	47 (24–70)	44 (24–64)	
Turnaround time (min)[d]			
Mean	24	57	.000[b]
<40 min	84 (98)	17 (32)	
≥40 min	2 (2)	36 (68)	
Frozen diagnosis[d]			.149[b]
Benign	23 (27)	12 (23)	
AH	20 (23)	8 (15)	
LT	3 (4)	4 (7)	
Malignancy	52 (60)	35 (66)	
PTC, conventional	43 (50)	29 (55)	
FVPTC	7 (8)	4 (7)	
PTC, oncocytic variant	1 (1)	0	
HC	0	1 (2)	
FC	1 (1)	1 (2)	
Follicular neoplasm	5 (6)	6 (11)	
Deferred	6 (7)	0	

Values are presented as number (%), unless otherwise indicated.
AH, adenomatous hyperplasia; LT, lymphocytic thyroiditis; PTC, papillary thyroid carcinoma; FVPTC, follicular variant papillary thyroid carcinoma; HC, Hurthle cell carcinoma; FC, follicular carcinoma, minimally invasive.
[a]Number of patients: control (n = 79), study group (n = 48); [b]Fisher exact test; [c]t test; [d]Number of nodules: control (n = 86), study group (n = 53).

in the diagnosis; two cases were initially diagnosed as adenomatous hyperplasia and lymphocytic thyroiditis on frozen sections, and then as conventional PTC and noninvasive capsulated FVPTC on permanent sections (discrepancy rate, 0.087); and one nodule was initially diagnosed as conventional PTC on frozen section, and then as lymphocytic thyroiditis on permanent section (discrepancy rate, 0.019). None of the study group had discrepancy between the frozen and permanent diagnoses (discrepancy rate, 0). Although they are not classified as a discrepancy, six malignant nodules in the control group turned out to be different histologic types in permanent sections (Table 2). In the control group, two out of five follicular neoplasms on frozen section turned out to be FVPTC on permanent sections. In the study group, two out of six follicular neoplasms on frozen section were diagnosed as oncocytic variant PTC and noninvasive capsulated FVPTC on permanent sections, due to different nuclear features and IHC profiles on permanent sections (Table 3). Four out of six deferred nodules of the control group were revealed to be FVPTC on permanent diagnosis (malignancy rate, 0.667) (Table 4). Immunophenotypes of 36 nodules in the study group are summarized in Table 5. All of nine nodules ($CK19^+$, $CD56^+$) were immunohistochemically matched with benign on permanent diagnosis, and all of 15 nodules ($CK19^+$, $CD56^-$) were matched with conventional PTC. Two nodules which were initially diagnosed as follicular neoplasm due to the

Table 2. Diagnostic discrepancy between frozen and permanent diagnoses in each group

Frozen diagnosis (No. of nodules)	Permanent diagnosis (No. of nodules)								Discrepancy rate
	Benign		Malignant						
	AH	LT	PTCc	FVPTC cap+, inv-	FVPTC cap+, inv+	FVPTC cap-	HC	FC	
Control group									
Benign (n = 23)									0.087
AH	19	0	1	0	0	0	0	0	
LT	0	2	0	1	0	0	0	0	
Malignant (n = 52)									0.019
PTCc	0	1	38	0	1	2	1	0	
FVPTC	0	0	0	0	0	6	0	1	
HC	0	0	0	0	0	0	0	0	
FC	0	0	0	1	0	0	0	0	
Study group									
Benign (n = 12)									0
AH	8	0	0	0	0	0	0	0	
LT	0	4	0	0	0	0	0	0	
Malignant (n = 35)									0
PTCc	0	0	29	0	0	0	0	0	
FVPTC	0	0	0	1	3	0	0	0	
HC	0	0	0	0	0	0	1	0	
FC	0	0	0	0	0	0	0	1	

AH, adenomatous hyperplasia; LT, lymphocytic thyroiditis; PTCc, papillary thyroid carcinoma, conventional; FVPTC, follicular variant papillary thyroid carcinoma; cap+, capsule present; inv-, no capsule invasion; inv+, capsule invasion present; cap-, no capsule; HC, Hurthle cell carcinoma; FC, follicular carcinoma, minimally invasive.

IHC staining results of $CK19^-$ and $CD56^+$ were finally diagnosed as oncocytic variant PTC in one and FVPTC in the other; the IHC stain results were reversed to $CK19^+$ and $CD56^-$ on permanent sections.

DISCUSSION

Application of IHC to frozen sections can diminish critical diagnostic discrepancy between the intraoperative frozen diagnosis and subsequent permanent diagnosis. In our study, those that were not subject to IHC on frozen sections showed a diagnostic discrepancy in 4%, a change in histologic subtype of malignant nodules in 11%, and a diagnostic deferral in 7%. In those with a diagnostic discrepancy, for example, FVPTC was misdiagnosed as lymphocytic thyroiditis intraoperatively, lymphocytic thyroiditis was mistaken for conventional PTC, and conventional PTC was missed due to a sampling error. In addition, six out of 52 malignant nodules in the control group showed altered histological subtypes, but there was no difference in the 35 malignant nodules of the study group. Most of the deferred lesions and lesions of follicular neoplasm were finally diagnosed as capsulated FVPTC. However, those to which IHC was applied intraoperatively did not have any diagnostic discrepancy and none of them were deferred.

With the introduction of FVPTC in 1977,[14] many cases previously thought to be follicular neoplasm were confirmed to be, in fact, FVPTC. This has led to a rather increased frequency of intra-

Table 3. Malignancy rate of FN between frozen and permanent diagnoses in each group

FN at frozen diagnosis (No. of nodules)	Permanent diagnosis (No. of nodules)										Malignancy rate
	Follicular neoplasm					Other					
	Benign		Malignant		Total	AH	PTCo	FVPTC cap+, inv-	FVPTC cap+, inv+	Total	
	FA	HA	HC	FC							
Control group (n=5)	1	0	1	1	3 (60)	0	0	1	1	2 (40)	0.800
Study group (n=6)	2	1	0	0	3 (50)	1	1[a]	1[a]	0	3 (50)	0.333

Values are presented as number (%).
FN, follicular neoplasm; FA, follicular adenoma; HA, hurthle cell adenoma; HC, hurthle cell carcinoma; FC, follicular carcinoma, minimally invasive; AH, adenomatous hyperplasia; PTCo, oncocytic variant of papillary thyroid carcinoma; FVPTC, follicular variant of papillary thyroid carcinoma; cap+, tumor capsule present; inv-, no capsule invasion; inv+, capsule invasion present.
[a]Although it showed CD56 positivity and cytokeratin 19 (CK19) negativity on rapid immunohistochemical stain of frozen section, focal loss of CD56 and focal reactivity of CK19 were revealed on permanent section of remained lesion.

Table 4. Malignancy rate of deferred lesion between frozen and permanent diagnoses in each group

Frozen diagnosis (deffered)	Permanent diagnosis (No. of nodules)								Malignancy rate
	Benign (n=2)			Malignant (n=4)					
	FA	HA	AH	PTCo	FVPTC cap+, inv-	FVPTC cap+, inv+	HC	FC	
Control group	1	0	1	0	4	0	0	0	0.667
Study group	0	0	0	0	0	0	0	0	0

FA, follicular adenoma; HA, hurthle cell adenoma; AH, adenomatous hyperplasia; PTCo, oncocytic variant of papillary thyroid carcinoma; FVPTC, follicular variant of papillary thyroid carcinoma; cap+, tumor capsule present; inv-, no capsule invasion; inv+, capsule invasion present; HC, hurthle cell carcinoma; FC, follicular carcinoma, minimally invasive.

Table 5. Immunophenotypes of the study group nodules that were subject to rapid immunohistochemical stain

Immunophenotype	Permanent diagnosis (No. of nodules)									Total No. of nodules (n = 36)
	Benign (n = 15)				Malignant (n = 21)					
	AH	LT	FA	HA	FC	HC	PTCc	PTCo	FVPTC	
$CK19^+/CD56^+$	6	3	0	0	0	0	0	0	0	9
$CK19^-/CD56^+$	3	0	2	1	1	1	0	0	0	8
$CK19^+/CD56^-$	0	0	0	0	0	0	15	1[a]	3[a]	19
$CK19^-/CD56^-$	0	0	0	0	0	0	0	0	0	0

AH, adenomatous hyperplasia; LT, lymphocytic thyroiditis; FA, follicular adenoma; HA, hurthle cell adenoma; FC, follicular carcinoma, minimally invasive; HC, hurthle cell carcinoma; PTCc, papillary thyroid carcinoma, conventional; PTCo, oncocytic variant of papillary thyroid carcinoma; FVPTC, follicular variant of papillary thyroid carcinom.
[a]Although it showed CD56 positivity and cytokeratin 19 (CK19) negativity on rapid immunohistochemical stain of frozen section, focal loss of CD56 and focal reactivity of CK19 were revealed on permanent section of remained lesion.

https://doi.org/10.4132/jptm.2017.05.25

operative pathologic consultation by frozen section in cases that had been preoperatively diagnosed as follicular neoplasm or reported to have some degree of nuclear atypia. Of course, these cases cannot be definitively diagnosed on frozen sections and they require meticulous sampling and ancillary IHC stain on permanent sections to reach definitive diagnosis.[11-13] To our knowledge, there has not yet been any report in thyroid lesions that employed the use of IHC in the intraoperative frozen diagnosis. Follicular neoplasm, by definition, cannot be a candidate for frozen diagnosis because its diagnosis depends on the histologic examination of the entire capsule of the mass.[15] However, as FVPTC has entered the diagnostic spectrum, a possible follicular neoplasm has also become a candidate for frozen diagnosis in order to rule out the possibility of FVPTC[16] which, in contrast to the follicular neoplasm, can be diagnosed on representative sections of the mass like other PTCs. At this point, we should note that considering the morphologic and gross features of FVPTC, there is always a hindrance of misinterpreting the microscopic appearance on frozen sections due to frozen artifacts.[17] In our institution, we have an experience of detecting micrometastasis in lymph nodes of breast cancer patients by applying IHC stain for cytokeratin on frozen sections.[18] With this previous experience, we applied IHC on frozen sections of the thyroid follicular lesions, expecting to distinguish between malignant and benign lesions intraoperatively and hence minimize the number of deferred or misdiagnosed lesions.

Many antibodies are now being used in the diagnosis of FVPTC,[11-13] but we chose CD56 and CK19 based on the integrated results of many antibodies and our accumulated experience heretofore. The combined results of CD56 negativity and CK19 positivity can maximize the diagnosis of PTC. Moreover, in contrast to HBME1, CK19 is often positive not only in PTC but also in adenomatous hyperplasia as well,[11-13] and this has led us to integrate the staining patterns of the two antibodies in the differential diagnosis of follicular patterned lesions. In our study, we could definitely diagnose PTC and FVPTC in follicular patterned lesions showing atypical nuclear features with a constant IHC staining pattern of $CK19^+$ and $CD56^-$. On the other hand, we could avoid overdiagnosis by confirming an IHC staining pattern of $CK19^+$ and $CD56^+$ in benign follicular lesions such as lymphocytic thyroiditis, even with nuclear atypia.

The study group showed a longer turnaround time, which was 33 minutes longer than that of the control group in average, and 68% of them took more than 40 minutes in the diagnosis. However, we should consider the total cost and psychological trauma of patients in the control group whose diagnoses were deferred (7%) or discrepant (4%). The time taken in IHC staining can be shortened to some extent although limited, but we expect to shorten the turnaround time more effectively if only we can decide with more speed whether the case in hand needs IHC on frozen section or not.

Most of the nodules diagnosed as follicular neoplasm were finally diagnosed as FVPTC. Four out of five nodules of the control group were diagnosed as follicular carcinoma in one, hurthle cell carcinoma in one, and as encapsulated FVPTC in two nodules with or without capsular invasion. In contrast, only one out of six nodules diagnosed as follicular neoplasm in the study group was finally diagnosed as noninvasive encapsulated FVPTC after an additional IHC staining and further evaluation of permanent sections. The other nodule was diagnosed as oncocytic PTC after further evaluation of the remaining specimen.

Deferred lesions or lesions of follicular neoplasm that are finally confirmed to be malignant on permanent sections need to undergo secondary surgical procedure or other additional treatment. As such, we should note that 80% of the follicular neoplasms and 67% of the deferred lesions in the control group were finally confirmed to be malignant, whereas 33% of the follicular neoplasms in the study group were finally confirmed to be malignant. In the control group, two patients diagnosed with follicular neoplasm underwent completion thyroidectomy and two times of radioiodine treatment. Three patients whose frozen diagnoses were deferred underwent additional radioiodine treatment. On the other hand, three patients in the study group, diagnosed as FVPTC (n = 2) and lymphocytic thyroiditis (n = 1), avoided secondary surgical procedure.

We do have two nodules (3.7%) in the study group that could not be diagnosed even with the aid of IHC, which is only natural because patterns of immunoexpression in FVPTC can vary even in permanent sections.[11-13] But, if we consider the fact that the number escalates to six (7.0%) in the control group without the aid of IHC, we can safely say that the IHC can make a rather significant difference in the accuracy of frozen diagnosis in follicular patterned lesions. Therefore, we propose that if more specific antibodies are selected and applied, an intraoperative IHC stain on frozen sections can significantly improve the diagnostic accuracy in thyroid follicular lesions.

In conclusion, although the significance of intraoperative IHC stain is somewhat compromised by longer turnaround time, it considerably diminishes the diagnostic discrepancy and inaccuracy. With consideration of the adverse effects of indefinite intraoperative diagnosis or discrepancy between the frozen and permanent diagnoses incurred on the patients, a development of more specific antibodies is necessary and their application to the intraoperative

diagnosis of thyroid follicular lesions will further increase the diagnostic accuracy.

Conflicts of Interest

No potential conflict of interest relevant to this article was reported.

Acknowledgments

This work is funded by a grant of 2015 Korean Thyroid Association.

REFERENCES

1. Franssila KO, Ackerman LV, Brown CL, Hedinger CE. Follicular carcinoma. Semin Diagn Pathol 1985; 2: 101-22.
2. Posillico SE, Wilhelm SM, McHenry CR. The utility of frozen section examination for determining the extent of thyroidectomy in patients with a thyroid nodule and "atypia/follicular lesion of undetermined significance". Am J Surg 2015; 209: 552-6.
3. Hirokawa M, Carney JA, Goellner JR, *et al*. Observer variation of encapsulated follicular lesions of the thyroid gland. Am J Surg Pathol 2002; 26: 1508-14.
4. Franc B, de la Salmonière P, Lange F, *et al*. Interobserver and intraobserver reproducibility in the histopathology of follicular thyroid carcinoma. Hum Pathol 2003; 34: 1092-100.
5. Lloyd RV, Erickson LA, Casey MB, *et al*. Observer variation in the diagnosis of follicular variant of papillary thyroid carcinoma. Am J Surg Pathol 2004; 28: 1336-40.
6. Elsheikh TM, Asa SL, Chan JK, *et al*. Interobserver and intraobserver variation among experts in the diagnosis of thyroid follicular lesions with borderline nuclear features of papillary carcinoma. Am J Clin Pathol 2008; 130: 736-44.
7. Min HS, Kim JH, Ryoo I, Jung SL, Jung CK. The role of core needle biopsy in the preoperative diagnosis of follicular neoplasm of the thyroid. APMIS 2014; 122: 993-1000.
8. Na DG, Kim JH, Sung JY, *et al*. Core-needle biopsy is more useful than repeat fine-needle aspiration in thyroid nodules read as nondiagnostic or atypia of undetermined significance by the Bethesda system for reporting thyroid cytopathology. Thyroid 2012;22:468-75.
9. Hakala T, Kholová I, Sand J, Saaristo R, Kellokumpu-Lehtinen P. A core needle biopsy provides more malignancy-specific results than fine-needle aspiration biopsy in thyroid nodules suspicious for malignancy. J Clin Pathol 2013; 66: 1046-50.
10. Asa SL. The role of immunohistochemical markers in the diagnosis of follicular-patterned lesions of the thyroid. Endocr Pathol 2005; 16: 295-309.
11. El Demellawy D, Nasr A, Alowami S. Application of CD56, P63 and CK19 immunohistochemistry in the diagnosis of papillary carcinoma of the thyroid. Diagn Pathol 2008; 3: 5.
12. de Matos LL, Del Giglio AB, Matsubayashi CO, de Lima Farah M, Del Giglio A, da Silva Pinhal MA. Expression of CK-19, galectin-3 and HBME-1 in the differentiation of thyroid lesions: systematic review and diagnostic meta-analysis. Diagn Pathol 2012; 7: 97.
13. Nechifor-Boila A, Borda A, Sassolas G, *et al*. Immunohistochemical markers in the diagnosis of papillary thyroid carcinomas: The promising role of combined immunostaining using HBME-1 and CD56. Pathol Res Pract 2013; 209: 585-92.
14. Chem KT, Rosai J. Follicular variant of thyroid papillary carcinoma: a clinicopathologic study of six cases. Am J Surg Pathol 1977; 1: 123-30.
15. LiVolsi VA, Baloch ZW. Follicular neoplasms of the thyroid: view, biases, and experiences. Adv Anat Pathol 2004; 11: 279-87.
16. Kesmodel SB, Terhune KP, Canter RJ, *et al*. The diagnostic dilemma of follicular variant of papillary thyroid carcinoma. Surgery 2003; 134: 1005-12.
17. Lin HS, Komisar A, Opher E, Blaugrund SM. Follicular variant of papillary carcinoma: the diagnostic limitations of preoperative fine-needle aspiration and intraoperative frozen section evaluation. Laryngoscope 2000; 110: 1431-6.
18. Lee IK, Lee HD, Jeong J, *et al*. Intraoperative examination of sentinel lymph nodes by immunohistochemical staining in patients with breast cancer. Eur J Surg Oncol 2006; 32: 405-9.

Journal of Pathology and Translational Medicine 2017; 51: 471-481
https://doi.org/10.4132/jptm.2017.06.02

■ ORIGINAL ARTICLE ■

Diverse Immunoprofile of Ductal Adenocarcinoma of the Prostate with an Emphasis on the Prognostic Factors

Se Un Jeong
Anuja Kashikar Kekatpure
Ja-Min Park[1] · Minkyu Han[2]
Hee Sang Hwang · Hui Jeong Jeong
Heounjeong Go · Yong Mee Cho

Department of Pathology, [1]Asan Institute for Life Sciences, [2]Department of Clinical Epidemiology and Biostatistics, Asan Medical Center, University of Ulsan College of Medicine, Seoul, Korea

Received: February 28, 2017
Revised: May 13, 2017
Accepted: June 2, 2017

Corresponding Author
Yong Mee Cho, MD, PhD
Department of Pathology, University of Ulsan College of Medicine, Asan Medical Center, 88 Olympic-ro 43-gil, Songpa-gu, Seoul 05505, Korea
Tel: +82-2-3010-5965
Fax: +82-2-3010-7898
E-mail: yongcho@amc.seoul.kr

Background: Ductal adenocarcinoma (DAC) of the prostate is an uncommon histologic subtype whose prognostic factors and immunoprofile have not been fully defined. **Methods:** To define its prognostic factors and immunoprofile, the clinicopathological features, including biochemical recurrence (BCR), of 61 cases of DAC were analyzed. Immunohistochemistry was performed on tissue microarray constructs to assess the expression of prostate cancer-related and mammalian target of rapamycin (mTOR) signaling-related proteins. **Results:** During the median follow-up period of 19.3 months, BCR occurred in 26 cases (42.6%). DAC demonstrated a wide expression range of prostate cancer-related proteins, including nine cases (14.8%) that were totally negative for pan-cytokeratin (PanCK) immunostaining. The mTOR signaling-related proteins also showed diverse expression. On univariate analysis, BCR was associated with high preoperative serum levels of prostate-specific antigen (PSA), large tumor volume, predominant ductal component, high Gleason score (GS), comedo-necrosis, high tumor stage (pT), lymphovascular invasion, and positive surgical margin. High expressions of phospho-mTOR (p-mTOR) as well as low expressions of PSA, phospho-S6 ribosomal protein (pS6) and PanCK were associated with BCR. On multivariable analysis, GS, pT, and immunohistochemical expressions of PanCK and p-mTOR remained independent prognostic factors for BCR. **Conclusions:** These results suggest GS, pT, and immunohistochemical expressions of PanCK and p-mTOR as independent prognostic factors for BCR in DAC. Since DAC showed diverse expression of prostate cancer–related proteins, this should be recognized in interpreting the immunoprofile of DAC. The diverse expression of mTOR-related proteins implicates their potential utility as predictive markers for mTOR targeted therapy.

Key Words: Prostatic neoplasms; Carcinoma, ductal; Immunohistochemistry; Prognosis

Ductal adenocarcinoma (DAC) is an uncommon histologic subtype of prostate cancer, accounting for 3.2% of prostate cancer cases.[1] DAC is usually combined with acinar adenocarcinoma (AAC), while its pure form comprises only 0.2%–0.4% of prostate cancers.[1] DAC is defined by large papillary or cribriform glands lined by tall pseudostratified columnar cells with prominent nucleoli, coarse chromatin, and mitotic figures, which are unusual for AAC.[1] DAC is histologically similar to endometrioid adenocarcinoma of the female genital tract,[2] and thus it was initially described as "endometrial carcinoma of the prostatic utricle" in 1967.[3] In addition, the histologic features are overlapping with adenocarcinomas of other organs, such as the gastrointestinal tract and lung.

DAC often presents at an advanced stage, frequently with metastasis.[4] Metastatic spread of DAC occurs commonly in the bone and lymph nodes, similar to AAC. DAC also metastasizes to unusual sites for ACC, such as the lung, liver, and rarely penis, testis, and skin.[1,5] When DAC presents as a metastatic disease, it poses a diagnostic challenge because of its overlapping features with adenocarcinomas of other organ sites.[1] In such cases, ancillary studies, like immunohistochemistry, may help make the differential diagnosis. However, the immunoprofile of DAC remains to be defined.

Prostate cancer is dependent on persistent androgen receptor (AR) signaling, which is obtained by overexpression, amplification, point mutations, and splice variants of AR. There are additional signaling pathways implicated in prostate cancer progression, among which the phosphoinositide 3-kinase (PI3K)/AKT/mammalian target of rapamycin (mTOR) pathway is notable because it is altered in nearly all advanced prostate cancers.[6] These findings suggest targeting both AR and PI3K/AKT/mTOR pathways as a new therapeutic approach in castration-resistant prostate cancer.[6] However, an immunohistochemical expression of the mTOR signaling pathway in DAC has not yet been reported.

In an effort to expand our understanding of this rare subtype

pISSN 2383-7837
eISSN 2383-7845

of prostate cancer, we examined the clinicopathological features of 61 cases of DAC and their immunoprofiles of prostate cancer-related and mTOR pathway-related proteins. Specific attention was paid to define prognostic factors for biochemical recurrence (BCR) and potential predictive markers for mTOR inhibitors.

MATERIALS AND METHODS

Study samples

This retrospective study initially included 87 cases that underwent radical prostatectomy for clinically localized prostate cancer and were pathologically diagnosed as DAC between January 1995 and December 2015 at Asan Medical Center (Seoul, Republic of Korea). None of these cases were treated with neoadjuvant androgen deprivation therapy. A total of 26 cases were excluded for the following reasons: 16 cases were reassessed as AAC during retrospective review; nine cases were excluded either because the tumor tissue was too small to construct two representative cores of tissue microarray (TMA) or because formalin-fixed paraffin-embedded tissue blocks were unavailable; and one case was excluded because clinical follow-up data was not available. As such, 61 cases of DAC were included in the final analysis.

Patients' clinicopathological information was obtained from electronic medical records and surgical pathology reports. BCR was defined as a serum prostate-specific antigen (PSA) level ≥0.2 ng/mL on two consecutive occasions after achieving undetectable PSA following radical prostatectomy.[7] All pathologic materials were reviewed for diagnostic reassessment according to the 2016 World Health Organization Tumor Classification.[1] Gleason score (GS) and pathologic tumor stage (pT) were assigned according to the 2015 modified Gleason grading system and the American Joint Committee on Cancer Staging System, seventh edition, respectively.[1,8] This study was approved by the Institutional Review Board of Asan Medical Center with a waiver of informed consent (2011-0499).

TMA construction

A TMA construct of 2-mm-diameter cores was generated from the 10% neutrally buffered formalin-fixed, paraffin-embedded tissue blocks of radical prostatectomy specimens using a tissue microarrayer (Quick-Ray, Unitma Co. Ltd., Seoul, Korea). Two representative cores from different DAC areas were included for each case.

Immunohistochemistry

Prostate cancer–related proteins analyzed in this study included pan-cytokeratin (PanCK), PSA, AR, enhancer of zeste homolog 2 (EZH2), p53, and ETS-related gene (ERG). Phosphatase and tensin homolog (PTEN), phospho-mammalian target of rapamycin (p-mTOR), phospho-S6 ribosomal protein (pS6), and 14-3-3 sigma protein were included as mTOR pathway–related proteins. Immunohistochemical staining was performed using an automated staining system (BenchMark XT, Ventana Medical Systems, Tucson, AZ, USA). The primary antibodies used in this study, their dilutions, and the subcellular location of each antigen are summarized in Table 1. Nuclei were counterstained with hematoxylin. Representative expression patterns of these proteins are presented in Fig. 1.

The immunohistochemical staining results were assessed in the DAC component only by two pathologists (S.U.J. and A. K.K.), both of whom were blinded to the associated clinicopathological information. The staining intensity of the antibodies was initially scored as negative, weak, moderate, or strong. Cases with moderate to strong intensity were regarded as positive, and then the average percentage of positive cells in all cores was recorded.

Immunohistochemistry on whole section

To exclude the issues of intratumoral heterogeneity, immunohistochemistry was performed on whole sections of one negative case, one intermediate case, and one positive case for each antibody. In addition, to exclude technical problems, such as poor formalin-fixation of radical prostatectomy specimens, immunohistochemistry for PanCK was performed on whole sections of all PanCK-negative cases.

Table 1. Antibodies used in the study

Antibody	Dilution	Company	Subcellular location
PanCK	1:400	Leica, Newcastle, UK	Cytoplasm
PSA	1:200	Dako Corp., Carpinteria, CA	Cytoplasm
AR	1:200	Cell Marque, Rocklin, CA	Nucleus
ERG	1:100	Epitomics, Burlingame, CA	Nucleus
p53	1:1500	Dako Corp., Carpinteria, CA	Nucleus
EZH2	1:25	Cell Signal Technology, Beverly, MA	Nucleus
PTEN	1:100	Cell Signal Technology, Beverly, MA	Cytoplasm/nucleus
p-mTOR	1:100	Cell Signal Technology, Beverly, MA	Cytoplasm
pS6	1:100	Cell Signal Technology, Beverly, MA	Cytoplasm
14-3-3 sigma	1:200	Sigma, St. Louis, MO	Cytoplasm

PanCK, pan-cytokeratin; PSA, prostate-specific antigen; AR, androgen receptor; ERG, ETS-related gene; EZH2, enhancer of zeste Homolog2; PTEN, phosphatase and tensin homolog; p-mTOR, phospho-mammalian target of rapamycin; pS6, phospho-S6 ribosomal protein.

https://doi.org/10.4132/jptm.2017.06.02

Statistical analysis

For descriptive statistics and univariate analyses, all continuous data were expressed as mean±standard deviation and were compared using Student's t tests. The optimal cut-off value of the protein expression was calculated from the receiver operating characteristic (ROC) curve analysis. Categorical data were compared with the chi-square test. BCR was estimated using the Kaplan-Meier method and the resulting curves were compared by log-rank test. In order to minimize the exclusion of variables that are important in this study, all variables with p-values of < .1 in the univariate analysis were included in the multivariate analysis, for which the Cox proportional hazards model was used. The overlapping variables were excluded in the multivariate analysis. Independent variables were chosen by the stepwise method. p-values of < .05 were considered statistically significant.

Table 2. Clinicopathological features of 61 cases of ductal adenocarcinoma

Variable	Value
Age (yr)	68.0±5.6
Preoperative PSA (ng/mL)	11.7±10.3
Total tumor volume (%)	28.5±21.5
DAC component (%)	48.3±32.5
Predominant component	
Ductal	32 (52.5)
Acinar	29 (47.5)
Predominant DAC pattern	
Papillary	48 (78.7)
Cribriform	9 (14.7)
PIN-like	4 (6.6)
Gleason score	
7	20 (32.8)
8	29 (47.5)
9	12 (19.7)
Pathologic tumor stage	
pT2a-c	17 (27.9)
pT3a	29 (47.5)
pT3b	15 (24.6)
Tertiary grade 5	12 (19.7)
Comedonecrosis	17 (27.9)
Extraprostatic extension	42 (68.9)
Lymphovascular invasion	26 (42.6)
Perineural invasion	52 (85.2)
Positive surgical margin	41 (67.2)
Seminal vesicle involvement	15 (24.6)
Lymph node metastasis	3 (4.9)
Biochemical recurrence	26 (42.6)
Death	2 (3.3)

Values are presented as mean±SD or number (%).
PSA, prostate-specific antigen; DAC, ductal adenocarcinoma; PIN-like, prostatic intraepithelial neoplasia-like; SD, standard deviation.

RESULTS

Clinicopathological features of DAC

The clinicopathological features of the 61 DAC cases are summarized in Table 2. The median age at the time of radical prostatectomy was 68 years (range, 51 to 77 years), with a median preoperative serum PSA level of 11.7 ng/mL (range, 0.6 to 66.4 ng/mL). The mean total tumor volume was 28.5% (range, 2% to 95%), in which the DAC component occupied 48.3% on average (range, 5% to 100%). Four cases (6.5%) were pure DAC. Among histologic DAC patterns, the papillary pattern was the most common (48 cases, 78.7%), followed by cribriform pattern (nine cases, 14.7%) and prostatic intraepithelial neoplasia-like pattern (four cases, 6.6%). A significant proportion of the cases were of high grade (GS ≥8: 41 cases, 67.2%) with accompanying comedo-necrosis in 17 cases (27.9%). The majority of the cases were of high stage (pT3: 44 cases, 72.1%) with frequent extraprostatic extension (42 cases, 68.9%), lymphovascular invasion (26 cases, 42.6%), positive surgical margin (41 cases, 67.2%), and seminal vesicle

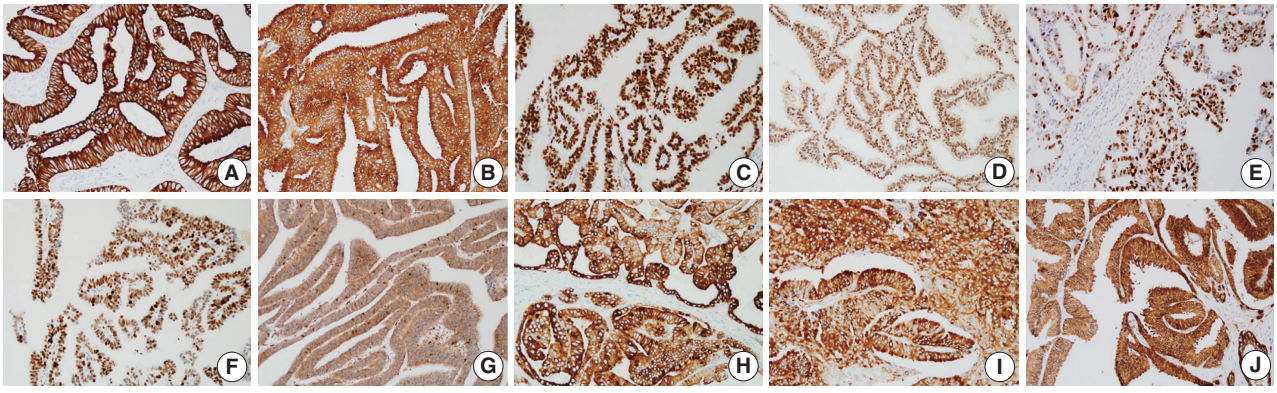

Fig. 1. Representative cases with strong intensity of each immunohistochemical staining: pan-cytokeratin (A), prostate-specific antigen (B), androgen receptor (C), ETS-related gene (D), p53 (E), enhancer of zeste homolog 2 (F), phosphatase and tensin homolog (G), phospho-mammalian target of rapamycin (H), phospho-S6 ribosomal protein (I), and 14-3-3 sigma (J).

http://jpatholtm.org/

Table 3. Correlation between expression of prostate cancer–related proteins and clinicopathological features of DAC

	PanCK			ERG			p53			AR			EZH2			PSA		
	Low	High	p-value	Low	High	p-value	Low	High	p-value	Low	High	p-value	Low	High	p-value	Low	High	p-value
No. of cases	30 (49.2)	31 (50.8)		58 (95.1)	3 (4.9)		46 (75.4)	15 (24.6)		42 (68.9)	19 (31.1)		38 (62.3)	23 (37.7)		33 (54.1)	28 (45.9)	
Age (yr)	68.3 (55–75)	67.7 (51–77)	.700	67.9 (51–77)	70.0 (65–75)	.526	67.5 (51–77)	69.3 (53–76)	.285	67.3 (51–77)	69.5 (59–76)	.163	67.7 (51–77)	68.4 (57–76)	.661	67.9 (54–77)	68.1 (51–76)	.875
PSA (ng/mL)	14.0 (3.1–66.4)	9.5 (0.6–24.1)	.363	11.8 (0.6–66.4)	9.0 (5.9–13.1)	.648	11.3 (0.6–32.8)	13.0 (3.4–66.4)	.573	12.7 (1.8–66.4)	9.5 (0.6–31.3)	.269	13.1 (1.8–66.4)	9.3 (0.6–30.3)	.160	11.0 (1.8–32.8)	12.5 (0.6–66.4)	.565
GS			.731			.175			.015			.025			.246			.006
7	10 (33.3)	10 (32.3)		20 (34.5)	0		19 (41.3)	1 (6.7)		11 (26.2)	9 (47.4)		14 (36.8)	6 (26.1)		5 (15.2)	15 (53.6)	
8	13 (43.3)	16 (51.6)		26 (44.8)	3 (100)		21 (45.7)	8 (53.3)		19 (45.2)	10 (52.6)		19 (50.0)	10 (43.5)		20 (60.6)	9 (32.1)	
9	7 (23.3)	5 (16.1)		12 (20.7)	0		6 (13.0)	6 (40.0)		12 (28.6)	0		5 (13.2)	7 (30.4)		8 (24.2)	4 (14.3)	
pT			.044			.543			.072			.350			.004			.348
T2a-c	5 (16.7)	12 (38.7)		17 (29.3)	0		16 (34.8)	1 (6.7)		14 (33.3)	3 (15.8)		16 (42.1)	1 (4.3)		7 (21.2)	10 (35.7)	
T3a	19 (63.3)	10 (32.3)		27 (46.6)	2 (66.7)		21 (45.7)	8 (53.3)		18 (42.9)	11 (57.9)		13 (34.2)	16 (69.6)		16 (48.5)	13 (46.4)	
T3b	6 (20.0)	9 (29.0)		14 (24.1)	1 (33.3)		9 (19.6)	6 (40.0)		10 (23.8)	5 (26.3)		9 (23.7)	6 (26.1)		10 (30.3)	5 (17.9)	
LVI			.912			.039			.030			.539			.025			.041
Absent	17 (56.7)	18(58.1)		35 (60.3)	0		30 (65.2)	5 (33.3)		23 (54.8)	12 (63.2)		26 (68.4)	9 (39.1)		15 (45.5)	20 (71.4)	
Present	13 (43.3)	13 (41.9)		23 (39.7)	3 (100)		16 (34.8)	10 (66.7)		19 (45.2)	7 (36.8)		12 (31.6)	14 (60.9)		18 (54.5)	8 (28.6)	
Comedo-necrosis			.715			.829			.011			.222			.034			.301
Absent	21 (70.0)	23 (74.2)		42 (72.4)	2 (66.7)		37 (80.4)	7 (46.7)		28 (66.7)	16 (84.2)		31 (81.6)	13 (56.5)		22 (66.7)	22 (78.6)	
Present	9 (30.0)	8 (25.8)		16 (27.6)	1 (33.3)		9 (19.6)	8 (53.3)		14 (33.3)	3 (15.8)		7 (18.4)	10 (43.5)		11 (33.3)	6 (21.4)	
Positive RM			.122			.215			.959			.297			.761			.921
Absent	7 (23.3)	13 (41.9)		20 (34.5)	0		15 (32.6)	5 (33.3)		12 (28.6)	8 (42.1)		13 (34.2)	7 (30.4)		11 (33.3)	9 (32.1)	
Present	23 (76.7)	18 (58.1)		38 (65.5)	3 (100)		31 (67.4)	10 (66.7)		30 (71.4)	11 (57.9)		25 (65.8)	16 (69.6)		22 (66.7)	19 (67.9)	
LN metastasis			.573			.686			.310			.232			.873			.102
Absent	29 (96.7)	29 (93.5)		55 (94.8)	3 (100)		43 (93.5)	15 (100)		39 (92.9)	19 (100)		36 (94.8)	22 (95.7)		30 (90.9)	28 (100)	
Present	1 (1.0)	2 (6.5)		3 (5.2)	0		3 (6.5)	0		3 (7.1)	0		2 (5.2)	1 (4.3)		3 (9.1)	0	

Values are presented as median (range) or number (%).
Cut-off for high expression of each protein is ≥ 50% for PanCK, 100 % for ERG, ≥ 10% for p53, 100% for AR, ≥ 25% for EZH2, and ≥ 70% for PSA.
DAC, ductal adenocarcinoma; PanCK, pan-cytokeratin; ERG, ETS-related gene; AR, androgen receptor; EZH2, enhancer of zeste homolog 2; PSA, prostate-specific antigen; GS, Gleason score; pT, pathologic tumor stage; LVI, lymphovascular invasion; RM, resection margin; LN, lymph node.

https://doi.org/10.4132/jptm.2017.06.02

Table 4. Correlation between expression of mTOR signaling–related proteins and clinicopathological features of DAC

	p-mTOR			14-3-3 sigma			pS6			PTEN		
	Low	High	p-value	Intact	Loss	p-value	Low	High	p-value	Intact	Loss	p-value
No. of cases	46 (75.4)	15 (24.6)		25 (41.0)	36 (59.0)		39 (63.9)	22 (36.1)		37 (60.7)	24 (39.3)	
Age (yr)	67.8 (51–77)	68.7 (59–76)	.589	69.6 (54–77)	66.9 (51–76)	.066	66.5 (54–76)	68.9 (51–77)	.109	68.7 (59–77)	66.8 (51–75)	.197
PSA (ng/mL)	11.6 (0.6–66.4)	12.0 (3.7–31.3)	.883	14.7 (0.6–66.4)	9.6 (1.8–32.8)	.088	14.1 (0.6–66.4)	10.3 (0.3–31.3)	.166	13.4 (3.4–66.4)	9.1 (0.6–30.3)	.106
GS			.307			.298			.105			.747
7	15 (32.6)	5 (33.3)		11 (44.0)	9 (25.0)		12 (30.8)	8 (36.4)		11 (29.7)	9 (37.5)	
8	20 (43.5)	9 (60.0))		10 (40.0)	19 (52.8)		22 (56.4)	7 (31.8)		19 (51.4)	10 (41.7)	
9	11 (23.9)	1 (6.7)		4 (16.0)	8 (22.2)		5 (12.8)	7 (31.8)		7 (18.9)	5 (20.8)	
pT			.138			.426			.790			.051
T2a–c	12 (26.1)	5 (33.3)		8 (32.0)	9 (25.0)		12 (30.8)	5 (22.7)		8 (21.6)	9 (37.5)	
T3a	25 (54.3)	4 (26.7)		13 (52.0)	16 (44.4)		18 (46.2)	11 (50.0)		16 (43.2)	13 (54.2)	
T3b	9 (19.6)	6 (40.0)		4 (16.0)	11 (30.6)		9 (23.1)	6 (27.3)		13 (35.1)	2 (8.3)	
LVI			.813			.730			.737			.903
Absent	26 (56.5)	9 (60.0)		15 (60.0)	20 (55.6)		23 (59.0)	12 (54.5)		21 (56.8)	14 (58.3)	
Present	20 (43.5)	6 (40.0)		10 (40.0)	16 (44.4)		16 (41.0)	10 (45.5)		16 (43.2)	10 (41.7)	
Comedonecrosis			.905			.574			.605			.687
Absent	33 (71.7)	11 (73.3)		19 (76.0)	25 (69.4)		29 (74.4)	15 (68.2)		26 (70.3)	18 (75.0)	
Present	13 (28.3)	4 (26.7)		6 (24.0)	11 (30.6)		10 (25.6)	7 (31.8)		11 (29.7)	6 (25.0)	
Positive RM			.224			.076			.904			.942
Absent	17 (37.0)	3 (20.0)		5 (20.0)	15 (41.7)		13 (33.3)	7 (31.8)		12 (32.4)	8 (33.3)	
Present	29 (63.0)	12 (80.0)		20 (80.0)	21 (58.3)		26 (66.7)	15 (68.2)		25 (67.6)	16 (66.7)	
LN metastasis			.310			.782			.919			.320
Absent	43 (93.5)	15 (100)		24 (96.0)	34 (94.4)		37 (94.9)	21 (95.5)		36 (97.3)	22 (91.7)	
Present	3 (6.5)	0		1 (4.0)	2 (5.6)		2 (5.1)	1 (4.5)		1 (2.7)	2 (8.3)	

Values are presented as number (%) or median (range).
Cut-off for each protein is as follows: ≥40% for high expression of p-mTOR, <80% for loss of 14-3-3 sigma, ≥10% for high expression of pS6, and <85% for loss of PTEN.
mTOR, mammalian target of rapamycin; DAC, ductal adenocarcinoma; p-mTOR, phospho-mammalian target of rapamycin; pS6, phospho-S6 ribosomal protein; PTEN, phosphatase and tensin homolog; PSA, prostate-specific antigen; GS, Gleason score; pT, pathologic tumor stage; LVI, lymphovascular invasion; RM, resection margin; LN, lymph node.

involvement (15 cases, 24.6%).

During the median follow-up period of 19.3 months (range, 1 to 70 months), BCR occurred in 26 cases (42.6%) at a median of 10.5 months (range, 1 to 44 months) after the surgery. Two patients (3.3%) died, and one died of prostate cancer (1.6%).

Expression of prostate cancer-related proteins in DAC

The prostate cancer–related proteins showed diverse expressions in DAC as shown in Fig. 2A. PanCK and PSA were heterogeneously expressed with a median value of 50% and 65%, respectively (range, 0% to 100%). Furthermore, nine cases (14.8%) were negative for PanCK and and two cases (3.3%) for PSA. AR was expressed in all DAC cases with a heterogeneous pattern and a median value of 85% (range, 10% to 100%). ERG expression was not observed in most cases (54 cases, 88.5%) and only seven cases (11.5%) showed focal or diffuse positivity. p53 and EZH2 were expressed at median values of 17.5% (range, 0% to 35%) and 20% (range, 0% to 95%), respectively.

Expression of mTOR signaling–related proteins in DAC

The mTOR signaling-related proteins also showed diverse expressions in DAC, as shown in Fig. 2B. DAC cases showed a high expression of PTEN (median, 100%) and a low expression of p-mTOR (median, 15%) and pS6 (median, 15%). Eight cases (13.1%) showed no immunoreactivity for PTEN. 14-3-3 sigma was also expressed variably with a median value of 60% (range, 0% to 100%).

Immunohistochemistry on whole section

Tumor heterogeneity was evaluated by immunohistochemistry using whole sections of one negative case, one intermediate case, and one positive case for each antibody. Although there was a slight variation in the cases of intermediate expression, a great degree of similarity was observed in all cases, especially in negative cases and entirely positive cases (data not shown). PanCK immunohistochemistry on whole sections of all PanCK-negative cases on the TMA construct showed immunopositivity in normal

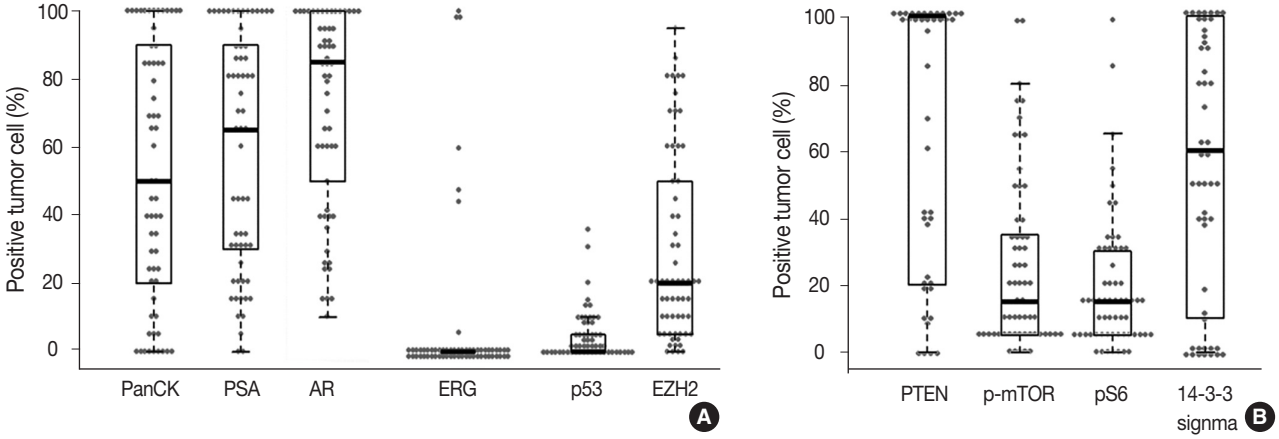

Fig. 2. (A) Box and whisker plot with overlying scatterplot to visualize distributions of the immunoreactive tumor cell proportions against the prostate cancer–related proteins in ductal adenocarcinoma. About 15% of the cases (9 of 61) exhibited a completely negative reaction for pan-cytokeratin (PanCK). (B) The same plot to demonstrate the positive tumor cell proportions against the proteins related to the mammalian target of rapamycin (mTOR) pathway. PSA, prostate-specific antigen; AR, androgen receptor; ERG, ETS-related gene; EZH2, enhancer of zeste homolog 2; PTEN, phosphatase and tensin homolog; p-mTOR, phospho-mammalian target of rapamycin; pS6, phospho-S6 ribosomal protein.

prostatic glands and AAC areas as shown in Fig. 3. However, PanCK was negative in eight cases among the nine cases; one case showed focal (15%) immunopositivity on the whole section. Therefore, technical problems were not an issue and the immunohistochemical data using the TMA construct were confirmed to be representative.

Correlation of protein expression with clinicopathological features

To define the prognostic significance of the prostate cancer-related proteins and mTOR signaling–related proteins, a cut-off expression value of each protein was determined according to the ROC curve analysis for BCR (Tables 3, 4). The correlation between expressions of prostate cancer-related proteins or mTOR signaling–related proteins and clinicopathological features are summarized in Tables 3 and 4, respectively.

Low expression of PanCK was associated with high pT ($p = .044$), whereas high GS was associated with low expressions of PSA and AR ($p = .006$ and $p = .025$, respectively) and high expression of p53 ($p = .015$). DAC cases with lymphovascular invasion showed high expressions of ERG, p53, and EZH2 ($p = .039$, $p = .030$, and $p = .025$, respectively) and low expression of PSA ($p = .041$).

Prognostic factors for BCR in DAC

As shown in Table 5, among the clinicopathological features, the univariate analysis showed that BCR was associated with high preoperative serum PSA level ($p < .001$), large tumor volume ($p < .001$), predominant ductal component ($p = .021$), high GS ($p = .004$), comedo-necrosis ($p = 0.015$), high pT ($p = .010$), lymphovascular invasion ($p = .002$), and positive surgical margin ($p = .015$). Among the protein expressions, high expressions of p-mTOR and low expression of PSA and pS6 were associated with BCR ($p = .049$, $p = .022$, and $p = .033$, respectively). Low expression of PanCK showed borderline significance ($p = .055$). On multivariable analysis, high GS ($p < .001$), high pT ($p = .025$), low expression of PanCK ($p = .007$), and high expression of p-mTOR ($p = .002$) remained independent prognostic factors for BCR. The Kaplan-Meier survival curves of these four independent prognostic factors are shown in Fig. 4.

DISCUSSION

Herein, we analyzed the clinicopathological features and immunoprofile of 61 cases of DAC. The results suggest GS, pT stage, and immunohistochemical expressions of PanCK and p-mTOR as independent prognostic factors for BCR. DAC demonstrated wide expression ranges of prostate cancer–related proteins, which should be recognized during interpretation of immunohistochemical results of DAC. Since DAC demonstrated diverse expression of mTOR-related proteins, these results cautiously suggest their potential utility as predictive markers for mTOR-targeted therapy.

Although previous studies regarding the immunohistochemical expression of DAC exist, they analyzed a small number of cases and mostly focused on PSA and a few other prostate cancer-related proteins.[9-17] Furthermore, they mostly presented the results as

 https://doi.org/10.4132/jptm.2017.06.02

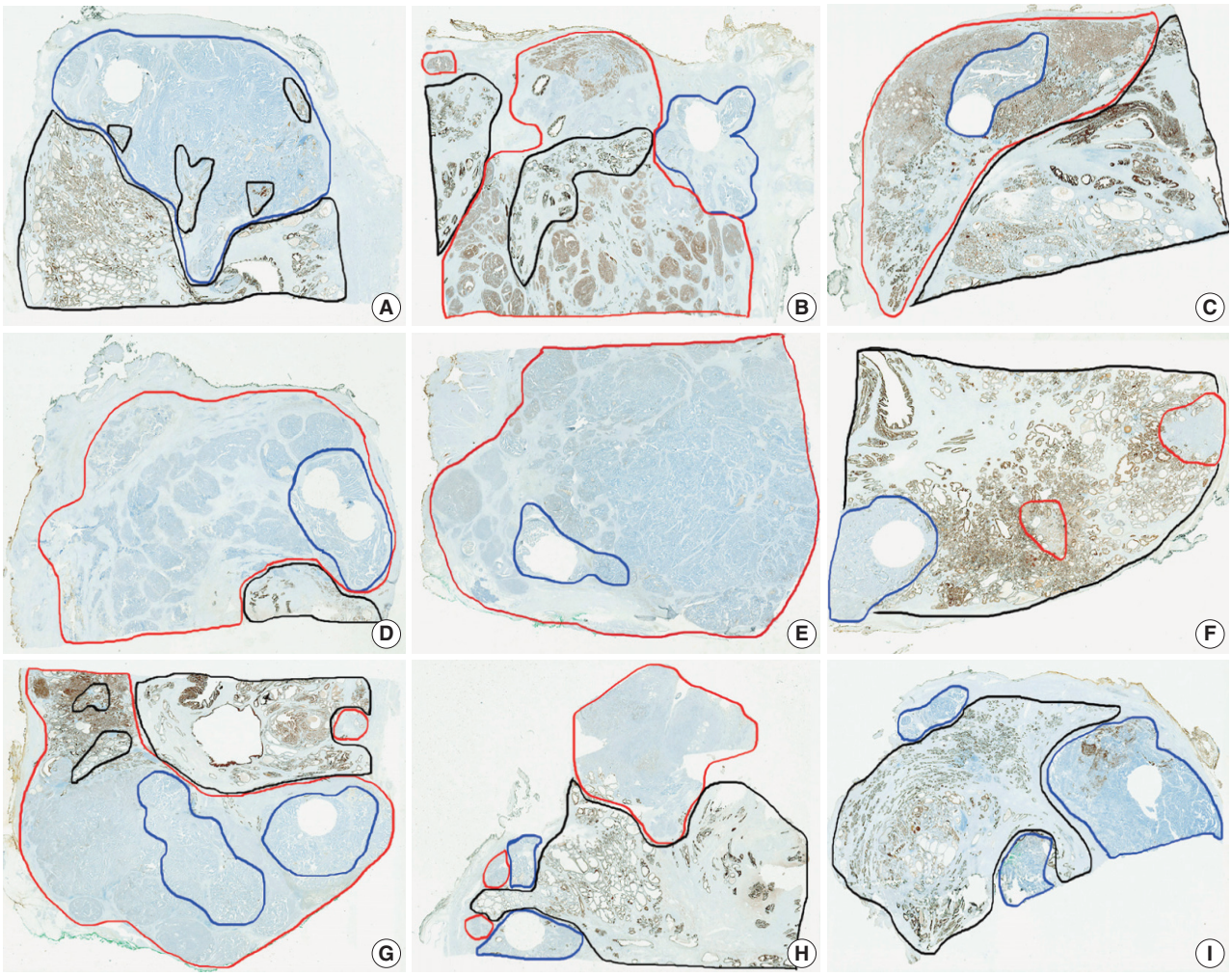

Fig. 3. Pan-cytokeratin (PanCK) immunohistochemistry on whole section slides. All nine cases of PanCK-negative on tissue microarray (TMA) were immunostained for PanCK on whole section, and then their scan view images were presented. PanCK was still negative in eight cases (A–H) on the whole sections except one case (I), which showed focal (15%) immunopositivity (ductal adenocarcinoma, blue line; acinar adenocarcinoma component, red line; normal prostate glands, black line; round empty space, TMA site).

positive, focally positive, or negative without an accurate range of expression. One recent study analyzed a large number of cases (n = 60) and showed high expressions of AR, PSA, and PTEN and low expression of ERG in 100%, 100%, 70.2%, and 38.3% of DAC cases, respectively.[18] Nevertheless, this present study is significant because of the detailed description of the expression range of each protein and the assessment of mTOR pathway–associated protein in DAC for the first time. Furthermore, we identified independent prognostic factors for BCR in DAC: GS, pT, and immunohistochemical expressions of PanCK and p-mTOR.

On light microscopic examination, histologic differences are apparent between DAC and AAC, but it appears that they are similar at the molecular level as assessed by gene expression profile.[19] In line with this notion, DAC cases in this study showed high expression of AR and low expression of p53, similar to AAC.[20-22] PanCK and PSA are drawing special attention among the prostate cancer-related proteins. Even though PanCK and PSA have been proven useful as an epithelial marker and a prostate lineage marker, respectively, the present study showed that they were expressed heterogeneously, including nine cases (14.8%) of PanCK-negative ones and two cases (3.3%) of PSA-negative ones. Previous studies showed that AAC was also focally positive or even negative for PanCK and PSA in a few cases (3.4% and 2%–7%, respectively), similar to DAC in present study.[23-27] Therefore, it is worth noting that both DAC and AAC could be focally positive and even negative for PanCK and PSA, especially in metastatic disease.

In AAC, fusions between the androgen-regulated transmembrane protease serine 2 gene (*TMPRSS2*) and the *ERG* gene are

Table 5. Univariate and multivariable analyses of the effect of clinicopathological factors and immunohistochemical markers on biochemical recurrence

Variable	Univariate analysis			Multivariable analysis		
	HR	95% CI	p-value	HR	95% CI	p-value
Age (yr)	1.010	0.941–1.083	.783	-	-	-
Preoperative PSA (ng/mL)	1.066	1.038–1.094	<.001	-	-	-
Total tumor volume (%)	1.029	1.013–1.047	<.001	-	-	-
Predominant component (ductal)	2.793	1.171–6.664	.021	-	-	-
Gleason score			.004			<.001
7	1			1		
8	12.04	1.588–91.21	.016	15.020	1.946–115.941	.009
9	26.79	3.406–210.66	.002	26.937	3.227–224.851	.002
Pathologic tumor stage			.010			.025
T2a–c	1			1		
T3a	5.400	1.205–24.190	.028	4.270	0.890–20.487	.070
T3b	10.190	2.237–46.400	.003	8.288	1.617–42.494	.011
Comedonecrosis	2.618	1.202–5.702	.015	-	-	-
Lymphovascular invasion	3.728	1.615–8.605	.002	-	-	-
Positive surgical margin	4.473	1.341–14.930	.015	-	-	-
Lymph node metastasis	0.616	0.082–4.624	.637	-	-	-
PanCK (high expression)	0.453	0.202–1.016	.055	0.274	0.108–0.700	.007
ERG (high expression)	1.626	0.382–6.931	.511	-	-	-
p53 (high expression)	2.082	0.938–4.621	.072	-	-	-
AR (high expression)	0.728	0.291–1.821	.498	-	-	-
EZH2 (high expression)	2.012	0.901–4.490	.088	-	-	-
PSA (high expression)	0.360	0.151–0.861	.022	-	-	-
p-mTOR (high expression)	2.266	1.004–5.117	.049	5.184	1.829–14.704	.002
14-3-3 sigma (loss of expression)	1.457	0.633–3.356	.376	-	-	-
pS6 (high expression)	0.431	0.199–0.935	.033	-	-	-
PTEN (loss of expression)	0.680	0.302–1.532	.352	-	-	-

HR, hazard ratio estimated by Cox proportional hazards regression model; CI, confidence interval of the estimated HR; PSA, prostate-specific antigen; PanCK, pan-cytokeratin; ERG, ETS-related gene; AR, androgen receptor; EZH2, enhancer of zeste homolog 2; p-mTOR, phospho-mammalian target of rapamycin; pS6, phospho-S6 ribosomal protein; PTEN, phosphatase and tensin homolog.

present in approximately 40%–50% of cases, where ERG immunohistochemistry correlates well with fusion-positive cancer.[24,26] In the Korean population, the ERG-positive rate by immunohistochemistry was 24.4%, which is lower than those of Western population-based studies.[23,27] Interestingly, Japanese population-based studies also showed low ERG-positive rates, similar to Korean population. These findings suggest that geographic variation may contribute to the lower rates of ERG-positive cases in Eastern Asian prostate cancer patients.[27] Since only seven cases (11%) were positive for ERG in the present study, it appears that the ERG-positive rate is even lower in DAC than in AAC.

EZH2 is the catalytic subunit of the polycomb repressive complex (PRC2) responsible for conducting histone methylation. It is important in cell cycle regulation and has a role in tumor cell proliferation and invasive growth.[28] High expression of EZH2 in AAC has been associated with aggressive clinicopathological features, such as GS ≥8, extraprostatic extension, positive surgical margins, and BCR.[29] In contrast to AAC, EZH2 expression was not associated with BCR in DAC by univariate and multivariable analyses, although it was correlated with poor prognostic clinicopathological features, such as comedo-necrosis, high pT, and lymphovascular invasion.

The mTOR pathway responds to diverse environmental cues, such as amino acids, stress, oxygen, energy, and growth factors, and it controls many biologic processes that generate or use large amounts of energy and nutrients.[30] mTOR signaling impacts most major cellular functions, giving it an important role in regulating basic cellular behaviors, such as cellular growth and proliferation.[30] Overactivation of mTOR signaling contributes to the initiation and development of many types of cancers, including prostate cancer, suggesting that mTOR inhibitors, such as sirolimus, everolimus, and temsirolimus, might lead to an improved patient survival.[31] However, the identification of biomarkers that predict which tumors will respond to mTOR inhibitors remains an unmet need.

 https://doi.org/10.4132/jptm.2017.06.02

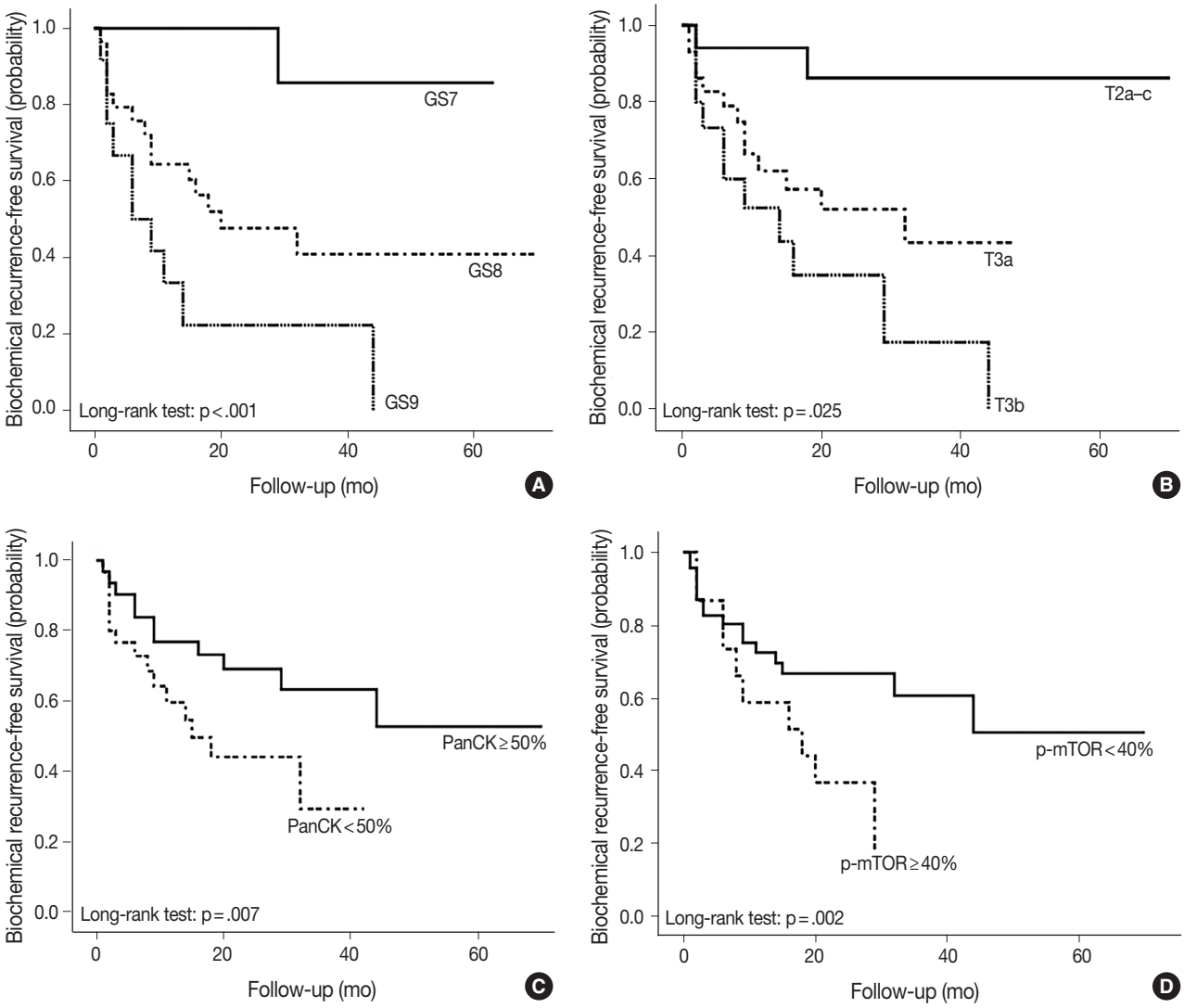

Fig. 4. Kaplan-Meier survival curves of four independent prognostic factors on biochemical recurrence. The Kaplan-Meier survival curves are well-established according to Gleason score (GS) and pT stage (A, B). The prognosis is worse with less than 50% expression in pan-cytokeratin (PanCK) staining (C), and with more than 40% expression in phospho-mammalian target of rapamycin (p-mTOR) staining (D).

As one of the diverse upstream regulators of the mTOR pathway, PTEN encodes a phosphatase that dephosphorylates phosphatidylinositol-3,4,5-trisphosphate (PIP3), a second messenger in the PI3K–protein kinase B (PKB) signaling pathway.[32] By negatively regulating the PI3K/PKB signaling pathway, it functions as a tumor suppressor. PTEN loss activates PI3K, which then activates not only mTOR complex 1 (mTORC1) by activating AKT, but also mTORC2 directly.[33] The mTORC1 and mTORC2 complexes are composed of mTOR and several common and unique proteins, allowing those different sensitivities to upstream regulators and diverse downstream output.[30] Many stresses, including low energy and oxygen levels and DNA damage, act through tuberous sclerosis 1 (TSC1) and 2 (TSC2), which are key upstream regulators of mTORC1. Adenosine monophosphate-activated protein kinase (AMPK), in response to hypoxia or a low energy state, phosphorylates TSC2 and communicates directly with mTORC1, leading to 14-3-3 binding.[30] The binding of 14-3-3 proteins, including 14-3-3 sigma on mTORC1, may promote mTORC1 signaling under growth factors, but also contributes to the regulatory mechanisms that suppress mTORC1 activity under conditions of cell stress.[34] mTORC1 also directly phosphorylates and activates ribosomal S6 kinase 1 (S6K1), of which the target substrate is the S6 ribosomal protein (pS6), which has been used as a surrogate for mTORC1 activity.[35] Phosphorylation of S6 induces protein synthesis in the ribosome.[30]

Few studies have been conducted on the mTOR signaling

pathway as a predictive marker in prostate cancer. In a clinical study to evaluate everolimus in castration-resistant prostate cancer, probably AAC type, deletion of PTEN assessed by fluorescence *in situ* hybridization was found in seven of 23 tumor samples and associated with longer progression-free survival and response. However, they argued that immunohistochemical expressions of PTEN, pS6, p-mTOR, and ERG were not predictive.[36] To the best of our knowledge, the present study is the first one to assess mTOR pathway-associated proteins in DAC where mTOR-related proteins are diversely expressed. Therefore, it would be interesting to define the usefulness of these proteins as predictive markers of mTOR inhibitors in DAC.

Although our present study examined a relatively large number of DAC cases, it had some limitations, including its retrospective design and the fact that all patients came from a single institution. Most cases were combined with AAC but the AAC component was not evaluated for immunohistochemical expression of prostate cancer- and mTOR signaling–related proteins. Since this present study showed GS, pT stage, and immunohistochemical expressions of PanCK and p-mTOR as independent prognostic factors, multi-institutional studies are necessary to validate the clinical utility of the results. Furthermore, remarkable advances in investigative tools, such as genomic microarray technologies and next-generation sequencing, may help find novel prognostic and predictive biomarkers. Therefore, efforts should be made to identify more accurate markers by integrating newly discovered biomarkers. Although mTOR-related proteins were cautiously suggested as immunohistochemical predictive markers for mTOR inhibitors, this result should be confirmed by immunohistochemical staining on whole section. It is also obvious that the assumption is still premature and should be investigated through a prospective clinical study.

Conflicts of Interest

No potential conflict of interest relevant to this article was reported.

Acknowledgments

This research was supported by the Basic Science Research Program through the National Research Foundation of Korea (NRF) funded by the Ministry of Science, ICT and Future Planning (2015R1A2A2A01006958).

REFERENCES

1. Moch H, Humphrey PA, Ulbright TM, Reuter VE. WHO classification of tumours of the urinary system and male genital organs. 4th ed. Lyon: International Agency for Research on Cancer, 2016.
2. Melicow MM, Pachter M. Endometrial carcinoma of proxtatic utricle (uterus masculinus). Cancer 1967; 20: 1715-22.
3. Tarjan M, Lenngren A, Hellberg D, Tot T. Immunohistochemical verification of ductal differentiation in prostate cancer. APMIS 2012; 120: 510-8.
4. Meeks JJ, Zhao LC, Cashy J, Kundu S. Incidence and outcomes of ductal carcinoma of the prostate in the USA: analysis of data from the Surveillance, Epidemiology, and End Results program. BJU Int 2012; 109: 831-4.
5. Tu SM, Lopez A, Leibovici D, *et al*. Ductal adenocarcinoma of the prostate: clinical features and implications after local therapy. Cancer 2009; 115: 2872-80.
6. Statz CM, Patterson SE, Mockus SM. mTOR inhibitors in castration-resistant prostate cancer: a systematic review. Target Oncol 2017; 12: 47-59.
7. Jung WY, Sung CO, Han SH, *et al*. AZGP-1 immunohistochemical marker in prostate cancer: potential predictive marker of biochemical recurrence in post radical prostatectomy specimens. Appl Immunohistochem Mol Morphol 2014; 22: 652-7.
8. Edge SB, Compton CC. The American Joint Committee on Cancer: the 7th edition of the AJCC cancer staging manual and the future of TNM. Ann Surg Oncol 2010; 17: 1471-4.
9. Bostwick DG, Kindrachuk RW, Rouse RV. Prostatic adenocarcinoma with endometrioid features: clinical, pathologic, and ultrastructural findings. Am J Surg Pathol 1985; 9: 595-609.
10. Ro JY, Ayala AG, Wishnow KI, Ordóñez NG. Prostatic duct adenocarcinoma with endometrioid features: immunohistochemical and electron microscopic study. Semin Diagn Pathol 1988; 5: 301-11.
11. Gong Y, Caraway N, Stewart J, Staerkel G. Metastatic ductal adenocarcinoma of the prostate: cytologic features and clinical findings. Am J Clin Pathol 2006; 126: 302-9.
12. Leite KR, Mitteldorf CA, Srougi M, *et al*. Cdx2, cytokeratin 20, thyroid transcription factor 1, and prostate-specific antigen expression in unusual subtypes of prostate cancer. Ann Diagn Pathol 2008; 12: 260-6.
13. Copeland JN, Amin MB, Humphrey PA, Tamboli P, Ro JY, Gal AA. The morphologic spectrum of metastatic prostatic adenocarcinoma to the lung: special emphasis on histologic features overlapping with other pulmonary neoplasms. Am J Clin Pathol 2002; 117: 552-7.
14. Oxley JD, Abbott CD, Gillatt DA, MacIver AG. Ductal carcinomas of the prostate: a clinicopathological and immunohistochemical

study. Br J Urol 1998; 81: 109-15.
15. Lee SS. Endometrioid adenocarcinoma of the prostate: a clinicopathologic and immunohistochemical study. J Surg Oncol 1994; 55: 235-8.
16. Millar EK, Sharma NK, Lessells AM. Ductal (endometrioid) adenocarcinoma of the prostate: a clinicopathological study of 16 cases. Histopathology 1996; 29: 11-9.
17. Tulunay O, Orhan D, Baltaci S, Gögüş C, Müftüoglu YZ. Prostatic ductal adenocarcinoma showing Bcl-2 expression. Int J Urol 2004; 11: 805-8.
18. Seipel AH, Samaratunga H, Delahunt B, Wiklund P, Clements M, Egevad L. Immunohistochemistry of ductal adenocarcinoma of the prostate and adenocarcinomas of non-prostatic origin: a comparative study. APMIS 2016; 124: 263-70.
19. Sanati S, Watson MA, Salavaggione AL, Humphrey PA. Gene expression profiles of ductal versus acinar adenocarcinoma of the prostate. Mod Pathol 2009; 22: 1273-9.
20. Ruizeveld de Winter JA, Janssen PJ, Sleddens HM, *et al*. Androgen receptor status in localized and locally progressive hormone refractory human prostate cancer. Am J Pathol 1994; 144: 735-46.
21. Henshall SM, Quinn DI, Lee CS, *et al*. Altered expression of androgen receptor in the malignant epithelium and adjacent stroma is associated with early relapse in prostate cancer. Cancer Res 2001; 61: 423-7.
22. Schlomm T, Iwers L, Kirstein P, *et al*. Clinical significance of p53 alterations in surgically treated prostate cancers. Mod Pathol 2008; 21: 1371-8.
23. Lee K, Chae JY, Kwak C, Ku JH, Moon KC. *TMPRSS2-ERG* gene fusion and clinicopathologic characteristics of Korean prostate cancer patients. Urology 2010; 76: 1268.e7-13.
24. Epstein JI, Egevad L, Humphrey PA, Montironi R, Members of the IIiDUPG. Best practices recommendations in the application of immunohistochemistry in the prostate: report from the International Society of Urologic Pathology consensus conference. Am J Surg Pathol 2014; 38: e6-19.
25. Berner A, Harvei S, Tretli S, Fosså SD, Nesland JM. Prostatic carcinoma: a multivariate analysis of prognostic factors. Br J Cancer 1994; 69: 924-30.
26. Morais CL, Herawi M, Toubaji A, *et al*. PTEN loss and ERG protein expression are infrequent in prostatic ductal adenocarcinomas and concurrent acinar carcinomas. Prostate 2015; 75: 1610-9.
27. Suh JH, Park JW, Lee C, Moon KC. ERG immunohistochemistry and clinicopathologic characteristics in Korean prostate adenocarcinoma patients. Korean J Pathol 2012; 46: 423-8.
28. Bachmann IM, Halvorsen OJ, Collett K, *et al*. EZH2 expression is associated with high proliferation rate and aggressive tumor subgroups in cutaneous melanoma and cancers of the endometrium, prostate, and breast. J Clin Oncol 2006; 24: 268-73.
29. van Leenders GJ, Dukers D, Hessels D, *et al*. Polycomb-group oncogenes EZH2, BMI1, and RING1 are overexpressed in prostate cancer with adverse pathologic and clinical features. Eur Urol 2007; 52: 455-63.
30. Laplante M, Sabatini DM. mTOR signaling in growth control and disease. Cell 2012; 149: 274-93.
31. Xu K, Liu P, Wei W. mTOR signaling in tumorigenesis. Biochim Biophys Acta 2014; 1846: 638-54.
32. Giannico GA, Arnold SA, Gellert LL, New and emerging diagnostic and prognostic immunohistochemical biomarkers in prostate pathology. Adv Anat Pathol 2017; 24: 35-44.
33. Sabatini DM. mTOR and cancer: insights into a complex relationship. Nat Rev Cancer 2006; 6: 729-34.
34. Morrison DK. The 14-3-3 proteins: integrators of diverse signaling cues that impact cell fate and cancer development. Trends Cell Biol 2009; 19: 16-23.
35. Templeton AJ, Dutoit V, Cathomas R, *et al*. Phase 2 trial of single-agent everolimus in chemotherapy-naive patients with castration-resistant prostate cancer (SAKK 08/08). Eur Urol 2013; 64: 150-8.
36. Vaishampayan U, Shevrin D, Stein M, *et al*. Phase II trial of carboplatin, everolimus, and prednisone in metastatic castration-resistant prostate cancer pretreated with docetaxel chemotherapy: a prostate cancer clinical trial consortium study. Urology 2015; 86: 1206-11.

Journal of Pathology and Translational Medicine 2017; 51: 482-487
https://doi.org/10.4132/jptm.2017.07.11

■ ORIGINAL ARTICLE ■

Acid-Fastness of *Histoplasma* in Surgical Pathology Practice

Madhu Rajeshwari · Immaculata Xess[1]
Mehar Chand Sharma · Deepali Jain

Departments of Pathology and [1]Microbiology, All India Institute of Medical Sciences, New Delhi, India

Received: May 10, 2017
Revised: June 27, 2017
Accepted: July 11, 2017

Corresponding Author
Deepali Jain, MD, DNB, FIAC
Department of Pathology, All India Institute of Medical Sciences, Ansari Nagar, New Delhi 110029, India
Tel: +91-9868895112
Fax: +91-11-26588663
E-mail: deepalijain76@gmail.com

Background: Histoplasmosis (HP) is diagnosed by visualizing intracellular microorganisms in biopsy and/or culture. Periodic-acid Schiff (PAS) and Gomori methenamine silver (GMS) staining methods are routinely used for identification. The acid-fast property of *Histoplasma* was identified decades ago, but acid-fast staining has not been practiced in current surgical pathology. Awareness of the acid-fast property of *Histoplasma*, which is due to mycolic acid in the cell wall, is important in distinguishing *Histoplasma* from other infective microorganisms. Here, we examined acid-fastness in previously diagnosed cases of *Histoplasma* using the Ziehl-Neelsen (ZN) stain and correlated those findings with other known fungal stains. **Methods:** All cases diagnosed as HP were retrieved and reviewed along with ZN staining and other fungal stains. We also stained cases diagnosed with *Cryptococcus* and *Leishmania* as controls for comparison. **Results:** A total of 54 patients ranging in age from 11 to 69 years were examined. The most common sites of infection were the skin, adrenal tissue, and respiratory tract. Of the total 43 tissue samples, 20 (46.5%) stained positive with the ZN stain. In viable cases, a significant proportion of microorganisms were positive while necrotic cases showed only rare ZN-positive yeasts. In comparison to PAS and GMS stains, there was a low burden of ZN-positive yeasts. *Cryptococcus* showed characteristic ZN staining and all cases of *Leishmania* were negative. **Conclusions:** Although the morphology of fungal organisms is the foundation of identification, surgical pathologists should be aware of the acid-fast property of fungi, particularly when there is the potential for confusion with other infective organisms.

Key Words: *Histoplasma*; Acid fast; Ziehl-Neelsen; Fungal organisms

Histoplasmosis (HP) is a major systemic fungal infection caused by two varieties of *Histoplasma*. *H. capsulatum* var. *capsulatum*, which causes the classic form of the disease, and var. *duboisii*, which causes African HP.[1] Despite the availability of serological and molecular tests, the gold standard for the diagnosis of the majority of fungal infections is demonstration of the organisms, either in tissue sections/aspirate smears, or by culture.[2] However, fungal culture is time consuming (a minimum of 15 days for *Histoplasma*) and the materials for culture may not be available in all cases.[2] Hence, histochemical staining for fungi can play a pivotal role in the timely diagnosis of fungal infections.

Gomori methenamine silver (GMS) and periodic-acid Schiff (PAS) are the two most commonly used broad-spectrum fungal stains in routine histopathology practice. These stains help to distinguish fungi based on morphologic characteristics such as size, type of budding, presence of hyphae, and branching. *Histoplasma* are characterized as 2–4 μm in size with round to oval uninucleate yeast cells that may show narrow-based budding. A clear space or artifactual halo may be apparent around the microorganisms due to retraction of the basophilic fungal cell cytoplasm from the poorly stained cell wall. They are usually intracellular, clustered within the histiocytes. Nonetheless, other yeast forms of similar size may be difficult to discriminate from one another. *Histoplasma* may be confused with capsule deficient *Cryptococcus neoformans*, *Candida glabrata*, *Leishmania donovani*, *Penicillium marneffei*, *Sporothrix schenckii*, the small form of *Blastomyces dermatitidis* and endospores of *Coccidioides* spp.[3]

Narrow spectrum fungal stains can help to solve the differentiation and identification problem of yeasts, the most well known being the mucicarmine stain, Alcian Blue and Fontana-Masson stains for *Cryptococcus*, and Congo red for *Blastomyces*.[4] The Ziehl-Neelsen (ZN) stain, commonly used to identify the mycobacteria, is a less known narrow spectrum fungal stain. Although the acid-fast property of *Histoplasma* was identified decades ago, it has never been used routinely for the diagnosis of HP. We propose that ZN staining can be used for the identification of fungal organisms, especially *Histoplasma*. Here, we aimed to examine acid-fastness in previously diagnosed cases of *Histoplasma* by ZN staining and the results were compared with PAS and GMS stains. We also stained 10 cases each of *Leishmania* and *Cryptococcus* infection,

pISSN 2383-7837
eISSN 2383-7845

the two most common morphologic mimickers, as controls for the ZN stain.

MATERIALS AND METHODS

All cases of HP diagnosed between 2010 and 2016 were retrieved from the Department of Pathology archives. The study was approved by the Institutional Ethics Committee (No. IEC-564/2.12.2016) and performed in accordance with the principles of the Declaration of Helsinki. Written informed consents were obtained. Hematoxylin and eosin, PAS, and GMS stained slides were reviewed and diagnosis reconfirmed. Cases with adequate tissue in paraffin blocks were selected and a modified ZN staining procedure was performed by the Kinyoun method. The acid-fastness of fungi was characterized in the ZN stains in all the cases.

The modified ZN staining procedure (Kinyoun method) was performed as follows. Paraffin-embedded sections were deparaffinized with xylene, rehydrated with graded concentrations of alcohol, and brought to water. The slides were flooded with carbol fuchsin for 30 minutes, washed, and then decolorized with 1% acid alcohol. The slides were then counterstained with 1% methylene blue. The number of ZN-positive yeasts was counted per 100 identified yeast cells. For comparison, ZN staining was performed in selected cases diagnosed as cryptococcosis (n = 10) and leishmaniasis (n = 10) and the results were compared with cases of HP. There were no cases of coccidioidomycosis or blastomycosis in our archive for comparison.

RESULTS

There were a total of 66 tissue samples from 54 patients diagnosed with HP during the study period. Adequate tissue for ZN staining was available only in 43 samples from 37 patients. Patients (33 men, four women) had an age range of 11 to 69 years. All of the specimens were from biopsies except for one case of intestinal resection. Culture/serology details were available in 18 cases, of which eight (44%) were positive. For rest of the cases, morphology was taken as the gold standard method of diagnosis. Immune status was known in 31 cases, of which 11 (35.5%) were immunocompromised with human immunodeficiency virus (HIV) infection and diabetes as the most common causes of immunosuppression. The most common sample site was the skin (37%) followed by adrenal tissue (23%) and the respiratory tract (11.6%, Table 1). Apart from the lungs, there was involvement of the nasopharynx, vocal cords, and trachea in one case each. Miscellaneous sites of involvement included bone marrow (n = 3), buccal mucosa (n = 1), tongue (n = 1), orbit (n = 1), lymph node (n = 1), ileum (n = 1), and retroperitoneum (n = 1). Fever, weight loss, pancytopenia and molluscum-like papules were common clinical presentations. Some of the rare presentations included subacute intestinal obstruction with ileal perforation, ulcerative lesion in the tongue mimicking a vesiculobullous lesion, tumor-like growth in the trachea and nasopharyngeal involvement in one case each. Twelve cases had disseminated disease (32.4%), four of which had more than one tissue sample available. Adrenal, skin, and bone marrow involvement were common in these disseminated cases. Two of the patients with disseminated HP were immunosuppressed (HIV-positive). Both of these cases had a rapid clinical course, which was fatal in one case.

Table 1. Summary of clinical details of all patients

Parameter	No.
Total No. of HP samples diagnosed during study period	66
ZN stain	43 (37 patients)
Sex, n (%)	
Males	33 (89.2)
Females	4 (10.8)
Age (yr)	11–69
Sites (%)	
Skin	37
Adrenal	23
Lung and respiratory tract	11.6
Others	28.4
Disseminated cases (%)	32.4
Immunocompromised state (%)	35.5
Culture/Serology positivity (%)	44
ZN positivity (%)	46.5
Culture positive cases that showed ZN positivity, n (%)	4/8 (50)

HP, histoplasmosis; ZN, Ziehl-Neelsen.

Of the 43 samples, 20 (46.5%) stained positive with the ZN procedure. The number of yeasts that showed positivity varied from less than 1% to 20% (Fig. 1A–D). Among the eight culture and serology positive cases, four exhibited ZN-positive staining. On morphology, four cases showed entirely necrotic tissue. In comparison to the entirely necrotic cases, viable cases showed more ZN-positive microorganisms. Out of the four necrotic cases, only one case showed ZN-positive yeasts. In comparison to PAS and GMS stains, ZN-positive yeasts were low in burden (Figs. 2A–C, 3A, B).

In contrast to *Histoplasma*, the cryptococcal yeasts displayed a peculiar staining pattern (Fig. 4A, B) where the capsule and cell wall stained a granular magenta to purple color. This pattern of staining could easily be differentiated from the crisp bright pink cytoplasmic staining of *Histoplasma*. Almost all of the yeasts in all of the cases stained uniformly, which made the cells easy to identify

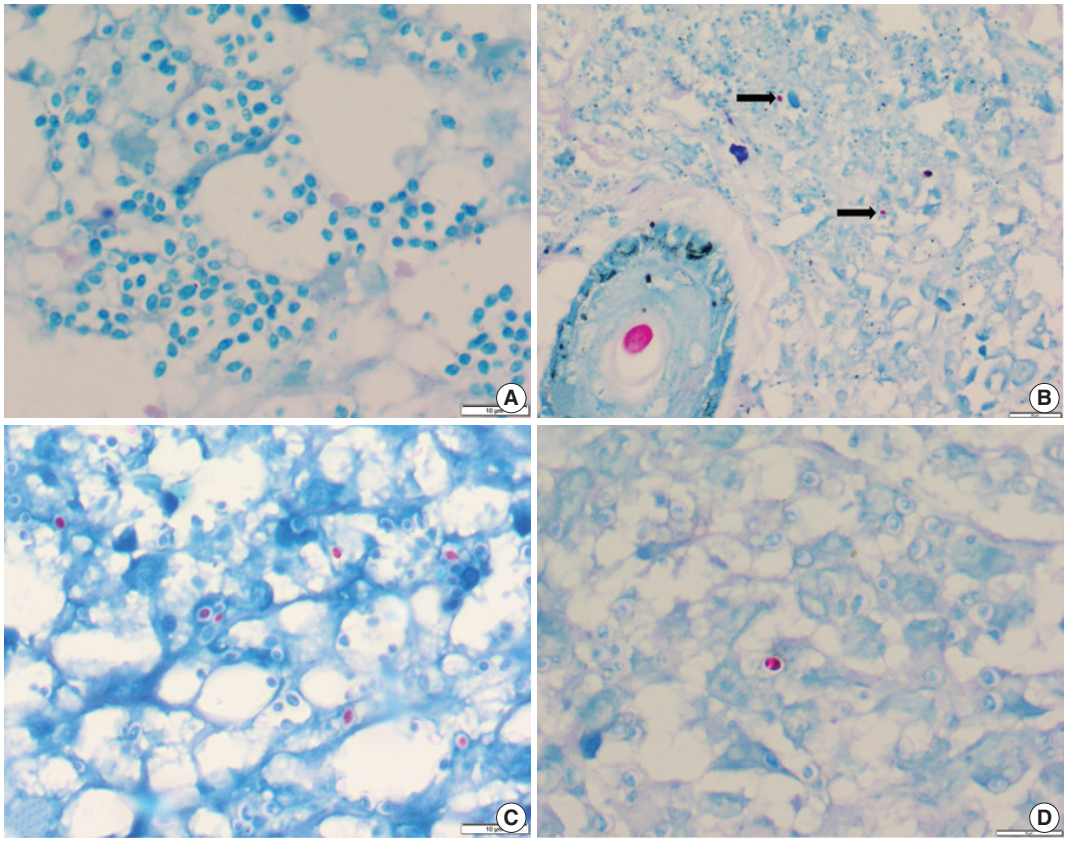

Fig. 1. (A) Photomicrograph of a histoplasmosis case showing Ziehl-Neelsen (ZN)-negative yeasts. (B) Skin biopsy showing ZN-positive *Histoplasma* yeast cells (arrows); ZN-positive hair shaft in a hair follicle is shown for color comparison. (C, D) Two different cases show numerous to few ZN-positive yeast cells.

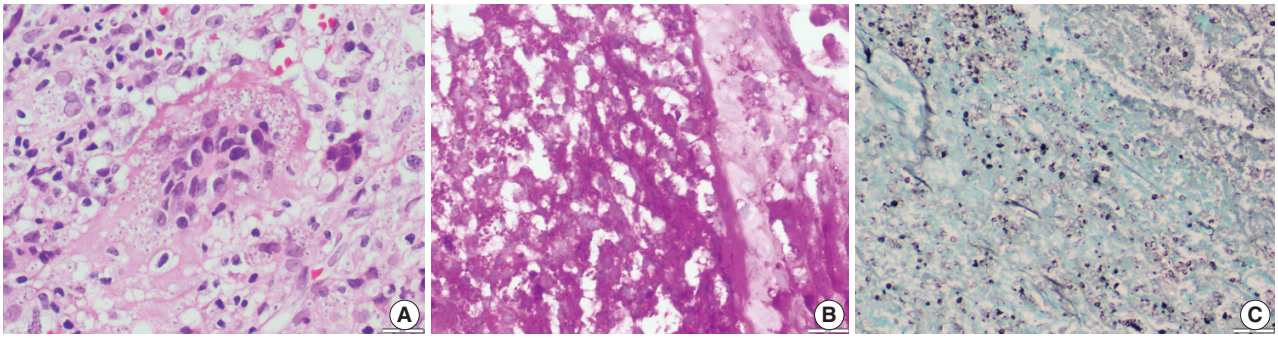

Fig. 2. (A) Photomicrograph shows numerous extracellular and intracellular *Histoplasma* yeast cells present within a giant cell. *Histoplasma* are round to oval in shape with an eccentric purple dot or crescent. (B, C) Periodic-acid Schiff and Gomori methenamine silver stains highlight fungal profiles.

even under low power objective microscopy. None of the cases of leishmaniasis showed positivity for ZN staining.

DISCUSSION

HP, initially thought to be endemic in the Eastern USA and Latin America, is being increasingly recognized in Asian countries like India with the majority of cases being reported from Eastern and North-Eastern regions.[1] A total of 38 cases were reported from India until 1996.[5] Another series from India reported 24 cases during a span of 10 years.[6] Because our hospital is a tertiary institute, we recorded 54 cases in six years, making it the largest

https://doi.org/10.4132/jptm.2017.07.11

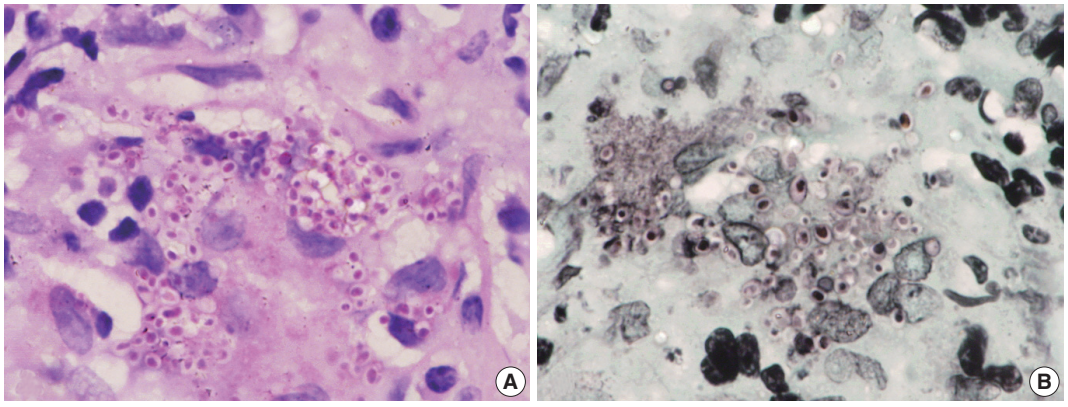

Fig. 3. Oil immersion magnification of periodic-acid Schiff (A) and Gomori methenamine silver (B) *Histoplasma* stains.

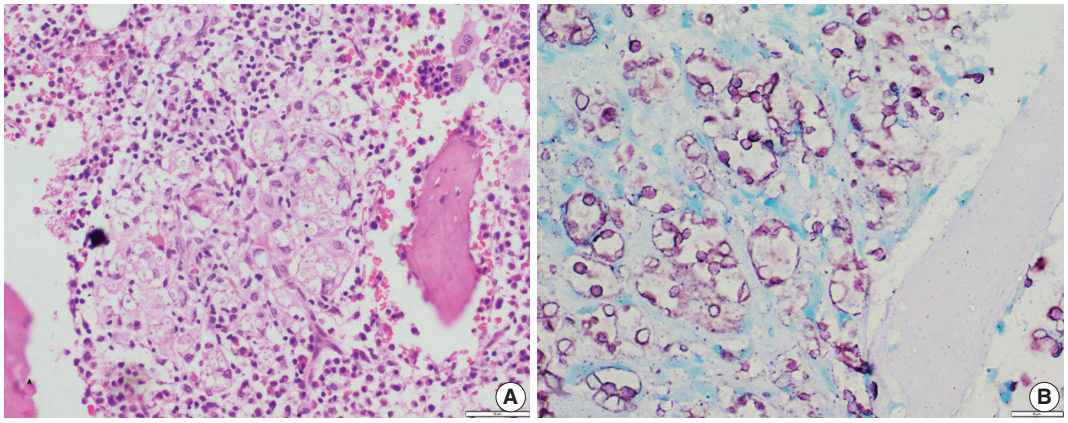

Fig. 4. (A) A case of cryptococcal infection involving bone marrow shows numerous fungal organisms that are round in shape and surrounded by a clear space. (B) Ziehl-Neelsen staining highlights all cryptococci and surrounding capsular halos with magenta color.

Table 2. Morphological mimics of *Histoplasma*

Morphological mimic	Differentiating feature(s)
Capsule deficient *Cryptococcus*	Size variation, weak positivity for mucin stains and positivity for FM stain; acid fast (present study)
Leishmania	Presence of kinetoplast
Small variant of *Blastomyces*	Broad-based budding
Candida albicans	Presence of pseudohyphae
Candida glabrata	More size variability, neutrophilic reaction
Penicillium marneffei	Presence of transverse septum
Endospores of *Coccidioides*	Presence of intact/ruptured spherules
Histoplasma	Round to oval intracellular yeasts with narrow based budding and surrounded by a halo, acid-fast ZN positive

FM, Fontana Masson; ZN, Ziehl-Neelsen.

series of HP from the Indian subcontinent. This large increase in cases indicates that the incidence of HP is increasing in India in recent times. HP is no longer a disease of immunocompromised patients;[7] in our series, only one-third of the patients had a known risk factor.

Classic diagnostic methods include microscopy, culture, antigen detection by enzyme immunoassay, antibody detection by complement fixation and immunodiffusion, and polymerase chain reaction assays.[7] The gold standard methods for the diagnosis of HP includes the demonstration of yeasts on microscopy and isolation of the mold by culture.[7,8] Although culture of the organism should always be sought and attempted, it is most effective only in cases of high fungal burden with chronic or disseminated forms of HP and culturing is often insensitive in sub-acute, acute, and mild forms of HP.[2] Time constraints for culture combined with a lack of specificity and sensitivity make histopatho-

logical examination an easy, rapid, and reliable diagnostic method.[9] We have used morphology as the gold standard for the diagnosis of HP where cultures were negative or unavailable. *Histoplasma* are characterized as 2–4 μm in size with round to oval uninucleate cells that are usually surrounded by a halo. However, many similar sized yeast varieties may be difficult to differentiate from *Histoplasma* (Table 2).

Parsons and Zarafonetis[10] first observed acid-fastness in *Histoplasma* as early as 1945, even before the discovery of GMS. Rawson[11] also found that the acid-fast property could be advantageously used to search for *Histoplasma*. Although acid-fastness of *Histoplasma* came to light decades ago, its utility in routine diagnostic practice has not been explored. In our study, nearly 46.5% of the samples were positive for ZN staining. The number of yeasts that were acid-fast varied from less than 1% to 20%. This is consistent with the one previous study available, where the authors noted that 47% of *Histoplasma* cases were acid-fast.[12] Similarly, only a few to one-third of yeast forms showed this property in their study as well as our previous reported case included in this series.[12,13] Until now, none of the fungi other than *Histoplasma* and *Blastomyces* were known to be acid-fast, and this property can be used to advantage in severely necrotic cases where the yeast forms may be scant and may be erroneously diagnosed as other common diseases like tuberculosis (TB). This is especially important in TB endemic countries such as India where we receive most of the cases of TB in routine practice and ZN staining is commonly performed for the diagnosis of TB. Therefore, knowledge about the ZN positivity of *Histoplasma* may be beneficial in recognizing yeast forms in necrotic cases of HP.

Acid-fast microorganisms are characterized by wax-like, nearly impermeable cell walls that contain mycolic acid and large amounts of fatty acids and complex lipids. Treatment with hot hydrochloric acid abolishes the acid-fastness of *Histoplasma*, suggesting that this property of *Histoplasma* is likely due to the presence of mycolic acid in the cell wall. However, *Blastomyces* resist this decolorization, signifying that fatty acids other than mycolic acid are responsible for acid-fastness.[12] We use a modified ZN stain in our laboratory for the diagnosis of TB and leprosy in routine services where the concentration of phenol (mordent) in carbol fuchsin was increased from 5% to 8%, which contributes to better stain penetration.

The acid-fastness of *Histoplasma* could not be demonstrated in cytology smears in our previous study.[14] Instead, *Histoplasma* yeasts were identified easily against the pale background of ZN stain in necrotic cases. However, the case numbers were too small to draw any conclusions and more studies are needed on aspirate smears. We have also observed the peculiar pattern of positivity of cryptococcal yeasts with the ZN stain. To the best of our knowledge, this finding has not been reported previously. In contrast to *Histoplasma*, almost all of the yeasts showed uniform positivity, making it one of the most sensitive and specific stains for the identification of cryptococci. Since the pattern of ZN positivity is different, this feature might also help to differentiate *Cryptococcus* and *Histoplasma* in combined infections, which is relatively common in immunosuppressed hosts. Endospores of *Coccidioides* resemble those of *Histoplasma*; however, we do not see *Coccidioides* in India so the comparison could not be made in this study.

In conclusion, this study is one of the largest series of HP where the acid-fastness of *Histoplasma* was evaluated. A comparative analysis of *Cryptococcus* and *Leishmania* revealed a different pattern of acid-fastness. Although morphology is the basis of fungal identification, a simple ZN stain may be included in the diagnostic armamentarium for fungal infections in surgical pathology. Although every organism is not acid-fast within a single case, approximately half of HP cases are positive on ZN staining. The difference in ZN positivity staining pattern between *Histoplasma* and *Cryptococcus* may serve as a useful distinguishing feature. Surgical pathologists should be aware of the acid-fast property of fungal organisms, which will be helpful in the correct identification of the microorganism and ultimately patient management in morphologically-challenging HP cases.

Conflicts of Interest

No potential conflict of interest relevant to this article was reported.

Acknowledgments

The abstract of the same work has been accepted for presentation in 2017 USCAP Annual Meeting; 4–10 Mar 2017; San Antonio, TX, USA.

REFERENCES

1. Antinori S. *Histoplasma capsulatum*: more widespread than previously thought. Am J Trop Med Hyg 2014; 90: 982-3.
2. Guimarães AJ, Nosanchuk JD, Zancopé-Oliveira RM. Diagnosis of histoplasmosis. Braz J Microbiol 2006; 37: 1-13.
3. Guarner J, Brandt ME. Histopathologic diagnosis of fungal infections in the 21st century. Clin Microbiol Rev 2011; 24: 247-80.
4. Youngberg GA, Wallen ED, Giorgadze TA. Narrow-spectrum histo-

chemical staining of fungi. Arch Pathol Lab Med 2003; 127: 1529-30.
5. Goswami RP, Pramanik N, Banerjee D, Raza MM, Guha SK, Maiti PK. Histoplasmosis in eastern India: the tip of the iceberg? Trans R Soc Trop Med Hyg 1999; 93: 540-2.
6. Gopalakrishnan R, Nambi PS, Ramasubramanian V, Abdul Ghafur K, Parameswaran A. Histoplasmosis in India: truly uncommon or uncommonly recognised? J Assoc Physicians India 2012; 60: 25-8.
7. Kauffman CA. Histoplasmosis: a clinical and laboratory update. Clin Microbiol Rev 2007; 20: 115-32.
8. Azar MM, Hage CA. Laboratory diagnostics for histoplasmosis. J Clin Microbiol 2017; 55: 1612-20.
9. Joseph Wheat L. Current diagnosis of histoplasmosis. Trends Microbiol 2003; 11: 488-94.
10. Parsons RJ, Zarafonetis CJ. Histoplasmosis in man: report of seven cases and review of 71 cases. Arch Intern Med 1945; 75: 1-23.
11. Rawson AJ. Acid-fast property of Histoplasma capsulatum. Am J Clin Pathol 1948; 18: 97.
12. Wages DS, Wear DJ. Acid-fastness of fungi in blastomycosis and histoplasmosis. Arch Pathol Lab Med 1982; 106: 440-1.
13. Jain D. Acid fast property of histoplasma: a concept revitalized. Int J Surg Pathol 2016; 24: 724-5.
14. Ranjan R, Jain D, Singh L, Iyer VK, Sharma MC, Mathur SR. Differentiation of histoplasma and cryptococcus in cytology smears: a diagnostic dilemma in severely necrotic cases. Cytopathology 2015; 26: 244-9.

Journal of Pathology and Translational Medicine 2017; 51: 488-498
https://doi.org/10.4132/jptm.2017.07.20

■ ORIGINAL ARTICLE ■

Placental Lesions in Meconium Aspiration Syndrome

Binnari Kim[1] · Soo-young Oh[2]
Jung-Sun Kim[1,3]

Departments of [1]Pathology and Translational Genomics and [2]Obstetrics and Gynecology, Samsung Medical Center, Sungkyunkwan University School of Medicine, Seoul; [3]Department of Health Sciences and Technology, Sungkyunkwan University, SAIHST, Seoul, Korea

Received: May 17, 2017
Revised: July 10, 2017
Accepted: July 20, 2017

Corresponding Author
Jung-Sun Kim, MD, PhD
Department of Pathology and Translational Genomics, Samsung Medical Center, Sungkyunkwan University School of Medicine, 81 Irwon-ro, Gangnam-gu, Seoul 06351, Korea
Tel: +82-2-3410-2767
Fax: +82-2-3410-0025
E-mail: jsunkim@skku.edu

Background: Meconium aspiration syndrome (MAS) is defined by respiratory distress requiring supplemental oxygen in a meconium-stained neonate. MAS is clinically subclassified as mild, moderate, and severe according to the oxygen requirement. The aims of this study were to compare the histological findings in the placentas of MAS neonates with those of meconium-stained but non-MAS neonates and to analyze the correlation between the severity of MAS and the grade of its histological parameters. **Methods:** We collected 160 singleton term placentas from neonates with meconium staining at birth from a tertiary medical center, Seoul, Republic of Korea. We reviewed hematoxylin and eosin sections of tissue samples (full-thickness placental disc, chorioamniotic membranes, and umbilical cord). **Results:** Funisitis was present more frequently in MAS than in non-MAS ($p < .01$), of which the stage was correlated with the severity of MAS ($p < .001$). The histological findings consistent with maternal underperfusion and chronic deciduitis were more frequent in MAS than in non-MAS ($p < .05$). There was a correlation between the degree of chorionic vascular muscle necrosis and the severity of MAS ($p < .05$). **Conclusions:** Our results suggest that fetal inflammatory response evidenced by funisitis occurs prenatally in MAS and that the stage of funisitis and of chorionic vascular muscle necrosis may be a predictive marker of the severity of MAS.

Key Words: Placenta; Meconium; Meconium aspiration syndrome; Chorioamnionitis; Chorionic vascular muscle necrosis

Meconium-stained neonates are quite common, accounting for about 10% to 16% of term pregnancies, in which a minority of cases suffer from respiratory distress requiring supplemental oxygen.[1-4] These cases are called meconium aspiration syndrome (MAS), occurring in 2% to 36% of meconium-stained neonates.[5,6] MAS is clinically subclassified as mild, moderate, and severe, according to the degree of respiratory distress and treatment requirements. In the past, the whole spectrum of MAS was considered as a group of diseases caused by meconium aspiration, but more recently it is understood that severe MAS is pathophysiologically different from mild and moderate MAS.[5,7] The time and amount of meconium exposure are not correlated to the severity of MAS.[8,9] The risk factors of severe MAS do not show a linear extension with those of mild and moderate MAS.[7] Moreover, the histologic and physiologic changes in severe MAS cases cannot be explained by aspiration of meconium per se.[10,11] Rather, it is proposed that severe MAS results from chronic asphyxia or infection accompanying meconium passage and lung damage.[5]

The placenta is an organ that connects the fetus to the uterus of the mother, thus providing the fetus with a safe environment rendering gas exchange and waste elimination. In a sense, the placenta is a unique organ that mirrors the status of a fetus and mother during pregnancy. For example, when the placental membranes are ruptured and amniotic fluid infection occurs, the placenta shows acute chorioamnionitis (as the maternal inflammatory response) and funisitis (as the fetal inflammatory response).[12] When the placenta does not carry adequate oxygen and nutrition for the fetus due to maternal underperfusion such as preeclampsia, the placental villi show increased syncytial knots, villous agglutination, intervillous fibrin, and distal villous hypoplasia, while maternal vessels in the decidua disclose atherosis or mural hypertrophy of the arterioles.[13] In contrast, the vascular thrombo-occlusion of a fetal origin is evidenced by avascular villi and villous stromal-vascular karyorrhexis accompanied by thrombus or intimal fibrin cushion of fetal vessels in the placenta.[14] Meanwhile, meconium-laden macrophages in the placenta are usually considered to be indicators of the meconium passage *in utero*.[15] In addition, acute chorioamnionitis, funisitis, chorionic vascular muscle necrosis, and amnion degeneration are accompanied by meconium exposure.[16,17]

MAS is one of the significant causes of neonatal respiratory

pISSN 2383-7837
eISSN 2383-7845

distress leading to various morbidities and mortality.[18,19] It is critical to know the risk factors of MAS, especially the severe one, as soon as possible before and/or after birth to manage a neonate predisposed to MAS. In order to find histopathological findings in the placenta to predict the occurrence and severity of MAS, we evaluated the histopathological findings in placentas from the MAS neonates, compared them with those from the meconium-stained but non-MAS neonates, and analyzed any correlation between the severity of MAS and the grade of the histological parameters.

MATERIALS AND METHODS

Among singleton term neonates with meconium staining at birth (n = 835) from all live deliveries (n = 16,264) in our institution from January 2006 to June 2014, a total of 160 cases whose placentas were available for histological examination were included in this retrospective study. The study was approved as a retrospective study without informed consent by the institutional review board of the hospital (2011-07-063). Multiple gestation, fetal deaths *in utero*, or other major anomalies were excluded. Clinical characteristics of the study population were reviewed in three categories: (1) maternal factors (age, parity, gestational age at delivery, mode of delivery); (2) neonatal factors (weight, sex, presence of fetal growth restriction, Apgar score, grade of meconium staining, neonatal intensive care unit admission and duration, arterial blood gas analysis of cord blood); and (3) intrapartum factors (presence of fever [≥ 38°C], rupture of membrane to delivery interval, oligohydramnios, use of labor epidural anesthesia, use of oxytocin, and fetal heart rate patterns). MAS was classified as follows: mild, requiring < 40% oxygen for < 48 hours; moderate, requiring ≥ 40% oxygen for at least 48 hours; or severe, requiring assisted mechanical ventilation for more than 48 hours.[5,6]

The tissue samples (the placental disc in full thickness, a cross section of the umbilical cord, and a roll of the chorioamniotic membranes) were fixed in 10% formalin and embedded in paraffin. The tissue sections stained with hematoxylin and eosin were reviewed by a pathologist who was blind to the clinical information. Placental histologic findings were categorized as those associated with amniotic fluid infection, maternal underperfusion, and fetal vascular obstructive lesions, according to the criteria proposed by the perinatal section of the Society for Pediatric Pathology.[12-14] Chronic placental inflammation such as chronic villitis, chronic chorioamnionitis, and chronic deciduitis were diagnosed according to the criteria reported previously.[14,20,21] Meconium-laden macrophages, amnion degeneration, chorionic vascular muscle necrosis were included as histological findings related to meconium staining (Fig. 1).[15-17] Tables 1 and 2 summarize the histological findings and their grading systems (if included).

For statistical analysis, SPSS Statistics ver. 23 (IBM Corp., Armonk, NY, USA) was used. For evaluation of the significance of clinical variables in MAS, we used chi-square test and Fisher exact test for the proportions and Kruskal-Wallis test and Mann-Whitney U test for the continuous variables. The relationship between histologic findings and MAS was verified by chi-square test and Fisher exact test. For evaluation of the correlation between the grades of histopathologic findings and the severity of MAS, linear-by-linear-association was used. The p-values less than .05 were considered to be statistically significant.

RESULTS

Clinical characteristics of meconium-stained neonates and the rate of MAS

The number of singleton term neonates with meconium staining at birth was 835 (5.13%) among all live neonates (n = 16,264) born in our institution from January 2006 to June 2014. MAS developed in 80 out of 835 (9.58%) term neonates with meconium staining. Placentas were available in 160 meconium-stained neonates; 41 of 80 cases (51%) with MAS; and 119 of 755 cases (15.7%) without MAS. Thirty-three neonates had mild MAS, four had moderate MAS, and four had severe MAS. The clinical factors indicating neonatal morbidity including Apgar score (1 minute) < 4, Apgar score (5 minutes) < 7, severe meconium staining, neonatal intensive care unit admission of long duration, low cord pH, cord base excess, and fetal tachycardia were detected more frequently in MAS group than in no MAS group. The clinical findings of 160 meconium-stained neonates are summarized in Table 3.

Comparison of the histopathologic findings between MAS and non-MAS

Among the findings associated with amniotic fluid infection, acute funisitis was more frequent in MAS than in non-MAS placentas (65.9% [27/41] vs 39.5% [47/119], p < .01). There was no significant difference in the frequency of acute chorioamnionitis between MAS and non-MAS placentas (58.5% [24/41] vs 47.9% [57/119], p > .05). The findings associated with maternal underperfusion were detected more frequently in MAS placentas than in non-MAS placentas (31.7% [13/41] vs 15.1% [18/119], p < .05), but the frequency of the findings associated with fetal vascular thrombo-occlusive disease was not significantly different

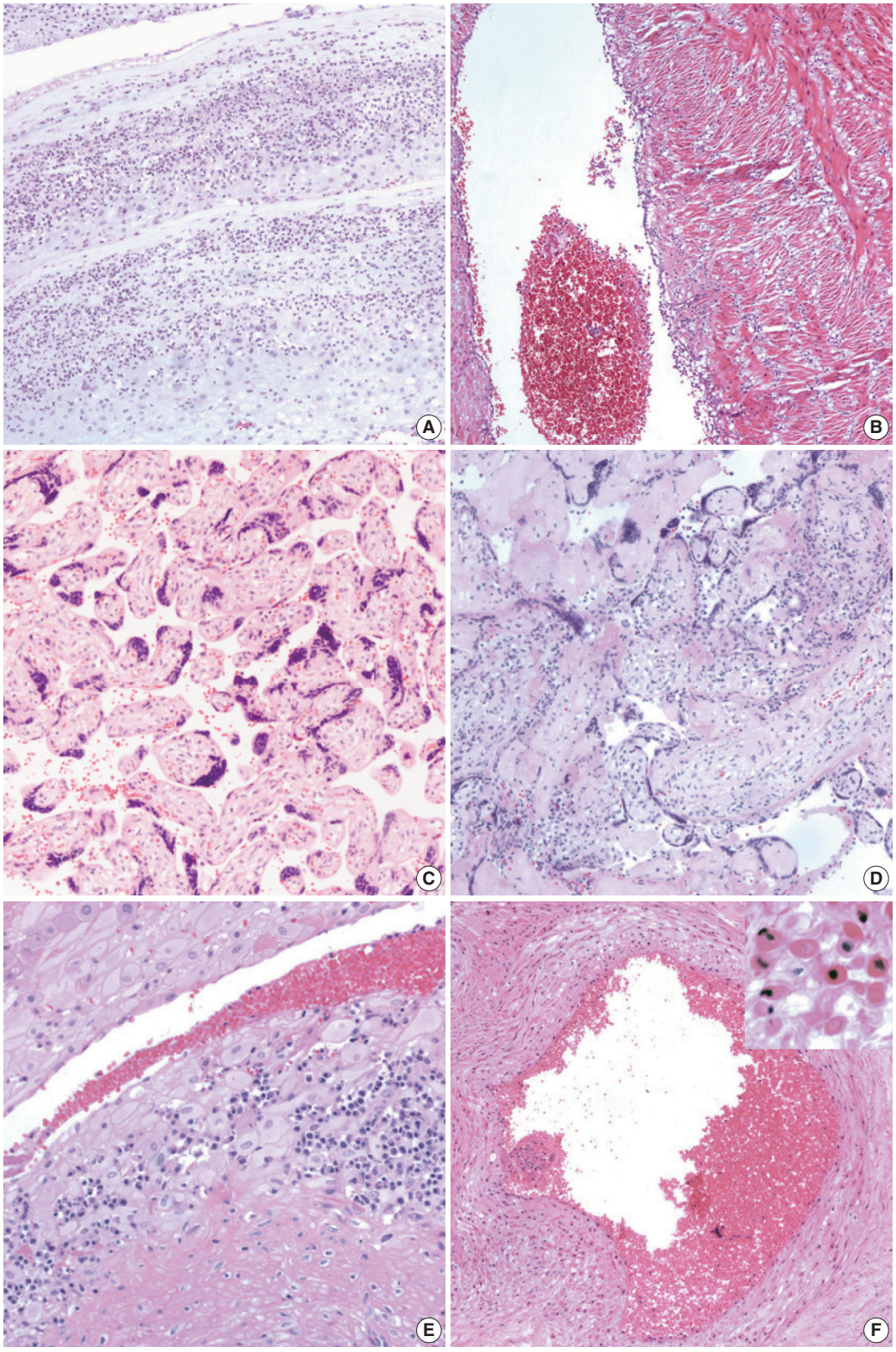

Fig. 1. Representative histological findings of the placenta. (A) Acute chorioamnionitis. (B) Funisitis. (C) Increased syncytial knots. (D) Chronic villitis. (E) Chronic deciduitis. (F) Chorionic vascular muscle necrosis.

https://doi.org/10.4132/jptm.2017.07.20

Table 1. Histologic findings of placentas evaluated in this study

Histologic finding
Findings consistent with amniotic fluid infection
Acute chorioamnionitis
Funisitis
Findings consistent with maternal underperfusion
Remote villous infarct
Recent villous infarct
Increased syncytial knots
Villous agglutination
Increased intervillous fibrin
Distal villous hypoplasia
Persistent muscularization of basal plate arteries
Mural hypertrophy of decidual arterioles
Acute atherosis of basal plate arteries and/or decidual arterioles
Findings consistent with fetal vascular thrombo-occlusive disease
Villous changes (villous stromal-vascular karyorrhexis, hyalinized avascular villi)
Thrombi, large fetal vessels
Intimal fibrin cushions, large fetal vessels
Fibromuscular sclerosis, intermediate-sized fetal vessels
Chronic inflammation
Chronic villitis (VUE) with obliterative fetal vasculopathy
Chronic chorioamnionitis
Chronic deciduitis
Findings associated with meconium staining
Amnion degeneration
Meconium-laden macrophages
Chorionic vascular muscle necrosis

VUE, villitis of unknown etiology.

Table 2. Histologic findings graded according to the severity

	Histologic finding
Acute chorioamnionitis	0: None
	1: Acute subchorionitis or chorionitis
	2: Acute chorioamnionitis
	3: Necrotizing chorioamnionitis or subacute chorioamnionitis
Funisitis	0: None
	1: Umbilical phlebitis or chorionic vasculitis
	2: Umbilical arteritis
	3: Concentric umbilical perivasculitis
Meconium-laden macrophages[a]	0: None
	1: The mean number of 10 fields (×200): <5
	2: The mean number of 10 fields (×200): 5–20
	3: The mean number of 10 fields (×200): >20
Chorionic vascular myonecrosis	0: None
	1: Necrosis of chorionic vessels
	2: Necrosis of umbilical cord vessels
	3: Necrosis of chorionic vessels and umbilical cord vessels
Maternal underperfusion	0: None
	1: One histologic finding of maternal underperfusion
	2: Two or three histologic findings of maternal underperfusion
	3: Four or more histologic findings of maternal underperfusion

[a]Meconium–laden macrophages were counted in membranes, chorionic plate, and umbilical cord respectively, of which the maximum score among these areas was chosen to evaluate the correlation with meconium aspiration syndrome.

between MAS and non-MAS placentas (0% [0/41] vs 7.6% [9/119], $p > .05$). Neither chronic villitis nor chronic chorioamnionitis was not increased in MAS placentas compared to non-MAS placentas (12.2% [5/41] vs 5.9% [7/119], 12.2% [5/41] vs 7.6% [9/119], $p > .05$), whereas chronic deciduitis showed a higher frequency in MAS than in non-MAS cases (7.3% [3/41] vs 0% [0/119], $p < .05$). The frequencies of meconium-laden macrophages, amnion degeneration, and chorionic vascular muscle necrosis were not related to MAS (95.1% [39/41] vs 96.6% [114/118], 91.3% [21/23] vs 97.3% [72/74], and 10.3% [4/39] vs 10.4% [11/106], respectively, $p > .05$) (Fig. 2).

Correlation between the severity of MAS and the grade of the placental histological findings

We analyzed the correlation between the severity of MAS and the grade of pathological findings and found out that the grade of funisitis and that of chorionic vascular muscle necrosis were higher as the severity of MAS increased ($p < .001$ and $p < .05$, respectively). Other parameters including acute chorioamnionitis, maternal underperfusion, and meconium-laden macrophages did not show any significant correlation with the severity of MAS (Fig. 3).

DISCUSSION

This study demonstrated that acute funisitis, histological findings associated with maternal underperfusion, and chronic deciduitis were frequently found in MAS. The grade of funisitis and chorionic vascular muscle necrosis was correlated with the severity of MAS.

Funisitis, which is characterized by the migration of polymorphonuclear leukocytes from the lumen to the wall of the umbilical vessels, was the most significant histological factor associated with MAS.[12] Funisitis is most commonly associated with intraamniotic infection as is acute chorioamnionitis. Acute chorioamnionitis represents a maternal inflammatory response to intraamniotic infection, whereas funisitis is an evidence of a fetal inflammatory response and reflects a systemic fetal inflammatory response syndrome.[22-28] Meconium may induce local inflammation following

tissue degeneration in the fetal membranes (chorioamnionitis) and umbilical cord (funitis) by its leukotactic activity, but it is less severe than that by intraamniotic infection is.[17] Intraamniotic inflammation occurs more frequently in meconium-stained amniotic fluid than in clear amniotic fluid.[29-34] The significant association of funisitis with MAS but not acute chorioamnionitis, in spite of the presence of both acute chorioamnionitis and funisitis in intraamniotic infection/inflammation, suggests that a fetal inflammatory response is crucial to MAS but not a general intraamniotic inflammatory response. It has been proposed that the combination of a local inflammatory response in the lung by meconium and capillary damage/leakage as a manifestation of systemic fetal inflammatory

Table 3. Clinical characteristics in non-MAS and MAS groups

Clinical factor	Non-MAS (n=119)	MAS (n=41)						p-value[d]
		Mild (n=33)	p-value[a]	Moderate (n=4)	p-value[b]	Severe (n=4)	p-value[c]	
Maternal factor								
Age (yr)[e]	32 (25 to 44)	32 (24 to 37)	>.05	34 (28 to 36)	>.05	34 (26 to 36)	>.05	>.05
Gestational age at delivery (wk)[e]	40.2 (37.2 to 41.5)	40.3 (37.3 to 41.6)	>.05	40.7 (39.5 to 41.4)	>.05	39.1 (38.2 to 40.1)	>.05	>.05
Primiparity (%)	88	94	>.05	75	>.05	75	>.05	>.05
Mode of delivery								
Elective C/S (%)	1.7	0	>.05	0	>.05	0	>.05	>.05
Emergency C/S (%)	54.6	42		75		100		
Vaginal (%)	43.7	58		25		0		
Neonatal factor								
Sex (male) (%)	53	60	>.05	75	>.05	50	>.05	>.05
Weight (kg)[e]	3.24 (1.98 to 4.57)	3.04 (1.98 to 4.06)	>.05	3.09 (2.91 to 3.56)	>.05	3.36 (2.6 to 4.4)	>.05	>.05
Growth restriction <10p (%)	22	33	>.05	0	>.05	25	>.05	>.05
Apgar score (1 min) <4 (%)	3.3	45	<.001	25	>.05	50	<.05	<.001
Apgar score (5 min) <7 (%)	0.8	24	<.001	25	>.05	50	<.01	<.001
Grade of meconium staining (%)								
1	39.7	30.2	>.05	0	>.05	25	<.05	<.01
2	21.6	36.4		50		0		
3	27.0	15.2		0		0		
4	11.7	18.2		50		75		
NICU admission (%)	6	90	<.001	100	<.001	100	<.001	<.001
Duration of admission (day)[e]	0 (0 to 6)	5 (0 to 13)	<.001	3.5 (0 to 7)	<.001	11 (8 to 22)	<.001	<.001
Cord pH at birth[e]	7.27 (6.99 to 7.53)	7.12 (6.85 to 7.29)	<.001	7.24 (7.08 to 7.32)	>.05	7.24 (7.02 to 7.41)	>.05	<.001
<7.0 (%)	2.3	26.3	<.001	0	>.05	0	>.05	<.01
<7.1 (%)	6.8	36.8	<.001	33.3	>.05	25.0	>.05	<.001
<7.2 (%)	25.0	63.2	<.001	33.3	>.05	50.0	>.05	<.01
Cord blood base excess at birth[e]	–4.45 (–19.5 to 15)	–10.75 (–3 to –19.9)	<.001	–2.20 (–12.1 to –1.7)	>.05	–6.45 (–15 to –1)	>.05	<.001
Intrapartum factor								
Fever ≥38°C (%)	35	57	>.05	66	>.05	50	>.05	>.05
Rupture of membranes to delivery (min)[e]	316 (0 to 1,400)	339.5 (0 to 1,178)	>.05	368 (0 to 472)	>.05	175.5 (0 to 876)	>.05	>.05
Use of oxytocin (%)	72.5	75	>.05	66	>.05	50	>.05	>.05
Use of epidural anesthesia (%)	81.4	93	>.05	66	>.05	50	>.05	>.05
Oligohydramnios (%)	9	9	>.05	33	>.05	0	>.05	>.05
Fetal tachycardia (%)	29	60	<.05	33	>.05	50	>.05	<.05
Fetal bradycardia (%)	1	0	>.05	0	>.05	25	>.05	>.05
Minimal fetal heart rate variability (%)	46	70	>.05	33	>.05	75	>.05	>.05

MAS, meconium aspiration syndrome; C/S, cesarean section; NICU, neonatal intensive care unit.
[a]Non-MAS vs mild MAS; [b]Non-MAS vs moderate MAS; [c]Non-MAS vs severe MAS; [d]Non-MAS vs mild MAS vs moderate MAS vs severe MAS; [e]Median (range).

https://doi.org/10.4132/jptm.2017.07.20

response explains the pathogenesis of MAS.[19] Upregulation of adhesion molecules in the umbilical cord was observed in the presence of funisitis, which was thought to result in increased concentrations of cytokines and soluble adhesion molecules in the fetal circulation. Activation of endothelium may affect not only the umbilical cord but also other fetal organs.[25] Funisitis is associated with adverse neonatal outcome including an Apgar score < 7 at 1 minute, small for gestational age and the rate of admission to

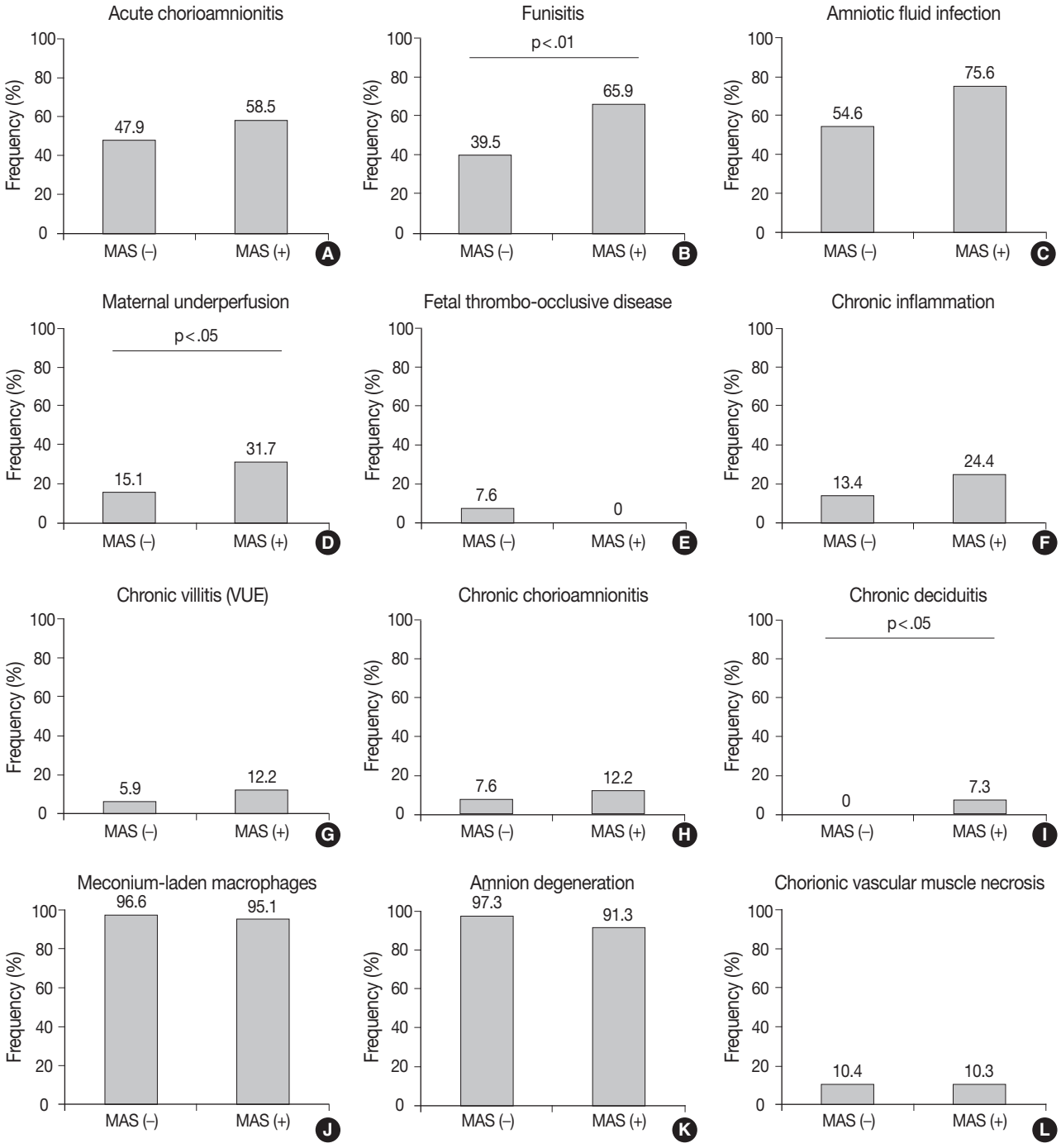

Fig. 2. Comparison of the frequencies of histological findings in the placentas between meconium aspiration syndrome (MAS) and non-MAS placentas. (A) Acute chorioamnionitis. (B) Funisitis. (C) Amniotic fluid infection. (D) Maternal underperfusion. (E) Fetal thrombo-occlusive disease. (F) Chronic inflammation. (G) Chronic villitis. (H) Chronic chorioamnionitis. (I) Chronic deciduitis. (J) Meconium-laden macrophages. (K) Amnion degeneration. (L) Chorionic vascular necrosis. VUE, villitis of unknown etiology.

the neonatal intensive care unit. It is also related to various clinical diseases such as chronic lung disease, intracranial hemorrhage, cerebral palsy, and negative long-term neurologic outcome.[25,35-45] The significant relationship of funisitis with MAS was supported by previous studies, but our study is the first to demonstrate the correlation of the severity between funisitis and MAS.[19]

The histological findings associated with maternal underperfusion were identified more frequently in MAS than in non-MAS placentas. Maternal blood from the spiral arteries of the basal plate flows into the intervillous spaces, and the exchange of oxygen and nutrients occurs with fetal blood in the villi. With maternal underperfusion, villi are less perfused, resulting in hypoxic damage and hence increased syncytial knots and villous agglutination.[13,46-48] Circulatory stasis due to underperfusion also induces intervillous fibrin.[13,46,47] Long-standing severe hypoxia may result in distal villous hypoplasia, manifested as decreased number, size, and branching.[13,49-53] Inadequate vascular remodeling and/or structural abnormality of maternal arteries, including mural hypertrophy of arterioles and persistent muscularization of arteries in the basal plate is a known cause of maternal underperfusion such as preeclampsia.[13,54-58] Villous ischemic changes were previously mentioned as a placental finding of MAS, but they were not studied thoroughly.[59] Maternal underperfusion is a major risk factor of fetal growth restriction, preterm rupture of membrane, and preterm labor.[13,60-63] Especially, it is frequently related to preeclampsia.[13,64] Chronic asphyxia is one of the possible causes of MAS.[5] Preeclampsia and maternal hypertension which bring about maternal underperfusion are known as risk factors of MAS.[65] Because maternal underperfusion can lead to pulmonary hypoplasia and immaturity, this situation is vulnerable to meconium-induced inflammation. Thus, conditions that can cause maternal underperfusion might increase the risk of MAS.

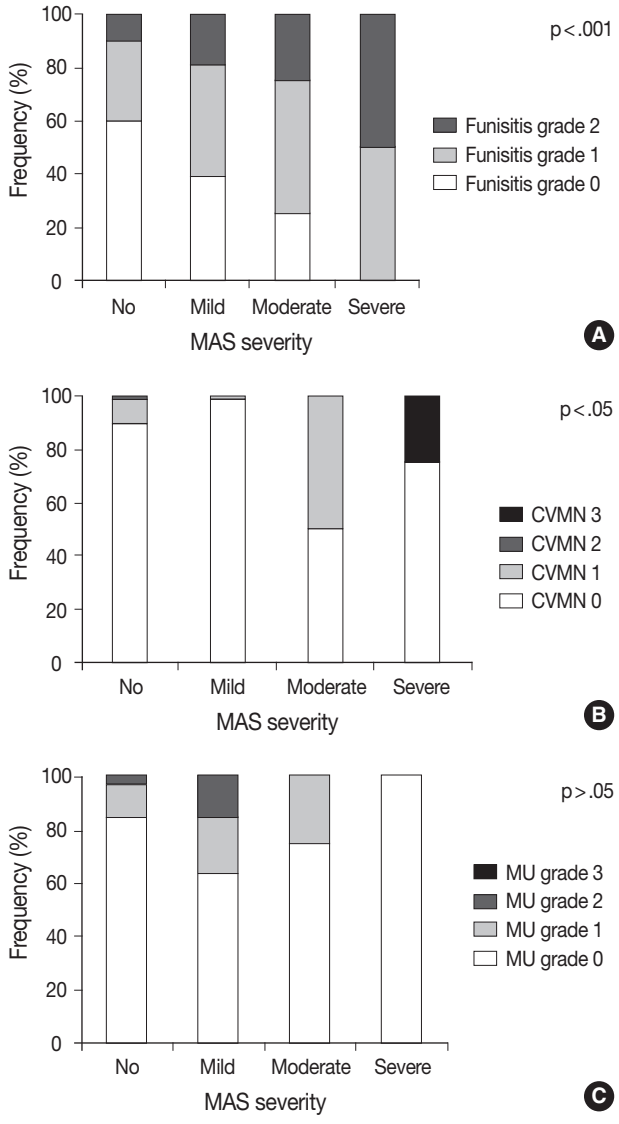

Fig. 3. Correlation of the severity of the histological findings in the placentas with the severity of meconium aspiration syndrome (MAS). (A) Funisitis vs MAS. (B) Chorionic vascular muscle necrosis (CVMN) vs MAS. (C) Maternal underperfusion (MU) vs MAS.

Chronic deciduitis is defined as the presence of lymphocytes and plasma cells in the basal plate of the placenta.[21,66] Chronic deciduitis has been associated with preterm labor and is also related to adverse outcomes such as intrauterine growth restriction and fetal death.[67,68] The etiology of chronic deciduitis is still not clear; however, chronic microbial infection and immune response to fetus antigen are thought to be involved.[66] The latter is supported by the association between chronic deciduitis and basal villitis, its presence in the placenta of pregnancies by egg donation, and the proximity of the plasma cells to trophoblast cells.[66] The relationship between chronic deciduitis and MAS has not been described before. An immunological predisposing factor to MAS may be suggested; however, the absence of significant association of MAS with chronic villitis and chronic chorioamnionitis, which are also representative of immune response to fetal antigens, does not support the hypothesis. It requires further studies to clarify.

Chorionic vascular muscle necrosis was frequent in MAS, and the severity was correlated with that of MAS. Chorionic vascular muscle necrosis can be diagnosed by observing eosinophilic cytoplasmic degeneration, nuclear pyknosis, discohesion, and rounding of peripheral vascular smooth muscle cells in vessels, resulting from apoptosis in chorionic vessels by prolonged meconium exposure.[69] It is associated with placental lesions resulting from hypoxia and poor neonatal outcome, including intrauterine growth restriction, intrauterine fetal demise, and fetal distress.[70]

https://doi.org/10.4132/jptm.2017.07.20

Collectively, our data support that fetal inflammatory response evidenced by funisitis and chorionic vascular muscle necrosis occurs prenatally in MAS. It is unlikely that MAS is simply caused by aspiration of meconium *in utero* or during the intrapartum period, which is relatively short, because these placental pathologic findings require a certain time period to be raised. Thureen *et al*.[59] reported that MAS is a kind of prenatal disease based on histopathologic pulmonary and placental evidences. Meconium passage normally occurs within the first 24 to 48 hours after birth, especially when the babies are 37 weeks or older. But, it is known to be associated with fetal distress such as hypoxia and infection in near-term or term babies.[2] There is also a hypothesis that the fetal swallowing of amniotic fluids containing various factors which evoke inflammation can lead to bowel peristalsis and meconium passage.[19] There are a variety of hypotheses on how meconium raises the respiratory distress in neonates. Nitric oxide (NO) has been known to damage lung epithelial cells responding to meconium. As such, Muller *et al*.[71] found that lipopolysaccharide and meconium-induced NO production is positively regulated by DMBT1. Ghidini and Spong[5] suggested that alternative mechanisms, such as chronic asphyxia, infection, and acute asphyxia, cause severe MAS that can result in meconium passage *in utero* and lung damage. There is a possibility that the above mechanisms are causative of both meconium passage and severe MAS, rather than that the meconium passage would be a direct cause of severe MAS.[5]

The limitations of this study include the followings: first, placentas were not collected consecutively from all births, and the placentas from neonates with MAS were enrolled for pathological examination at a higher rate than those without MAS. This selection bias explains the high frequency of MAS and inconsistent statistics of clinical characteristics in this study compared with those reported previously.[1-4,7] Second, the relatively small number of moderate and severe MAS cases included may have limited the statistical significance of the results. This is partly supported by that some clinical factors found to be significantly different between mild MAS and non-MAS did not show statistically significant difference between moderate/severe MAS and non-MAS. Further studies with consecutive collection of a larger number of cases could confirm our results and also may find additional placental findings as risk factors.

Our results suggest that fetal inflammatory response evidenced by funisitis occurs prenatally in MAS, and the stage of funisitis and the severity of chorionic vascular muscle necrosis may be predictive markers of the severity of MAS. If meconium staining is detected during delivery and MAS is clinically suspected, the placenta should be fully examined to determine whether these abnormal findings exist and at what stages they are. If the placenta shows high-grade funisitis or extensive chorionic vascular muscle necrosis, the neonate should be treated aggressively from the very beginning to prevent severe MAS.

Conflicts of Interest

No potential conflict of interest relevant to this article was reported.

Acknowledgments

This study was supported by the Basic Science Research Program through the National Research Foundation of Korea (NRF) funded by the Ministry of Science, ICT and Future Planning (NRF-2012R1A1A3012668), Republic of Korea.

REFERENCES

1. Fischer C, Rybakowski C, Ferdynus C, Sagot P, Gouyon JB. A population-based study of meconium aspiration syndrome in neonates born between 37 and 43 weeks of gestation. Int J Pediatr 2012; 2012: 321545.
2. Ahanya SN, Lakshmanan J, Morgan BL, Ross MG. Meconium passage *in utero*: mechanisms, consequences, and management. Obstet Gynecol Surv 2005; 60: 45-56.
3. Hofmeyr GJ, Xu H. Amnioinfusion for meconium-stained liquor in labour. Cochrane Database Syst Rev 2010; (1): CD000014.
4. Lauzon L, Hodnett E. Labour assessment programs to delay admission to labour wards. Cochrane Database Syst Rev 2001; (3): CD000936.
5. Ghidini A, Spong CY. Severe meconium aspiration syndrome is not caused by aspiration of meconium. Am J Obstet Gynecol 2001; 185: 931-8.
6. Wiswell TE, Bent RC. Meconium staining and the meconium aspiration syndrome. Unresolved issues. Pediatr Clin North Am 1993; 40: 955-81.
7. Choi W, Jeong H, Choi SJ, *et al*. Risk factors differentiating mild/moderate from severe meconium aspiration syndrome in meconium-stained neonates. Obstet Gynecol Sci 2015; 58: 24-31.
8. Hernández C, Little BB, Dax JS, Gilstrap LC 3rd, Rosenfeld CR. Prediction of the severity of meconium aspiration syndrome. Am J Obstet Gynecol 1993; 169: 61-70.
9. Spong CY, Ogundipe OA, Ross MG. Prophylactic amnioinfusion for meconium-stained amniotic fluid. Am J Obstet Gynecol 1994; 171: 931-5.
10. Cornish JD, Dreyer GL, Snyder GE, *et al*. Failure of acute perinatal

asphyxia or meconium aspiration to produce persistent pulmonary hypertension in a neonatal baboon model. Am J Obstet Gynecol 1994; 171: 43-9.
11. Jovanovic R, Nguyen HT. Experimental meconium aspiration in guinea pigs. Obstet Gynecol 1989; 73: 652-6.
12. Redline RW, Faye-Petersen O, Heller D, *et al*. Amniotic infection syndrome: nosology and reproducibility of placental reaction patterns. Pediatr Dev Pathol 2003; 6: 435-48.
13. Redline RW, Boyd T, Campbell V, *et al*. Maternal vascular underperfusion: nosology and reproducibility of placental reaction patterns. Pediatr Dev Pathol 2004; 7: 237-49.
14. Redline RW, Ariel I, Baergen RN, *et al*. Fetal vascular obstructive lesions: nosology and reproducibility of placental reaction patterns. Pediatr Dev Pathol 2004; 7: 443-52.
15. Altshuler G, Arizawa M, Molnar-Nadasdy G. Meconium-induced umbilical cord vascular necrosis and ulceration: a potential link between the placenta and poor pregnancy outcome. Obstet Gynecol 1992; 79(5 Pt 1): 760-6.
16. Miller PW, Coen RW, Benirschke K. Dating the time interval from meconium passage to birth. Obstet Gynecol 1985; 66: 459-62.
17. Burgess AM, Hutchins GM. Inflammation of the lungs, umbilical cord and placenta associated with meconium passage *in utero*: review of 123 autopsied cases. Pathol Res Pract 1996; 192: 1121-8.
18. Espinheira MC, Grilo M, Rocha G, Guedes B, Guimarães H. Meconium aspiration syndrome: the experience of a tertiary center. Rev Port Pneumol 2011; 17: 71-6.
19. Lee J, Romero R, Lee KA, *et al*. Meconium aspiration syndrome: a role for fetal systemic inflammation. Am J Obstet Gynecol 2016; 214: 366.e1-9.
20. Kim CJ, Romero R, Kusanovic JP, *et al*. The frequency, clinical significance, and pathological features of chronic chorioamnionitis: a lesion associated with spontaneous preterm birth. Mod Pathol 2010; 23: 1000-11.
21. Khong TY, Bendon RW, Qureshi F, *et al*. Chronic deciduitis in the placental basal plate: definition and interobserver reliability. Hum Pathol 2000; 31: 292-5.
22. Kim CJ, Romero R, Chaemsaithong P, Chaiyasit N, Yoon BH, Kim YM. Acute chorioamnionitis and funisitis: definition, pathologic features, and clinical significance. Am J Obstet Gynecol 2015; 213(4 Suppl): S29-52.
23. Overbach AM, Daniel SJ, Cassady G. The value of umbilical cord histology in the management of potential perinatal infection. J Pediatr 1970; 76: 22-31.
24. Maudsley RF, Brix GA, Hinton NA, Robertson EM, Bryans AM, Haust MD. Placental inflammation and infection: a prospective bacteriologic and histologic study. Am J Obstet Gynecol 1966; 95: 648-59.
25. D'Alquen D, Kramer BW, Seidenspinner S, *et al*. Activation of umbilical cord endothelial cells and fetal inflammatory response in preterm infants with chorioamnionitis and funisitis. Pediatr Res 2005; 57: 263-9.
26. Pacora P, Chaiworapongsa T, Maymon E, *et al*. Funisitis and chorionic vasculitis: the histological counterpart of the fetal inflammatory response syndrome. J Matern Fetal Neonatal Med 2002; 11: 18-25.
27. Naccasha N, Hinson R, Montag A, Ismail M, Bentz L, Mittendorf R. Association between funisitis and elevated interleukin-6 in cord blood. Obstet Gynecol 2001; 97: 220-4.
28. Yoon BH, Romero R, Park JS, *et al*. The relationship among inflammatory lesions of the umbilical cord (funisitis), umbilical cord plasma interleukin 6 concentration, amniotic fluid infection, and neonatal sepsis. Am J Obstet Gynecol 2000; 183: 1124-9.
29. Romero R, Hanaoka S, Mazor M, *et al*. Meconium-stained amniotic fluid: a risk factor for microbial invasion of the amniotic cavity. Am J Obstet Gynecol 1991; 164: 859-62.
30. Mazor M, Furman B, Wiznitzer A, Shoham-Vardi I, Cohen J, Ghezzi F. Maternal and perinatal outcome of patients with preterm labor and meconium-stained amniotic fluid. Obstet Gynecol 1995; 86: 830-3.
31. Halliday HL, Hirata T. Perinatal listeriosis: a review of twelve patients. Am J Obstet Gynecol 1979; 133: 405-10.
32. Cassell GH, Davis RO, Waites KB, *et al*. Isolation of *Mycoplasma hominis* and *Ureaplasma urealyticum* from amniotic fluid at 16-20 weeks of gestation: potential effect on outcome of pregnancy. Sex Transm Dis 1983; 10(4 Suppl): 294-302.
33. Mazor M, Froimovich M, Lazer S, Maymon E, Glezerman M. Listeria monocytogenes: the role of transabdominal amniocentesis in febrile patients with preterm labor. Arch Gynecol Obstet 1992; 252: 109-12.
34. Mazor M, Hershkovitz R, Bashiri A, *et al*. Meconium stained amniotic fluid in preterm delivery is an independent risk factor for perinatal complications. Eur J Obstet Gynecol Reprod Biol 1998; 81: 9-13.
35. Jessop FA, Lees CC, Pathak S, Hook CE, Sebire NJ. Funisitis is associated with adverse neonatal outcome in low-risk unselected deliveries at or near term. Virchows Arch 2016; 468: 503-7.
36. Du H, Liu E, Xu C, Zhao S, Xiang H, Li Z. Prognostic value of funisitis and/or chorionic vasculitis compared to histologic chorioamnionitis in full-term infants. J Matern Fetal Neonatal Med 2017; 30: 169-73.
37. Kim CJ, Yoon BH, Romero R, *et al*. Umbilical arteritis and phlebitis mark different stages of the fetal inflammatory response. Am J Obstet Gynecol 2001; 185: 496-500.
38. Matsuda T, Nakajima T, Hattori S, *et al*. Necrotizing funisitis: clinical significance and association with chronic lung disease in premature infants. Am J Obstet Gynecol 1997; 177: 1402-7.

39. DiSalvo D. The correlation between placental pathology and intraventricular hemorrhage in the preterm infant. The Developmental Epidemiology Network Investigators. Pediatr Res 1998; 43: 15-9.
40. Yoon BH, Romero R, Park JS, *et al*. Fetal exposure to an intra-amniotic inflammation and the development of cerebral palsy at the age of three years. Am J Obstet Gynecol 2000; 182: 675-81.
41. Leviton A, Paneth N, Reuss ML, *et al*. Maternal infection, fetal inflammatory response, and brain damage in very low birth weight infants. Developmental Epidemiology Network Investigators. Pediatr Res 1999; 46: 566-75.
42. Mittendorf R, Montag AG, MacMillan W, *et al*. Components of the systemic fetal inflammatory response syndrome as predictors of impaired neurologic outcomes in children. Am J Obstet Gynecol 2003; 188: 1438-46.
43. Shatrov JG, Birch SC, Lam LT, Quinlivan JA, McIntyre S, Mendz GL. Chorioamnionitis and cerebral palsy: a meta-analysis. Obstet Gynecol 2010; 116(2 Pt 1): 387-92.
44. Watterberg KL, Demers LM, Scott SM, Murphy S. Chorioamnionitis and early lung inflammation in infants in whom bronchopulmonary dysplasia develops. Pediatrics 1996; 97: 210-5.
45. Moscuzza F, Belcari F, Nardini V, *et al*. Correlation between placental histopathology and fetal/neonatal outcome: chorioamnionitis and funisitis are associated to intraventricular haemorrage and retinopathy of prematurity in preterm newborns. Gynecol Endocrinol 2011; 27: 319-23.
46. Tominaga T, Page EW. Accommodation of the human placenta to hypoxia. Am J Obstet Gynecol 1966; 94: 679-91.
47. Mayhew TM, Barker BL. Villous trophoblast: morphometric perspectives on growth, differentiation, turnover and deposition of fibrin-type fibrinoid during gestation. Placenta 2001; 22: 628-38.
48. Huppertz B, Kingdom J, Caniggia I, *et al*. Hypoxia favours necrotic versus apoptotic shedding of placental syncytiotrophoblast into the maternal circulation. Placenta 2003; 24: 181-90.
49. Jackson MR, Walsh AJ, Morrow RJ, Mullen JB, Lye SJ, Ritchie JW. Reduced placental villous tree elaboration in small-for-gestational-age pregnancies: relationship with umbilical artery Doppler waveforms. Am J Obstet Gynecol 1995; 172(2 Pt 1): 518-25.
50. Karsdorp VH, Dirks BK, van der Linden JC, van Vugt JM, Baak JP, van Geijn HP. Placenta morphology and absent or reversed end diastolic flow velocities in the umbilical artery: a clinical and morphometrical study. Placenta 1996; 17: 393-9.
51. Macara L, Kingdom JC, Kohnen G, Bowman AW, Greer IA, Kaufmann P. Elaboration of stem villous vessels in growth restricted pregnancies with abnormal umbilical artery Doppler waveforms. Br J Obstet Gynaecol 1995; 102: 807-12.
52. Krebs C, Macara LM, Leiser R, Bowman AW, Greer IA, Kingdom JC. Intrauterine growth restriction with absent end-diastolic flow velocity in the umbilical artery is associated with maldevelopment of the placental terminal villous tree. Am J Obstet Gynecol 1996; 175: 1534-42.
53. Madazli R, Somunkiran A, Calay Z, Ilvan S, Aksu MF. Histomorphology of the placenta and the placental bed of growth restricted foetuses and correlation with the Doppler velocimetries of the uterine and umbilical arteries. Placenta 2003; 24: 510-6.
54. Kaplan C, Lowell DM, Salafia C. College of American Pathologists Conference XIX on the Examination of the Placenta: report of the Working Group on the Definition of Structural Changes Associated with Abnormal Function in the Maternal/Fetal/Placental Unit in the Second and Third Trimesters. Arch Pathol Lab Med 1991; 115: 709-16.
55. Khong TY. The Robertson-Brosens-Dixon hypothesis: evidence for the role of haemochorial placentation in pregnancy success. Br J Obstet Gynaecol 1991; 98: 1195-9.
56. Kliman HJ. Uteroplacental blood flow: the story of decidualization, menstruation, and trophoblast invasion. Am J Pathol 2000; 157: 1759-68.
57. Khong TY, De Wolf F, Robertson WB, Brosens I. Inadequate maternal vascular response to placentation in pregnancies complicated by pre-eclampsia and by small-for-gestational age infants. Br J Obstet Gynaecol 1986; 93: 1049-59.
58. Barth WH Jr, Genest DR, Riley LE, Frigoletto FD Jr, Benacerraf BR, Greene MF. Uterine arcuate artery Doppler and decidual microvascular pathology in pregnancies complicated by type I diabetes mellitus. Ultrasound Obstet Gynecol 1996; 8: 98-103.
59. Thureen PJ, Hall DM, Hoffenberg A, Tyson RW. Fatal meconium aspiration in spite of appropriate perinatal airway management: pulmonary and placental evidence of prenatal disease. Am J Obstet Gynecol 1997; 176: 967-75.
60. De Wolf F, Brosens I, Renaer M. Fetal growth retardation and the maternal arterial supply of the human placenta in the absence of sustained hypertension. Br J Obstet Gynaecol 1980; 87: 678-85.
61. Lackman F, Capewell V, Richardson B, daSilva O, Gagnon R. The risks of spontaneous preterm delivery and perinatal mortality in relation to size at birth according to fetal versus neonatal growth standards. Am J Obstet Gynecol 2001; 184: 946-53.
62. Arias F, Victoria A, Cho K, Kraus F. Placental histology and clinical characteristics of patients with preterm premature rupture of membranes. Obstet Gynecol 1997; 89: 265-71.
63. Naeye RL. Pregnancy hypertension, placental evidences of low uteroplacental blood flow, and spontaneous premature delivery. Hum Pathol 1989; 20: 441-4.
64. Lain KY, Roberts JM. Contemporary concepts of the pathogenesis

and management of preeclampsia. JAMA 2002; 287: 3183-6.
65. Edmonds P. An introduction to meconium. Midwifery Today Int Midwife 2014; (111): 32-3.
66. Kim CJ, Romero R, Chaemsaithong P, Kim JS. Chronic inflammation of the placenta: definition, classification, pathogenesis, and clinical significance. Am J Obstet Gynecol 2015; 213(4 Suppl): S53-69.
67. Naeye RL. Functionally important disorders of the placenta, umbilical cord, and fetal membranes. Hum Pathol 1987; 18: 680-91.
68. Katzman PJ. Chronic inflammatory lesions of the placenta. Semin Perinatol 2015; 39: 20-6.
69. King EL, Redline RW, Smith SD, Kraus FT, Sadovsky Y, Nelson DM. Myocytes of chorionic vessels from placentas with meconium-associated vascular necrosis exhibit apoptotic markers. Hum Pathol 2004; 35: 412-7.
70. Cimic A, Baergen RN. Meconium-associated umbilical vascular myonecrosis: correlations with adverse outcome and placental pathology. Pediatr Dev Pathol 2016; 19: 315-9.
71. Müller H, Weiss C, Renner M, Felderhoff-Müser U, Mollenhauer J. DMBT1 promotes basal and meconium-induced nitric oxide production in human lung epithelial cells *in vitro*. Histochem Cell Biol 2017; 147: 389-97.

 https://doi.org/10.4132/jptm.2017.07.20

Journal of Pathology and Translational Medicine 2017; 51: 499-504
https://doi.org/10.4132/jptm.2017.07.28

■ ORIGINAL ARTICLE ■

Intraosseous Hibernoma: A Rare and Unique Intraosseous Lesion

Boram Song[1] · Hye Jin Ryu[2]
Cheol Lee[1] · Kyung Chul Moon[1,3]

Departments of [1]Pathology and [2]Radiology, Seoul National University College of Medicine, Seoul; [3]Kidney Research Institute, Medical Research Center, Seoul National University College of Medicine, Seoul, Korea

Received: July 4, 2017
Revised: July 26, 2017
Accepted: July 27, 2017

Corresponding Author
Kyung Chul Moon, MD
Department of Pathology, Kidney Research Institute, Medical Research Center, Seoul National University College of Medicine, 103 Daehak-ro, Jongno-gu, Seoul 03080, Korea
Tel: +82-2-2072-1767
Fax: +82-2-743-5530
E-mail: blue7270@snu.ac.kr

Background: Hibernoma is a rare benign tumor of adults that is composed of multivacuolated adipocytes resembling brown fat cells. Hibernoma typically occurs in soft tissue, and intraosseous examples are very rare. Intraosseous hibernomas can radiologically mimic metastatic carcinoma and other tumorous conditions. **Methods:** To collect the intraosseous hibernomas, we searched the pathologic database and reviewed the hematoxylin and eosin (H&E)–stained slides of bone biopsy samples performed to differentiate radiologically abnormal bone lesions from 2006 to 2016. A total of six intraosseous hibernoma cases were collected, and clinical and radiological information was verified from electronic medical records. H&E slide review and immunohistochemical staining for CD68, pan-cytokeratin, and S-100 protein were performed. **Results:** Magnetic resonance imaging of intraosseous hibernomas showed low signal intensity with slightly hyperintense foci on T1 and intermediate to high signal intensity on T2 weighted images. Intraosseous hibernomas appeared as heterogeneous sclerotic lesions with trabecular thickening on computed tomography scans and revealed mild hypermetabolism on positron emission tomography scans. Histopathologically, the bone marrow space was replaced by sheets of multivacuolated, foamy adipocytes resembling brown fat cells, without destruction of bone trabeculae. In immunohistochemical analysis, the tumor cells were negative for CD68 and pan-cytokeratin and positive for S-100 protein. **Conclusions:** Intraosseous hibernoma is very rare. This tumor can be overlooked due to its rarity and resemblance to bone marrow fat. Pathologists need to be aware of this entity to avoid misdiagnosis of this rare lesion.

Key Words: Hibernoma; Bone neoplasms; Pathology; Immunohistochemistry

Hibernoma is a rare benign adipocytic tumor of brown fat.[1] This tumor was originally described as a "pseudolipoma" by Merkel in 1906.[2] In 1914, Gery[3] noticed a histological resemblance to the brown fat in hibernating animals and renamed the tumor "hibernoma". The typical histologic feature of the tumor is multivacuolated adipocytes with centrally located nuclei resembling a brown fat cell.[1]

Hibernomas commonly occur in the soft tissue of the thigh, followed by the shoulder, back, and neck.[1] Intraosseous location has been rarely reported. Less than 20 cases are currently reported in the English literature.[4-13] Radiologically, intraosseous hibernomas can mimic metastatic carcinoma and other bone lesions, such as a hemangioma, bone island, or benign notochordal lesion.[5,8,10] Only bone biopsy and pathologic diagnosis can distinguish intraosseous hibernomas from other common conditions. In this study, we present six cases of intraosseous hibernomas with clinical, radiologic, and pathological findings.

MATERIALS AND METHODS

Cases and clinicopathologic information

The pathologic database of the Department of Pathology, Seoul National University Hospital, from 2006 to 2016 was searched with the keywords of hibernoma or brown fat, and three intraosseous hibernomas were found.

We also reviewed the hematoxylin and eosin (H&E)–stained slides of bone biopsy cases with radiologic and clinical impressions of bone marrow involvement of metastatic carcinoma, lymphoma, chronic osteomyelitis, and hemangioma cases between 2006 and 2016, and three additional intraosseous hibernoma cases were newly identified.

A total of six cases were included in this study. In all cases, the bone biopsy was performed with a 14-gauge core needle under computed tomography (CT) or fluoroscopy guidance. We reevaluated the H&E slides to confirm the adequacy of the initial diagnosis and to analyze the various pathological features. Imaging studies were also reviewed by the musculoskeletal radiologist. The corresponding clinical data were obtained from the patient's

pISSN 2383-7837
eISSN 2383-7845

medical records.

This study was approved by the Institutional Review Board (IRB) of Seoul National University Hospital (H-1611-004-803). The informed consent was waived by IRB.

Immunohistochemical staining

Immunohistochemical (IHC) staining for S-100 protein (Dako, Santa Clara, CA, USA), cytokeratin (Dako) and CD68 (Dako) was performed on formalin-fixed, paraffin-embedded tissue for all cases to validate the diagnosis of hibernoma. All IHC analyses were performed using the Ventana Benchmark XT automated staining system (Ventana Medical Systems, Tucson, AZ, USA).

RESULTS

Clinical and radiologic features

The clinical and radiologic features of the six patients are summarized in Table 1. The patients' ages ranged from 45 to 71 years. Three patients were male, and three were female. Five of six cases occurred in the axial skeleton; two in a thoracic vertebral body, two in a lumbar vertebral body, and one in the sacrum. The other case presented in the distal femur. Five of six patients initially presented with musculoskeletal pain (low back pain in four and knee pain in one patient), and the intraosseous hibernomas were identified during the diagnostic work-up to determine the cause of pain. The remaining case was asymptomatic and detected incidentally during preoperative work-up for a hepatocellular carcinoma. In three patients presenting with low back pain, imaging studies revealed disc bulging and spinal canal stenosis in addition to the bone lesion at the pain site. The remaining two patients complaining of pain revealed intramedullary bone lesions only; however, the pain of these two patients was controlled by analgesics without additional intervention.

In all cases, magnetic resonance imaging (MRI) consistently showed hypointensity intermingled with slightly hyperintense foci on T1-weighted images and intermediate to high signal intensity on T2-weighted images (Fig. 1A, B). CT mainly demonstrated mild osteosclerosis (Fig. 1C). Positron emission tomography (PET) scanning was performed in one patient and revealed mild hypermetabolism in the lesion, supporting the suspicion of malignancy (Fig. 1D). A bone scan was performed in one hepatocellular carcinoma patient as part of a liver transplantation work-up and showed increased uptake mimicking metastatic carcinoma. Involvement of cortical bone and extraosseous mass formation was not present. Radiologic impressions of the lesions were reported as intraosseous hemangioma, bone marrow involvement of lymphoma, metastatic carcinoma, or osteomyelitis.

Histological and IHC findings

Histopathological examination of the core biopsy showed aggregates of large polygonal cells with finely vacuolated voluminous cytoplasm resembling brown fat cell (Fig. 2A). The multivacuolated fat cells were arranged in sheets and clusters or scattered singularly intermingled with fatty and hematopoietic marrow elements (Fig. 2B). They had small, centrally located nuclei indented by vacuolated cytoplasm. Neither mitotic figures nor nuclear atypia were identified. The tumor cells infiltrated and replaced marrow space between the bony trabeculae without destroying the anatomy, although lamellar bony trabeculae within the lesion were slightly hypertrophied and showed mild sclerosis (Fig. 2C). The lesions also had small to medium sized blood vessels inside (Fig. 2D). Hibernoma cells with vacuolated cytoplasm may look

Table 1. Clinical and radiologic data

Case	Age (yr)	Sex	Reason for investigation	Site	Radiologic finding	Radiologic impression
1	71	F	Low back pain	L3 VB	MR: T1, low, heterogenous; T2, high CT: sclerosis PET: mild hypermetabolism	Metastasis Lymphoma Osteomyelitis Hemangioma
2	49	M	Low back pain	T12 VB	MR: T1, low, heterogenous; T2, high Simple X-ray: sclerosis	Metastasis Hemangioma
3	65	M	Hepatocellular carcinoma	T12 VB	MR: T1, low, heterogenous; T2, high CT: sclerosis Bone scan: increased uptake	Metastasis
4	68	M	Low back pain	Sacral ala	MR: T1, low, heterogenous; T2, high CT: osteolysis with peripheral sclerosis	Hemangioma
5	45	F	Knee pain	Distal femur	MR: T1, low, heterogenous; T2, high CT: mild sclerosis	Hemangioma Lymphoma Osteomyelitis
6	56	F	Low back pain	L3–4 VB	MR: T1, low, heterogenous; T2, high CT: sclerosis	Hemangioma Metastasis

F, female; VB, vertebral body; MR, magnetic resonance; CT, computed tomography; PET, positron emission tomography; M, male.

https://doi.org/10.4132/jptm.2017.07.28

like lipoblasts or foamy histiocytes. Among our cases, one was initially misdiagnosed as lipoblast in marrow space, and another was misinterpreted as a foamy histiocyte collection.

With IHC staining, the vacuolated cells were positive for S-100 protein in nuclei and cytoplasm and negative for CD68 and pan-cytokeratin (AE1/AE3) (Fig. 3). These IHC findings were consistent with intraosseous hibernoma and excluded histiocytic lesion or hidden metastatic carcinoma as possible diagnoses.

DISCUSSION

Hibernoma is a rare benign tumor composed of brown fat.[1] Brown fat is known to exist in restricted portions of the body of newborn humans and hibernating animals, performing a role in thermogenesis without shivering. Brown fat gradually disappears postnatally within a few years[14,15] but can remain focally in the paravertebral and neck region, mediastinum, and retroperitoneum in adults.[1,15]

In the study of a large series of hibernomas from the Armed Forces Institute of Pathology (AFIP), USA, soft tissue hibernomas were reported to usually occur in 30- to 40-year-old adults, varying from 2 to 72 years of age, with almost equal distribution between the sexes. These tumors most commonly occur in the subcutaneous or intramuscular region of the thigh, which is not the normal

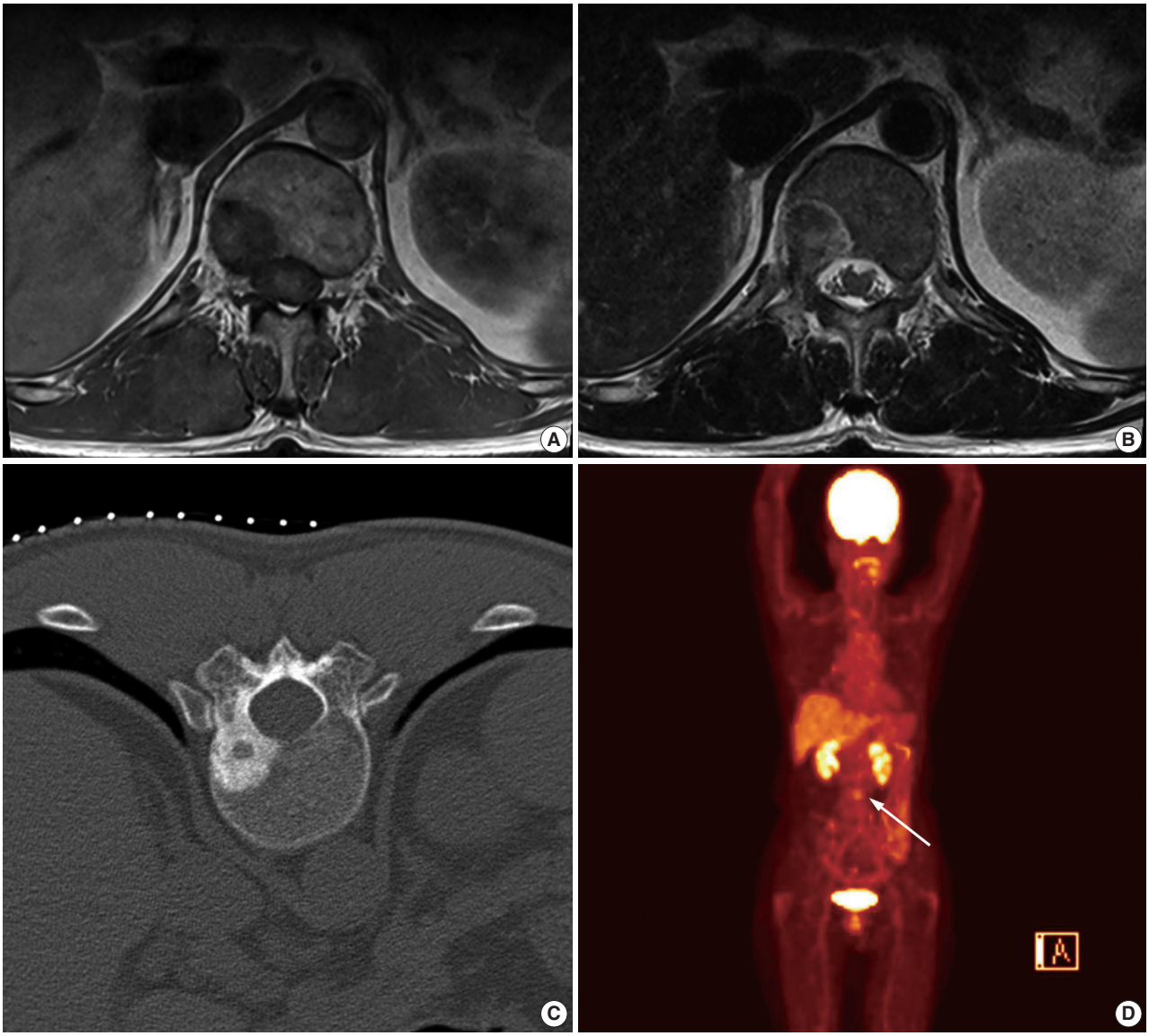

Fig. 1. Radiologic findings of intraosseous hibernoma. (A) Low signal intensity on T1-weighted magnetic resonance imaging (MRI). (B) Heterogeneous T2 high signal intensity on T2-weighted MRI. (C) Sclerotic change on computed tomography. (D) Mild hypermetabolism on positron emission tomography scan (arrow).

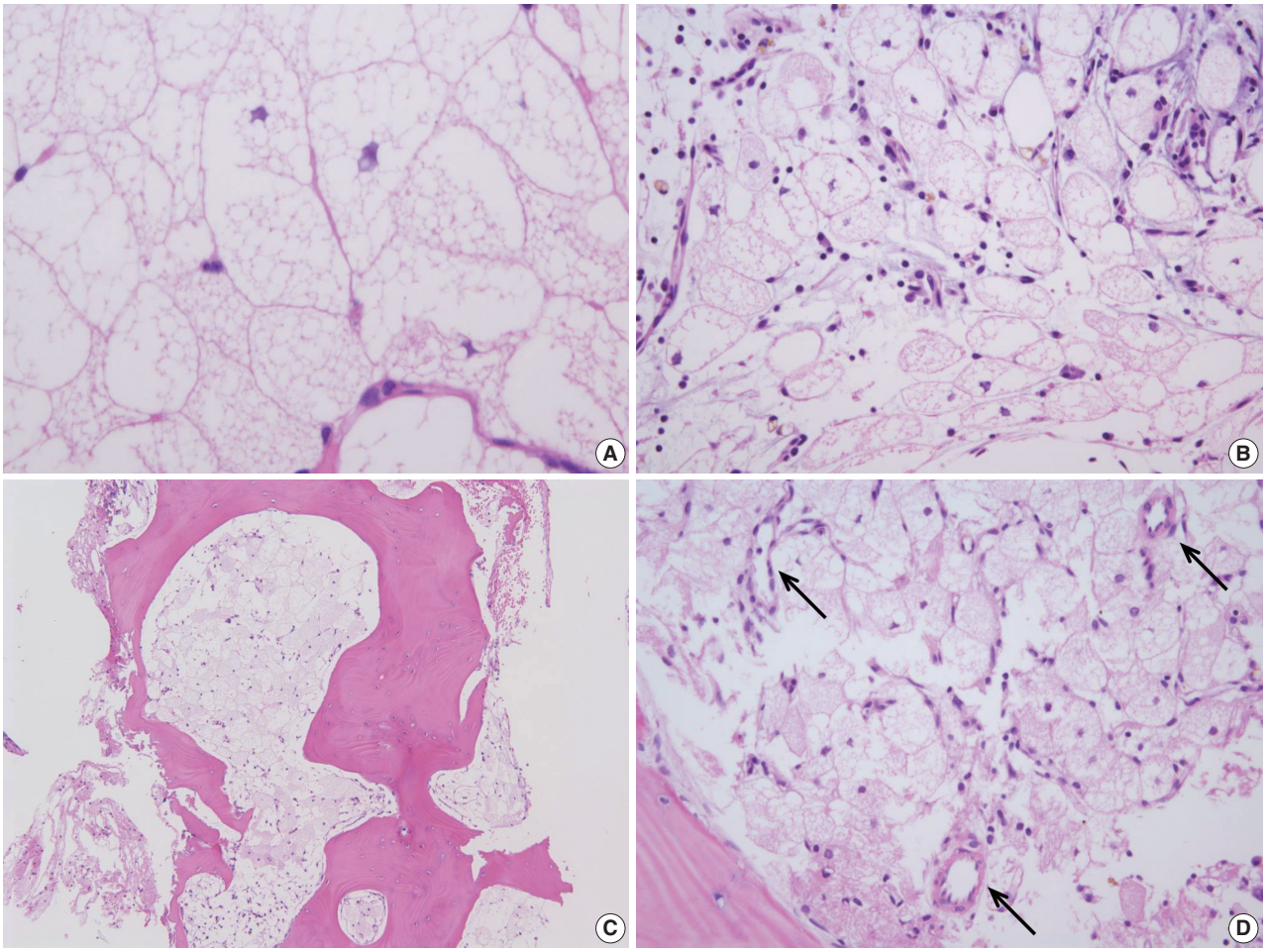

Fig. 2. Pathologic features of intraosseous hibernoma. (A) Brown fat cells with multivacuolated or granular cytoplasm indenting centrally located small nuclei. (B) Brown fat cells are intermingled with hematopoietic cells. (C) Bony trabeculae shows mild sclerosis. (D) Small to medium sized vessels (arrows) within the lesion.

location of brown fat.[1]

Hibernomas are very rarely found in an intraosseous location, with a total of 12 cases reported in the English literature up to now.[4-8,10] Previous study of intraosseous hibernomas described slight female predominance and an age range of 40 to 85 years.[10] In this study, we presented six additional cases of intraosseous hibernomas diagnosed at Seoul National University Hospital between 2006 and 2016. Our cohort showed similar sex and age distribution to the previous study, with three males and three females varying in ages from 45 to 71 years. Most of our cases (five of six patients) initially presented with musculoskeletal pain and underwent imaging work-up to determine the cause. Detected bone lesions were generally accompanied by disc herniation or spinal stenosis at the pain site. This finding had suggested that musculoskeletal pain, which had led the patient to seek medical attention, may be irrelevant to the bone lesion. To date, intraosseous hibernomas are usually considered to be asymptomatic.[10] Only one previous case was reported symptomatic due to the resolution of symptoms after radioablation therapy.[9] In our cohort, two of five patients presenting with pain had no other lesions that could cause pain besides the intraosseous lesion, allowing the possibility of intraosseous hibernoma-induced bone pain. However, the patients' pain was controlled by analgesics without additional interventions such as radioablation or curettage, suggesting that the pain was not actually caused by the intraosseous hibernoma.

Most reported intraosseous hibernomas were located in the axial skeleton,[4-13] and five of our cases were also found in the axial skeleton. However, one case in our study was found in the distal femur and presented with leg pain. Radiologic features of the lesions were consistent with those described in the previous studies.[5,7,8,10] Intraosseous hibernomas appeared as a sclerotic lesion on CT, with MRI showing T1 hypointensity with internal hyperintense foci, T2 heterogenous hyperintensity, and moderate contrast

 https://doi.org/10.4132/jptm.2017.07.28

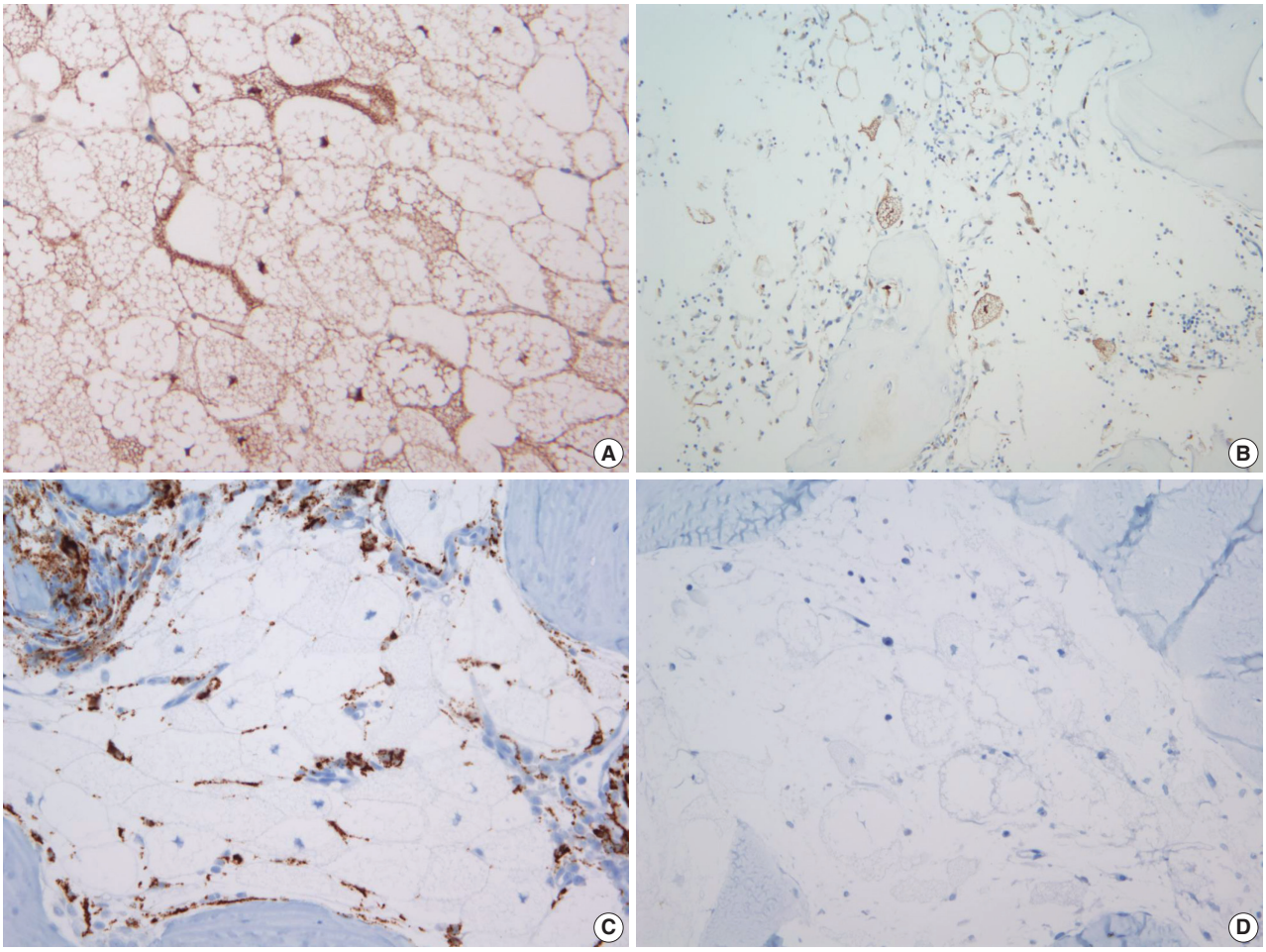

Fig. 3. Immunohistochemical stain of intraosseous hibernoma. (A) Immunohistochemical stain for S-100 protein shows diffuse positive staining in the nuclei and vacuolated cytoplasm. (B) S-100 protein immunohistochemistry highlights scattered brown fat cells intermingled with white adipose tissue. (C) CD68 staining are negative in brown fat cells. (D) Pan-cytokeratin also shows negative staining.

enhancement on post-contrast T1-weighted image. The lesions also revealed mildly increased uptake on PET scans and bone scans. The heterogeneous signals and contrast enhancement on MRI[16,17] and increased uptake on bone scan[8] are due to the increased vascularity within the lesions. Brown fat cells of hibernomas have numerous mitochondria in the cytoplasm. These mitochondria-rich brown fat cells present mild glucose hypermetabolism and increased ^{18}F fluorodeoxyglucose uptake on PET/CT scans.[18] Sclerosis on the CT scan is a nonspecific finding that may be seen in other lesions as a reactive change.[5] Imaging findings of intraosseous hibernomas usually suggest a more common diagnosis of metastases and hemangiomas, not a hibernoma.[5,7,8,10] The possibility of metastasis requires a histologic examination of the lesion to rule out malignancy. In our cohort, differential diagnoses for the imaging results were intraosseous hemangioma, bone marrow involvement of lymphoma, metastatic carcinoma, and osteomyelitis.

Microscopically, intraosseous hibernoma shows sheets and clusters of brown fat cells with voluminous multivacuolated cytoplasm and central small nuclei with minimal nuclear atypia. Unlike intraosseous lipomas, which destroy bony trabeculae and form a mass lesion,[19] intraosseous hibernomas keep the bony trabeculae intact and infiltrate between them.[4,7] This growth pattern is associated with reactive sclerosis of bony trabeculae affected by a lesion and was observed in most of the biopsied specimens of our cases. Sclerosis of bony trabeculae is a nonspecific finding that may be seen in other lesions that grow in the marrow space, including intraosseous hemangioma, lymphoma, and osteoblastic metastasis.[5] Hibernoma cells with vacuolated cytoplasm may mimic lipoblasts of liposarcoma, foamy histiocytes, and granular cell tumors. Immunohistochemically, brown fat cells are positive for S-100 protein in the nuclei and cytoplasm and negative for CD68. Histiocytes can be distinguished by CD68 positivity. Lipoblasts are smaller and have fewer vacuoles than brown fat cells and show definite nuclear atypia. Absence of intracytoplasmic

vacuoles can differentiate granular cell tumors from brown fat cells. In our cohort, there were misdiagnoses in two cases: one as lipoblasts in the marrow space, and the other as foamy histiocytes collection. The diagnosis of intraosseous hibernoma was confirmed by IHC testing for S-100 protein and CD68.

Osteoblasts and adipocytes are known to originate from common mesenchymal stem cells.[20] Recently, it is known that differentiation of brown fat cells is associated with PRD1-BF1-RIZ1 homologous domain-containing 16 (PRDM16) under regulation by bone morphogenetic protein 7 (BMP7), which stimulates bone formation.[21] Considering the function of BMP7 in bone formation and brown adipogenesis helps explain how brown fat cells and sclerotic bony trabeculae are mixed in intraosseous hibernomas.[7]

Whether the brown fat cells in the marrow space are non-neoplastic resting cells or a neoplastic lesion is arguable. IHC staining does not help in this matter. In contrast to the intraosseous lipoma, which develops into a mass without hematopoietic marrow or bony trabeculae within the tumor,[19] the fact that the intraosseous hibernoma is confined to the marrow spaces without forming a destructive mass suggests the former explanation. However, the radiologically distinct lesions described previously and in our studies support the lesion as being benign but neoplastic.

Intraosseous hibernomas are extremely rare and benign tumors. However, imaging findings for intraosseous hibernomas are non-specific, and bone biopsy with histologic confirmation is usually required to distinguish it from other common conditions such as metastases. If pathologists do not consider the possibility of intraosseous hibernomas, the presence of brown fat cells in a bone biopsy specimen can be overlooked or misdiagnosed, leading to repeated biopsy to confirm the radiologically abnormal bone lesion. Therefore, pathologists need to be aware of intraosseous hibernomas to avoid missing this rare lesion.

Conflicts of Interest

No potential conflict of interest relevant to this article was reported.

REFERENCES

1. Furlong MA, Fanburg-Smith JC, Miettinen M. The morphologic spectrum of hibernoma: a clinicopathologic study of 170 cases. Am J Surg Pathol 2001; 25: 809-14.
2. Merkel H. On a pseudolipoma of the breast. Beitr Pathol Anat 1906; 39: 152-7.
3. Gery L. In discussion of MF Bonnel's paper. Bull Mem Soc Anat (Paris) 1914; 89: 111-2.
4. Thorns C, Schardt C, Katenkamp D, Kähler C, Merz H, Feller AC. Hibernoma-like brown fat in the bone marrow: report of a unique case. Virchows Arch 2008; 452: 343-5.
5. Kumar R, Deaver MT, Czerniak BA, Madewell JE. Intraosseous hibernoma. Skeletal Radiol 2011; 40: 641-5.
6. Lynch DT, Dabney RS, Andrews JM. Intraosseous hibernoma or unusual location of brown fat? J Hematopathol 2013; 6: 151-3.
7. Bai S, Mies C, Stephenson J, Zhang PJ. Intraosseous hibernoma: a potential mimic of metastatic carcinoma. Ann Diagn Pathol 2013; 17: 204-6.
8. Botchu R, Puls F, Hock YL, *et al*. Intraosseous hibernoma: a case report and review of the literature. Skeletal Radiol 2013; 42: 1003-5.
9. Ringe KI, Rosenthal H, Langer F, Callies T, Wacker F, Raatschen HJ. Radiofrequency ablation of a rare case of an intraosseous hibernoma causing therapy-refractory pain. J Vasc Interv Radiol 2013; 24: 1754-6.
10. Bonar SF, Watson G, Gragnaniello C, Seex K, Magnussen J, Earwaker J. Intraosseous hibernoma: characterization of five cases and literature review. Skeletal Radiol 2014; 43: 939-46.
11. Dannheim K, Bhargava P. A rare finding of brown fat in bone marrow as a mimic for metastatic disease. Am J Hematol 2016; 91: 545-6.
12. Vlychou M, Teh J, Whitwell D, Athanasou NA. Intraosseous hibernoma: a rare adipocytic bone tumour. Skeletal Radiol 2016; 45: 1565-9.
13. Westacott L, Collins A, Dickenson I. Intraosseous hibernoma in the sacrum of an adult. Int J Surg Pathol 2016; 24: 749-52.
14. Himms-Hagen J. Brown adipose tissue thermogenesis: interdisciplinary studies. FASEB J 1990; 4: 2890-8.
15. van Marken Lichtenbelt WD, Vanhommerig JW, Smulders NM, *et al*. Cold-activated brown adipose tissue in healthy men. N Engl J Med 2009; 360: 1500-8.
16. Peer S, Kühberger R, Dessl A, Judmaier W. MR imaging findings in hibernoma. Skeletal Radiol 1997; 26: 507.
17. Lee JC, Gupta A, Saifuddin A, *et al*. Hibernoma: MRI features in eight consecutive cases. Clin Radiol 2006; 61: 1029-34.
18. Gaffney EF, Hargreaves HK, Semple E, Vellios F. Hibernoma: distinctive light and electron microscopic features and relationship to brown adipose tissue. Hum Pathol 1983; 14: 677-87.
19. Eyzaguirre E, Liqiang W, Karla GM, Rajendra K, Alberto A, Gatalica Z. Intraosseous lipoma: a clinical, radiologic, and pathologic study of 5 cases. Ann Diagn Pathol 2007; 11: 320-5.
20. Nombela-Arrieta C, Ritz J, Silberstein LE. The elusive nature and function of mesenchymal stem cells. Nat Rev Mol Cell Biol 2011; 12: 126-31.
21. Celi FS. Brown adipose tissue: when it pays to be inefficient. N Engl J Med 2009; 360: 1553-6.

Journal of Pathology and Translational Medicine 2017; 51: 505-508
https://doi.org/10.4132/jptm.2017.01.04

■ CASE STUDY ■

A Rare Case of Aggressive Melanotic Schwannoma Occurred in Spinal Nerve of a 59-Year-Old Male

Sung-eun Choi* · Yoon Jin Cha*
Jisup Kim · Hyunseo Cha
Jayeong Seo · Sung-Uk Kuh[1]
Sung-Jun Kim[2] · Se Hoon Kim[3]

Departments of Pathology, [1]Neurosurgery, and [2]Radiology, Gangnam Severance Hospital, Yonsei University College of Medicine, Seoul; [3]Department of Pathology, Severance Hospital, Yonsei University College of Medicine, Seoul, Korea

Received: October 17, 2016
Revised: December 6, 2016
Accepted: January 4, 2017

Corresponding Author
Se Hoon Kim, MD
Department of Pathology, Severance Hospital, Yonsei University College of Medicine, 50-1 Yonsei-ro, Seodaemun-gu, Seoul 03722, Korea
Tel: +82-2-2228-1764
Fax: +82-2-362-0860
E-mail: paxco@yuhs.ac

*Sung-eun Choi and Yoon Jin Cha contributed equally to this work.

Melanotic schwannoma (MS) is a rare variant of nerve sheath neoplasm that shows ultrastructural and immunophenotypical features of Schwann cells but also has cytoplasmic melanosomes and is reactive for melanocytic markers as well. Unlike conventional schwannoma, which is totally benign, MS has an unpredictable prognosis and is thought to have low-malignant potential. Herein, we present a rare case of recurrent MS in lumbar spine of a 59-year-old male.

Key Words: Melanotic schwannoma; Spine; Recurrence; Metastasis

Melanotic schwannoma (MS) is a rare, distinctive tumor which is categorized as a variant of schwannoma. Approximately 50% of MS have psammomatous calcifications, which is related to Carney complex, an autosomal dominant disorder.[1] Tumor cells of MS are thought to be Schwann cells that characteristically have melanosomes and are immunophenotypically reactive for melanocytic markers.[2] We report a case of MS that had occurred in lumbar spinal nerve of a 59-year-old male, which locally recurred 5 years after the surgical removal of the primary tumor and also metastasized to the lung.

CASE REPORT

This study was approved by the Institutional Review Board of Gangnam Severance Hospital with a waiver of informed consent (IRB No. 3-2016-0255).

A 59-year-old male presented with right buttock pain and radiating leg pain. He had a medical history of hypertension on medication for 10 years. Five years ago, he had a hemi-laminectomy with removal of a spinal cord mass of left L4 level, at the outside hospital, and the diagnosis was MS. On spinal magnetic resonance imaging, tumor in previous operative site, L4 level of spinal cord, was recognized with involvement of L4 vertebral body (Fig. 1A). Tumor recurrence was considered based on the patient's history. Subsequent positron emission tomography–computed tomography revealed strong fluorodeoxyglucose (FDG) uptake in the L4/5 level. Multiple lung nodules with increased FDG uptake were found in the left upper lobe, right middle lobe, and right lower lobe, which appeared to be consistent with metastatic nodules (Fig. 1B). Patient received total laminectomy of L4 and subtotal laminectomy of L3 lower and L5 upper bodies. The resected specimen submitted in fresh

pISSN 2383-7837
eISSN 2383-7845

state consisted of a product of L4 corpectomy, including a body of L4 spinal bone and separately sent soft tissue. A 3.3×2.2-cm-sized black, soft mass was located in the posterior side of the L4 body. On cut section, the black mass was infiltrating into the bone (Fig. 2A).

On histological examination, a cellular pigmented mass was infiltrating the bone marrow (Fig. 2B). Discohesive tumor cells were arranged in solid sheets or nests. Tumor cells had eosinophilic ample cytoplasm, long cytoplasmic process with fuzzy cell borders, and variable amounts of cytoplasmic melanin pigments. Nuclear pleomorphism and prominent macronucleoli were observed with a few mitoses up to 2/10 high power fields (HPFs) (Fig. 2C). Foci of tumor necrosis were observed (Fig. 2D). Immunohistochemical staining for human melanoma black 45 (HMB45; 1:100, clone HMB45, Dako, Carpinteria, CA, USA), S-100 protein (1:2,000, clone bBS/NC/VI-H14, Dako), Ki-67

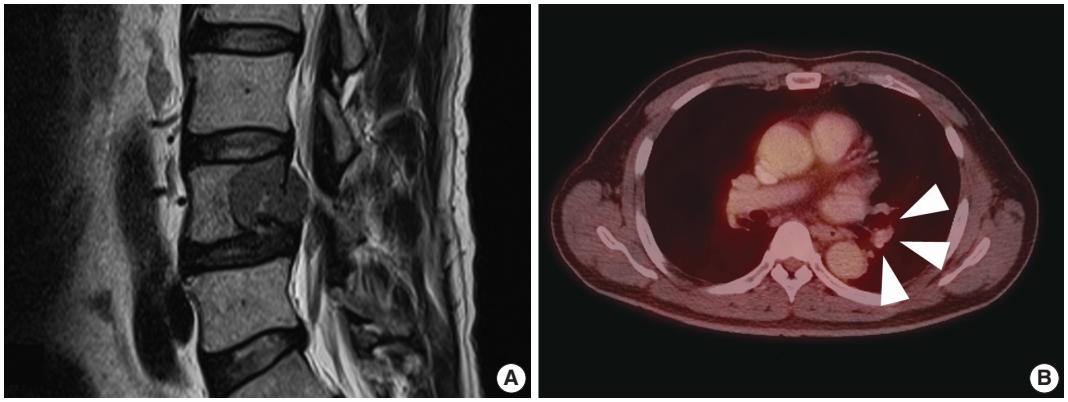

Fig. 1. Radiologic findings of spinal melanotic schwannoma. (A) Magnetic resonance imaging of lumbar spine reveals a destructive mass of the vertebral body. (B) Metastatic pulmonary nodule in left upper lobe with increased fluorodeoxyglucose uptake on positron emission tomography–computed tomography (arrowheads).

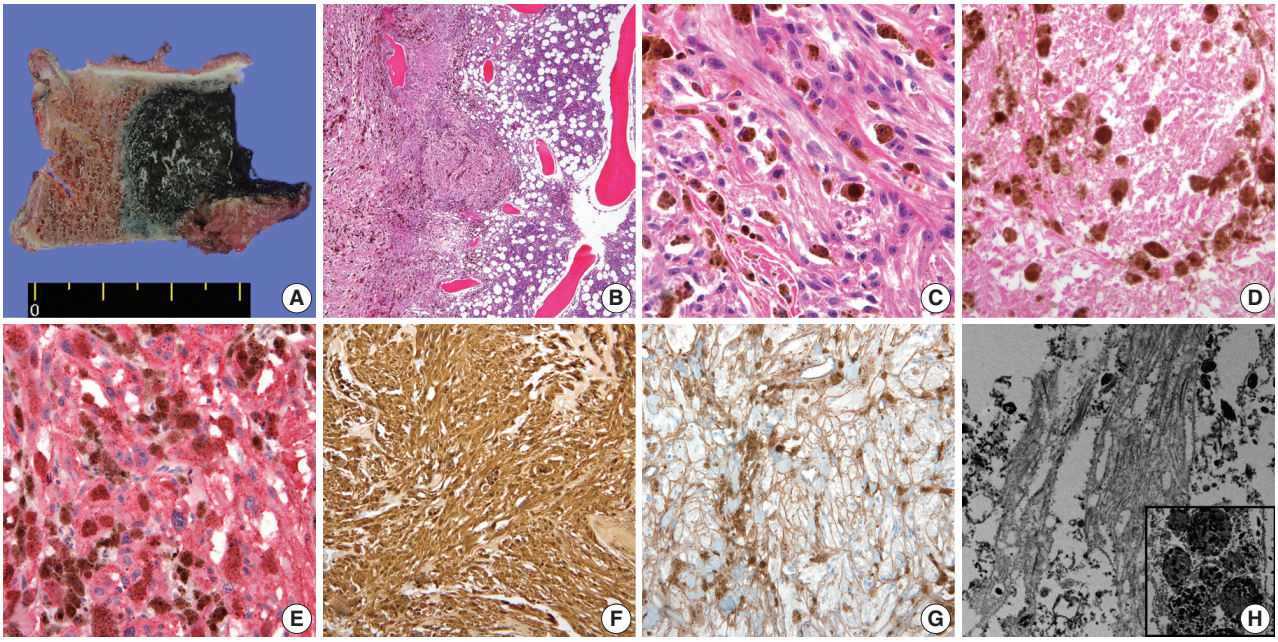

Fig. 2. Gross, microscopic and ultrastructural findings of melanotic schwannoma. (A) A heavily pigmented black round mass of vertebral body has infiltrative margin. (B) Tumor cells permeate the bone marrow space of vertebra (left). Note the right sided normal bone marrow that shows retained trabecular bone and marrow space containing hematopoietic cells. (C) Epithelioid tumor cells have discernible cytoplasmic membrane, pleomorphic nuclei, and cytoplasmic melanin pigments. Note the mitosis (center) and prominent nucleolus. (D) Foci of tumor necrosis are seen. Human melanoma black 45 (E) and S-100 protein (F) are diffusely and strongly positive in tumor cells. (G) Collagen type IV staining reveals pericellular membranous staining of tumor cells, implying the presence of basal lamina. (H) On electron microscopy, abundant basal lamina of tumor cell is evident with cytoplasmic melanosomes (×12,000) (inset, ×5,000).

https://doi.org/10.4132/jptm.2017.01.04

Table 1. Previously reported melanotic schwannomas with metastasis

Case No.	Sex	Age (yr)	Primary site	Metastasis site	References
1	M	27	Bronchus	Brain	Rowlands *et al*.[15] (1987)
2	F	48	T9–T10	Lung, skin	Killeen *et al*.[16] (1988)
3	M	27	L5	Lung, pleura	Vallat-Decouvelaere *et al*.[7] (1999)
4	F	35	L3–L5	Bone, lymph node	Vallat-Decouvelaere *et al*.[7] (1999)
5	F	45	T6	Lung, bone, liver	Vallat-Decouvelaere *et al*.[7] (1999)
6	M	35	C4–C5	Leptomeninges	Santaguida *et al*.[10] (2004)
7	M	61	T7	Leptomeninges	Tawk *et al*.[11] (2005)
8	M	33	L5–S1	Lung	Shields *et al*.[12] (2011)
9	F	32	C4–C5	Lung	Faria *et al*.[13] (2013)
10	F	15	Cervical paraspinal	Leptomeninges, parascapular, and neck soft tissues	Torres-Mora *et al*.[8] (2014)
11	F	23	L4	Liver	Torres-Mora *et al*.[8] (2014)
12	F	25	Sacrum	Lung, pleura, lymph nodes	Torres-Mora *et al*.[8] (2014)
13	M	27	L2–L3	Lung, lymph nodes, abdomen	Torres-Mora *et al*.[8] (2014)
14	M	32	C2 nerve root	Lung, skeleton	Torres-Mora *et al*.[8] (2014)
15	M	40	Paraspinal L3–L4	Spine (T12)	Torres-Mora *et al*.[8] (2014)
16	F	44	T5–6	Lung, posterior chest wall	Torres-Mora *et al*.[8] (2014)
17	M	47	L3–L4	Lung, liver, pleura, leptomeninges, bone	Torres-Mora *et al*.[8] (2014)
18	M	47	C5	Lumbar/thoracic, brain	Torres-Mora *et al*.[8] (2014)
19	M	61	T6–T8	Spinal cord	Torres-Mora *et al*.[8] (2014)
20	F	67	T10	Liver	Torres-Mora *et al*.[8] (2014)
21	M	46	L3	Brain, leptomeninges	Khoo *et al*.[14] (2016)

M, male; F, female; T, thoracic spine; L lumbar spine; C, cervical spine.

(1:150, clone MIB-1, Dako), and collagen type IV (1:100, clone CIV 22, Dako) was performed. Tumor cells showed diffuse and strong expression of HMB45 and S-100 protein (Fig. 2E, F). Collagen type IV was expressed along the pericellular membrane (Fig. 2G). Ki-67 was positive in approximately 1% of the tumor cells. Under electron microscopy, abundant basal lamina (Fig. 2H) was observed along with the cytoplasmic melanosomes (Fig. 2H, inset).

DISCUSSION

We reported a rare case of spinal MS that showed local recurrence and pulmonary metastasis. MS is a rare variant of nerve sheath neoplasm of which less than 200 cases have been reported to date with three cases in Korean reports.[2-5] MS can be divided into psammomatous and nonpsammomatous type,[2] and approximately half of the psammomatous MS are related to Carney complex, an autosomal dominant disease with cardiac myxomas and Cushing syndrome.[6] Nonpsammomatous MS is considered to be a sporadic type and commonly affects spinal nerves and paraspinal ganglia, whereas psammomatous type often involves autonomic nerves of viscera. In contrast to the typical encapsulation of conventional schwannoma, MS is a circumscribed but unencapsulated tumor, which may reflect the potential of more aggressive nature of MS such as an invasive growth pattern. In present study, the tumor showed infiltrative border that permeated the bone marrow space. Unlike the conventional schwannoma, which is a totally benign neoplasm, MS follows an unpredictable clinical course. Even devoid of overt histologic atypia, approximately 10% of MS follow a malignant course.[2,7] Although MS could demonstrate nuclear pleomorphism and macronucleoli with expression of melanocytic markers, findings mimicking malignant melanoma, these histologic features are poorly correlated with the clinical outcome. However, unlike malignant melanoma which usually has frequent mitosis, MS has rare mitosis. In addition, histologic features of ample cytoplasm, cytoplasmic process, and indiscernable cell border as well as low proliferative index contribute to the diagnosis of MS rather than malignant melanoma. Presence of mitosis itself, particularly over one mitosis/10HPFs, is the only known risk factor of metastasis in MS.[8] In present case, the tumor had histologic atypia—nuclear pleomorphism, prominent macronucleoli—and foci of necrosis which are worrisome histologic features in routine pathologic diagnosis. Moreover, more importantly, the mitotic count was up to 2 /10HPFs, which may have been a factor attributing to the lung metastasis.

Recently, Torres-Mora *et al*.[8] carried out gene microarray study covering over 1,700 genes, showed different gene expression profile of MS from conventional schwannoma or malignant melanoma, and suggested that MS is a distinctive neoplasm, belonging neither to the conventional schwannoma nor malignant mel-

anoma. Among pigmented lesions of central nervous system, MS lacks *GNAQ* codon 209 mutations, which is one of mutational descriptors found in leptomeningeal melanocytic lesions.[9] Although MS is a genetically interesting and ambiguous tumor, a genetic study of the present case was not available. Instead, immunohistochemical staining and electron microscopy helped to identify the abundant basal lamina and cytoplasmic melanosomes, which elucidated the features of both Schwann cell and melanocyte. Previous study described different basement membrane staining patterns of MS from conventional schwannoma and leptomeningeal melanocytic lesion.[9] MS demonstrated pericellular staining of basement membrane on collagen type IV, similar to that of conventional schwannoma with or without a nesting pattern, whereas other melanocytic lesions had predominant nesting pattern.[9]

So far, only about 20 cases of metastatic MS have been reported,[7,8,10-16] which are shown in Table 1. This is the first metastatic and recurrent MS case in a Korean patient. The sporadic, spinal MS showed an aggressive biologic behavior—local recurrence and pulmonary metastasis—and the ancillary examination delineated the pericellular basal lamina and cytoplasmic melanosomes.

Conflicts of Interest

No potential conflict of interest relevant to this article was reported.

Acknowledgments

This study was supported by a faculty research grant of Yonsei University College of Medicine for 6-2015-0147.

The authors are deeply indebted to Dr. Yeon-Lim Suh in the Department of Pathology, Samsung Medical Center, for her insightful discussion that greatly improved the manuscript.

REFERENCES

1. Carney JA. Carney complex: the complex of myxomas, spotty pigmentation, endocrine overactivity, and schwannomas. Semin Dermatol 1995; 14: 90-8.
2. Louis DN, Ohgaki H, Wiestler OD, Cavenee WK. WHO classification of tumours of the central nervous system. Lyon: IARC Press; 2007.
3. Yim H, Go JH, Ahn CS, Hong SW, Jung WH. Pigmented (melanotic) schwannoma of the cervical spinal canal: a case report. Korean J Pathol 1995; 29: 256-62.
4. Yi S, Chin DK, Jin BH, Cho YE, Kim YS. Melanotic schwannoma in cervical spine: a case report. J Korean Neurosurg Soc 2001; 30: 916-20.
5. You SH, Suh YL, Kim JH. Melanotic acoustic schwannoma. J Korean Neurosurg Soc 2002; 31: 485-7.
6. Carney JA. Psammomatous melanotic schwannoma: a distinctive, heritable tumor with special associations, including cardiac myxoma and the Cushing syndrome. Am J Surg Pathol 1990; 14: 206-22.
7. Vallat-Decouvelaere AV, Wassef M, Lot G, *et al*. Spinal melanotic schwannoma: a tumour with poor prognosis. Histopathology 1999; 35: 558-66.
8. Torres-Mora J, Dry S, Li X, Binder S, Amin M, Folpe AL. Malignant melanotic schwannian tumor: a clinicopathologic, immunohistochemical, and gene expression profiling study of 40 cases, with a proposal for the reclassification of "melanotic schwannoma". Am J Surg Pathol 2014; 38: 94-105.
9. Kusters-Vandevelde HV, van Engen-van Grunsven IA, Kusters B, *et al*. Improved discrimination of melanotic schwannoma from melanocytic lesions by combined morphological and GNAQ mutational analysis. Acta Neuropathol 2010; 120: 755-64.
10. Santaguida C, Sabbagh AJ, Guiot MC, Del Maestro RF. Aggressive intramedullary melanotic schwannoma: case report. Neurosurgery 2004; 55: 1430.
11. Tawk RG, Tan D, Mechtler L, Fenstermaker RA. Melanotic schwannoma with drop metastases to the caudal spine and high expression of CD117 (c-kit). J Neurooncol 2005; 71: 151-6.
12. Shields LB, Glassman SD, Raque GH, Shields CB. Malignant psammomatous melanotic schwannoma of the spine: a component of Carney complex. Surg Neurol Int 2011; 2: 136.
13. Faria MH, Doria-Netto RH, Osugue GJ, Queiroz Lde S, Chaddad-Neto FE. Melanotic schwannoma of the cervical spine progressing with pulmonary metastasis: case report. Neurol Med Chir (Tokyo) 2013; 53: 712-6.
14. Khoo M, Pressney I, Hargunani R, Tirabosco R. Melanotic schwannoma: an 11-year case series. Skeletal Radiol 2016; 45: 29-34.
15. Rowlands D, Edwards C, Collins F. Malignant melanotic schwannoma of the bronchus. J Clin Pathol 1987; 40: 1449-55.
16. Killeen RM, Davy CL, Bauserman SC. Melanocytic schwannoma. Cancer 1988; 62: 174-83.

Journal of Pathology and Translational Medicine 2017; 51: 509-512
https://doi.org/10.4132/jptm.2017.03.22

■ CASE STUDY ■

Cytologic Characteristics of Thymic Adenocarcinoma with Enteric Differentiation: A Study of Four Fine-Needle Aspiration Specimens

Ah-Young Kwon · Joungho Han
Hae-yon Cho · Seokhwi Kim
Heejin Bang · Jiyeon Hyeon

Department of Pathology, Samsung Medical Center, Sungkyunkwan University School of Medicine, Seoul, Korea

Received: February 17, 2017
Revised: March 14, 2017
Accepted: March 22, 2017

Corresponding Author
Joungho Han, MD
Department of Pathology, Samsung Medical Center, Sungkyunkwan University School of Medicine, 81 Irwon-ro, Gangnam-gu, Seoul 06351, Korea
Tel: +82-2-3410-2765
Fax: +82-2-3410-0025
E-mail: hanjho@skku.edu

Thymic adenocarcinoma is extremely rare. Although its histologic features have been occasionally reported, a lack of description of the cytologic features has hampered the prompt and accurate diagnosis of this condition. Herein, we describe the cytologic findings and histology of four aspiration cytology specimens of thymic adenocarcinoma. The specimens were obtained from primary tumors, metastatic lymph nodes, and pericardial effusions. All four specimens showed three-dimensional glandular clusters with a loss of polarity and nuclear overlapping. One specimen had extensive extracellular mucinous material. Three specimens contained tumor cells with intracytoplasmic vacuoles. While the specimen with extracellular mucin showed relatively mild cytologic atypia, other specimens exhibited more atypical cytologic changes: irregular nuclear membranes, a coarse chromatin pattern, and prominent nucleoli. The cytologic features were correlated with the histologic features in each case of enteric type thymic adenocarcinoma. The differential diagnosis included other thymic carcinomas, yolk sac tumors, and metastatic adenocarcinoma from the lung or colorectum.

Key Words: Mediastinum; Thymus gland; Adenocarcinoma; Cytology; Aspiration

Primary thymic adenocarcinoma is a very rare neoplasm that accounts for 0.48% of all thymic epithelial tumors.[1] Only 58 cases have been reported to date.[2] Based on histology, thymic adenocarcinoma is classified into four subtypes: mucinous, papillary, not otherwise specified (NOS), and a type with adenoid cystic carcinoma-like features.[3] Recently, Moser *et al*.[4] and our institute[2] reported that both mucinous and NOS types showed enteric differentiation, suggesting that enteric type thymic adenocarcinoma could be an appropriate term in regards to the histology of this condition.

Previous studies have focused on the diagnosis and classification of thymic adenocarcinoma according to its clinical, histologic, and immunohistochemical features. However, the cytologic features of thymic adenocarcinoma have not yet been reported. In this study, we investigated the characteristics of thymic adenocarcinoma in aspiration cytology based on four specimens from three patients. The clinical and histologic features of these specimens were reported in our previous study.[2] We analyzed the cytologic features and histologic characteristics as well as the differential diagnosis of thymic adenocarcinoma.

CASE REPORT

The clinicopathologic characteristics of four thymic adenocarcinoma specimens are summarized in Table 1. These four specimens were obtained from three patients, who were reported in our previous study[2] as cases 6, 7, and 8. All cytology specimens were obtained by fine-needle aspiration (FNA) from the subaortic and right supraclavicular lymph nodes, pericardial effusion, and tumors. This study was approved by the Institutional Review Board of Samsung Medical Center (IRB file No. 2016-07-064), and informed consent was waived.

Patient 1 (specimen 1)

A 70-year-old man visited Samsung Medical Center complaining of chest wall pain. Chest computed tomography (CT) revealed a 9.6-cm-sized cystic lesion in the anterior and left upper mediastinum with direct extension to the mediastinal fat and the

pISSN 2383-7837
eISSN 2383-7845

Table 1. Clinicopathologic characteristics of cases

Case No.	Sex	Age (yr)	Smoking history	Past history	Masaoka stage	Specimen of aspiration	Cytologic diagnosis	Histologic diagnosis
1	M	70	40 PY	HTN, DM	II	Mediastinal LN (subaortic LN)	Metastatic carcinoma, showing glandular clusters of atypical cells	Thymic adenocarcinoma, enteric type
2	M	50	20 PY	Angina	IVB	Supraclavicular LN	Metastatic carcinoma, showing glandular clusters of atypical cells	Thymic adenocarcinoma, enteric type
						Pericardial effusion	Metastatic carcinoma, showing glandular clusters of atypical cells	-
3	M	62	5 PY	HTN, DM	IVB	Tumor	A few clusters of atypical cells in mucinous background	Thymic adenocarcinoma, enteric mucinous type

M, male; PY, pack-year; HTN, hypertension; DM, diabetes mellitus; LN, lymph node.

left upper lobe of the lung. Multiple enlarged lymph nodes were found in the mediastinum. The patient underwent endobronchial ultrasound (EBUS)–transbronchial needle aspiration (TBNA) of the subaortic lymph node. FNA slides revealed some epithelial clusters in bloody background (Fig. 1A). Three-dimensional (3D) clusters consisted of variably sized cells with moderate to high nuclear atypia. Their nuclei had irregular contours, margination, a coarse chromatin pattern, and single or two prominent nucleoli. Cytoplasmic borders were indistinct, and the amount of cytoplasm was variable (Fig. 1B). Some of the tumor cells contained intracytoplasmic vacuoles (Fig. 1A, arrow). Core needle biopsy (CNB) was conducted a day after the EBUS-TBNA. The tumor was diagnosed as thymic adenocarcinoma with enteric differentiation (Fig. 1C). The histologic characteristics were well correlated with the features identified in cytologic specimens: a tubulo-glandular pattern with nuclear atypia and occasional intracytoplasmic mucin.

Patient 2 (specimens 2 and 3)

A 50-year-old man visited the hospital for an evaluation of his weight loss (8 kg during the past two months). Chest CT revealed an 8.1-cm-sized, heterogeneously enhancing mass in the anterior mediastinum with sternum destruction. Multiple small nodules in the lung parenchyma and necrotic lymphadenopathy in the right supraclavicular area were also identified. FNA of the right supraclavicular lymph node revealed a large amount of three-dimensional epithelial cell clusters in a background of blood and inflammatory cells (Fig. 1D, E). The cells at the edge of the clusters were stratified. Small to large clusters consisted of columnar cells with abundant eosinophilic cytoplasm and occasional intracytoplasmic vacuoles (Fig. 1F). The elongated nuclei of the columnar cells had irregular membranes with margination, coarse to vesicular chromatin, and prominent nucleoli. CNB for the mediastinal mass was subsequently performed. A tubular growth pattern, pseudostratified nuclei with atypia, and a few instances of intracytoplasmic mucin were also found in the CNB specimen (Fig. 1I). Considering the cytology and histology of the tumor, enteric type adenocarcinoma was an appropriate diagnosis.

After 6 months of prolonged chemotherapeutic treatment, pericardial effusion from the patient was obtained by aspiration. Liquid-based cytology showed crowded epithelial cells with nuclear overlapping (Fig. 1G). Pleomorphic nuclei, vesicular chromatin, and single or two prominent nucleoli were also shown (Fig. 1H).

Patient 3 (specimen 4)

A 62-year-old man presented to the hospital with chest discomfort. Chest CT showed an infiltrative anterior mediastinal mass, measuring 3.2 cm in size, along with massive pericardial effusion. The possibility of lymphoma or thymic malignancy was suggested considering the patient's clinical and radiologic features. FNA of the anterior mediastinum was conducted. In the aspirated specimen, a few cells could be identified with extensive mucinous material in the background (Fig. 1J). Tumor cells were round and small to medium in size. A relatively fine chromatin pattern and indistinct nucleoli favored benign cells; however, slight nuclear margination, irregular arrangement, and cellular overlapping suggested malignancy (Fig. 1K). The patient underwent surgical excision. According to the cytologic and histologic features of the specimen, a diagnosis of enteric type mucinous adenocarcinoma was made (Fig. 1L). One major histologic characteristic of the surgical specimen was floating tumor clusters in the extracellular mucin that were cribriform, tubular, or single cell types.

DISCUSSION

Thymic adenocarcinoma is rarely encountered in routine practice. However, with the increasing frequency of EBUS, pathologists

 https://doi.org/10.4132/jptm.2017.03.22

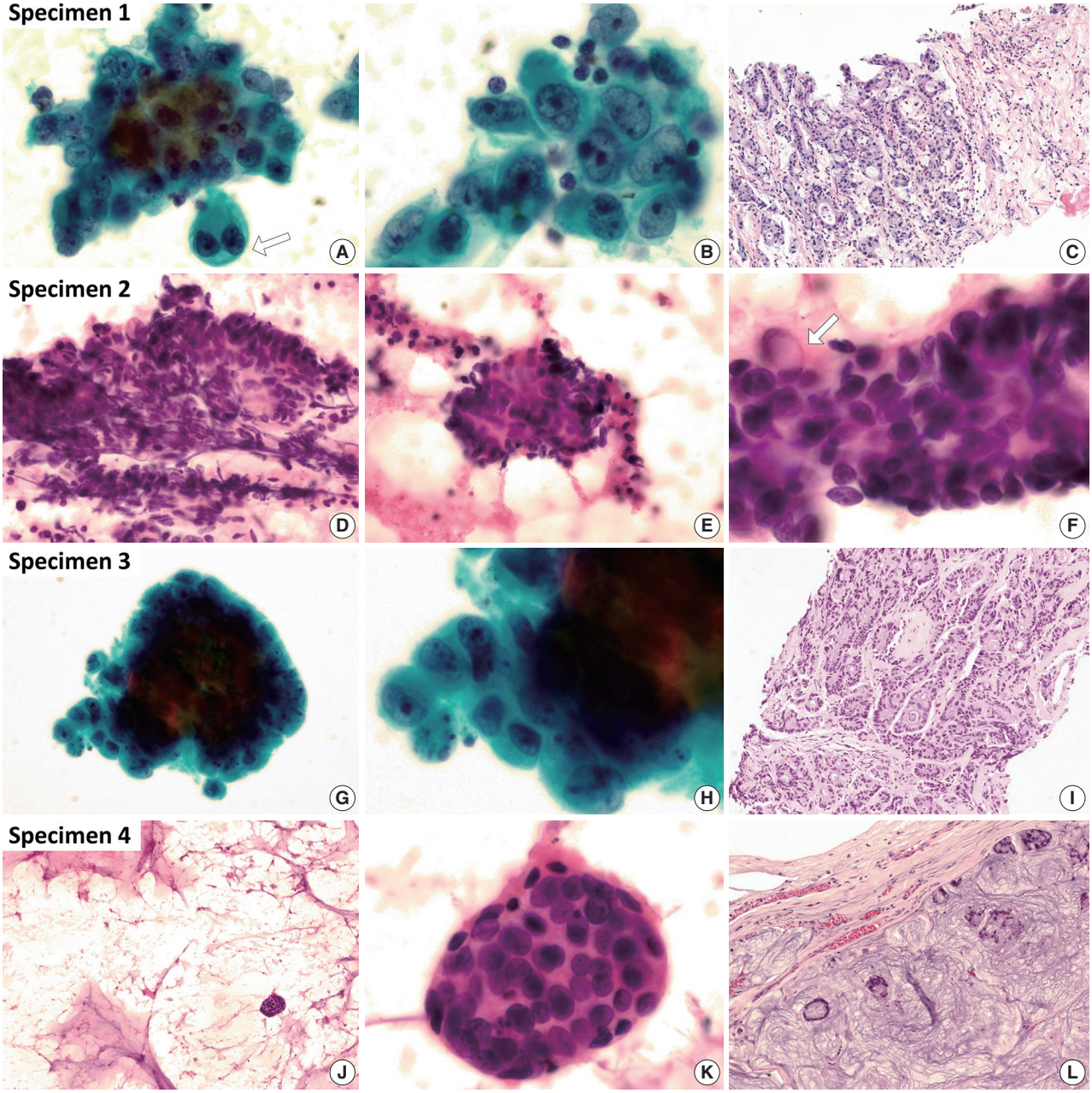

Fig. 1. Cytologic characteristics of thymic adenocarcinoma with histology. (A–C) The fine-needle aspiration (FNA) specimen was obtained from a mediastinal lymph node. Some epithelial cell clusters with a three-dimensional glandular structure are shown. The variably-sized cells have atypical nuclei showing an irregular margin, distinct margination, vesicular chromatin, and prominent nucleoli. Loss of polarity is also present. The cytoplasm is moderately abundant, and intracytoplasmic vacuoles are not infrequently seen (arrow). Adenocarcinoma with a tubular pattern is revealed in the histomorphology of the core biopsy from the tumor. Glandular structure, atypical nuclei, eosinophilic cytoplasm, intracytoplasmic vacuoles, and surrounding inflammatory cells and fibrotic stroma are identical findings with aspiration cytology (A and B, Wright-Giemsa stain). (D–I) Two separate FNAs were carried out in a supraclavicular lymph node (D–F) and the pericardial effusion (G, H). There are glandular- and cribriform-patterned clusters with an inflammatory background. Palisading and stratification are frequently found in clusters. An irregular nuclear margin, vesicular chromatin, prominent nucleoli, and an occasional intracytoplasmic vacuole (arrow) are shown in this sample from patient 2. A core biopsy specimen was obtained from the mediastinal tumor. The tumor shows a tubular and cribriform pattern, stratified nuclei, eosinophilic cytoplasm, intracytoplasmic vacuoles, and inflammatory cells (G and H, Wright-Giemsa stain). (J–L) Most of the aspiration specimen obtained from the tumor is mucinous material. Only a few clusters can be detected. A round cluster of tumor cells reveals relatively mild nuclear atypia. Nuclear overlapping and irregular arrangement are still observed. The excisional specimen reveals floating tumor cells with a tubular or cribriform pattern within the extensive extracellular mucin.

should be aware of the cytologic features of thymic adenocarcinoma in aspiration. In addition, thymic adenocarcinomas often accompany metastasis at the time of diagnosis. Therefore, the importance of an accurate diagnosis of aspiration cytology in mediastinal tumors, lymph nodes, or effusion is increasing.

Thymic adenocarcinoma may be classified into four categories based on histology. We previously reported that mucinous adenocarcinoma and adenocarcinoma NOS could be referred to as enteric type adenocarcinoma.[2] This enteric type is the most common; all 14 cases reported in Korea have been of this type.[2] Although some individual reports have mentioned the diagnosis of thymic adenocarcinoma in aspiration specimens,[5-7] a detailed description of the cytologic diagnosis of thymic adenocarcinoma has not been reported to date.[2,8-12]

In our FNA specimens, thymic adenocarcinoma cells demonstrated 3D clusters with nuclear crowding and overlapping. Other cytologic findings were similar to histomorphology. In specimens 1 and 2, the columnar cells had stratified nuclei and occasional intracytoplasmic vacuoles. The nuclei had the following signs, which suggest malignancy: irregularity of the nuclear membrane, nuclear margination, coarse chromatin, and prominent nucleoli. A dirty background containing blood and inflammatory cells could aid in a confirmative diagnosis. Malignant features of the nuclei were not clear for the mucinous type (specimen 4). However, extensive extracellular mucin and loss-of-polarity of clusters were characteristically identified. Their cytologic features were more prominent when compared with histologic specimens.

The differential diagnosis of thymic adenocarcinoma includes thymic epithelial malignancies, direct invasion of pulmonary adenocarcinoma, metastatic adenocarcinoma, and germ cell tumors, especially yolk sac tumors. Aspiration cytology of yolk sac tumors might show similar cytologic features to thymic adenocarcinoma, such as atypical cells with a glandular pattern and a dirty background. The serum α-fetoprotein level and immunohistochemical staining could be helpful in the differential diagnosis. Other thymic carcinomas might reveal epithelial cell clusters with nuclear atypia and crowding. Glandular tumor clusters and intracellular or extracellular mucin favor a diagnosis of adenocarcinoma. Metastatic adenocarcinoma from other organs should be regarded as an important differential diagnosis. In particular, colonic adenocarcinoma and pulmonary enteric type adenocarcinoma might be difficult to differentiate from primary thymic adenocarcinoma because their histologic features and immunohistochemical profile are very similar. Therefore, clinical and radiologic findings such as location, size, and the presence of metastasis of the tumor should be rigorously analyzed and carefully considered.

Conflicts of Interest

No potential conflict of interest relevant to this article was reported.

REFERENCES

1. Ahmad U, Yao X, Detterbeck F, *et al*. Thymic carcinoma outcomes and prognosis: results of an international analysis. J Thorac Cardiovasc Surg 2015; 149: 95-100.
2. Kwon AY, Han J, Chu J, *et al*. Histologic characteristics of thymic adenocarcinomas: clinicopathologic study of a nine-case series and a review of the literature. Pathol Res Pract 2017; 213: 106-12.
3. Marx A, Chan JK, Coindre JM, *et al*. The 2015 World Health Organization classification of tumors of the thymus: continuity and changes. J Thorac Oncol 2015; 10: 1383-95.
4. Moser B, Schiefer AI, Janik S, *et al*. Adenocarcinoma of the thymus, enteric type: report of 2 cases, and proposal for a novel subtype of thymic carcinoma. Am J Surg Pathol 2015; 39: 541-8.
5. Banki F, Khalil K, Kott MM, Cota AL. Adenoid cystic carcinoma of the thymus gland: a rare tumor. Ann Thorac Surg 2010; 90: e56-8.
6. Furtado A, Nogueira R, Ferreira D, Tente D, Eisele R, Parente B. Papillary adenocarcinoma of the thymus: case report and review of the literature. Int J Surg Pathol 2010; 18: 530-3.
7. Zaitlin N, Rozenman J, Yellin A. Papillary adenocarcinoma in a thymic cyst: a pitfall of thoracoscopic excision. Ann Thorac Surg 2003; 76: 1279-81.
8. Abdul-Ghafar J, Yong SJ, Kwon W, Park IH, Jung SH. Primary thymic mucinous adenocarcinoma: a case report. Korean J Pathol 2012; 46: 377-81.
9. Cho EN, Park HS, Kim TH, *et al*. A rare case of primary thymic adenocarcinoma mimicking small cell lung cancer. Tuberc Respir Dis 2015; 78: 112-9.
10. Jung HY, Cho H, Chung JH, *et al*. A rare case of primary tubular adenocarcinoma of the thymus, enteric immunophenotype: a case study and review of the literature. J Pathol Transl Med 2015; 49: 331-4.
11. Ra YJ, Bae MJ, Kim YS, Choi KU. Difficulties in diagnosis and treatment of thymic adenocarcinoma producing beta-human chorionic gonadotropin in anterior mediastinum. Interact Cardiovasc Thorac Surg 2010; 11: 114-6.
12. Seon HJ, Kim KH, Choi YD, *et al*. Angina pectoris caused by the extrinsic compression of coronary artery by primary thymic mucinous adenocarcinoma. Int J Cardiol 2012; 156: e13-5.

Journal of Pathology and Translational Medicine 2017; 51: 513-515
https://doi.org/10.4132/jptm.2017.04.25

■ BRIEF CASE REPORT ■

Iatrogenic Gastric Pseudolipomatosis during Endoscopic Submucosal Dissection

Sang Wook Kim · Woo Sung Moon[1]

Division of Gastroenterology, Department of Internal Medicine and [1]Department of Pathology, Research Institute of Clinical Medicine of Chonbuk National University-Biomedical Research Institute of Chonbuk National University Hospital and Research Institute for Endocrine Sciences, Chonbuk National University Medical School, Jeonju, Korea

Mucosal pseudolipomatosis of the stomach is a rare lesion. It is characterized by the presence of gas-filled vacuoles in the lamina propria.[1] The etiology of this lesion is uncertain. Herein, we present a case of gastric pseudolipomatosis with an unusual iatrogenic artifact while performing injection of submucosal solution during endoscopic submucosal dissection (ESD).

CASE REPORT

The patient had provided written informed consent for publication of this case study.

A 63-year-old woman was admitted for evaluating gastric submucosal lesion incidentally detected during a health check-up. Upon endoscopic examination, a single smooth surfaced polypoid lesion sized 1 cm was identified. Under the clinical impression of submucosal benign mesenchymal tumor, ESD was performed. Normal saline and indigo carmine dye mixed with hyaluronic acid was injected into the submucosal layer to lift up the lesion and distinguish the muscle layer from the submucosal layer. The endoscopist did not detect any visible mucosal changes before injecting the solution (Fig. 1A). However, the release of air bubbles from the lesion was clearly observed during the submucosal dissection (Fig. 1B). Microscopic examination of the submucosal tumor was consistent with inflammatory fibroid polyp. The lamina propria contained numerous unlined empty spaces without inflammatory reaction, measuring 40–600 μm in diameter and extending to the submucosa and submucosal tumor (Fig. 2A, B). Neither specific cytological abnormalities nor architectural destruction was found in the mucosa. *Helicobacter pylori* was not identified. The lesion showed negative immunohistochemical staining results for D2-40, CD31, CD34, vimentin, and S100 protein. Therefore, lymphangiomatous lesion and lipomatous metaplasia were ruled out (Fig. 2C). These histologic findings were similar, if not identical, to those of gastrointestinal pseudolipomatosis reported previously.[1,2] Based on histological and immunohistochemical findings, a final diagnosis of gastric pseudolipomatosis was made.

DISCUSSION

Gastrointestinal pseudolipomatosis is characterized by the presence of gas-filled vacuoles of various sizes within the lamina propria. It is named as gastrointestinal pseudolipomatosis because it resembles fatty infiltration.[1,2] Histologically, differential diagnoses of pseudolipomatosis include lymphangiomatous lesion and lipomatous metaplasia which can be easily excluded by using appropriate immunohistochemical staining. The etiology of pseudolipomatosis is unclear. Penetration of gas into the injured mucosa associated with air pressure during endoscopy,[1] *H. pylori* infection,[3] and the use of disinfectant hydrogen peroxide solution have been proposed as possible etiologies.[4] We propose that our case is an artifact caused by infusion of incompletely removed air inside the syringe caused by inadequate flushing when injecting the submucosal solution (Fig. 2D). Several facts

Corresponding Author
Woo Sung Moon, MD, PhD
Department of Pathology, Chonbuk National University Medical School, 567 Baekje-daero, Deokjin-gu, Jeonju 54896, Korea
Tel: +82-63-270-3086, Fax: +82-63-270-3135, E-mail: mws@chonbuk.ac.kr

Received: March 16, 2017 **Revised:** April 18, 2017
Accepted: April 24, 2017

pISSN 2383-7837
eISSN 2383-7845

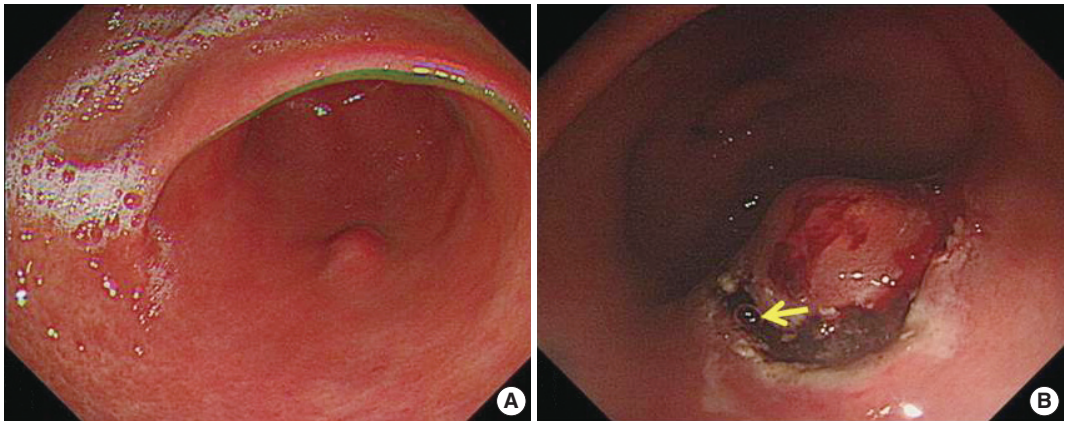

Fig. 1. Endoscopic findings. (A) Endoscopic appearance of a single polypoid lesion without any visible mucosal changes. (B) Appearance of air bubble during submucosal dissection (arrow).

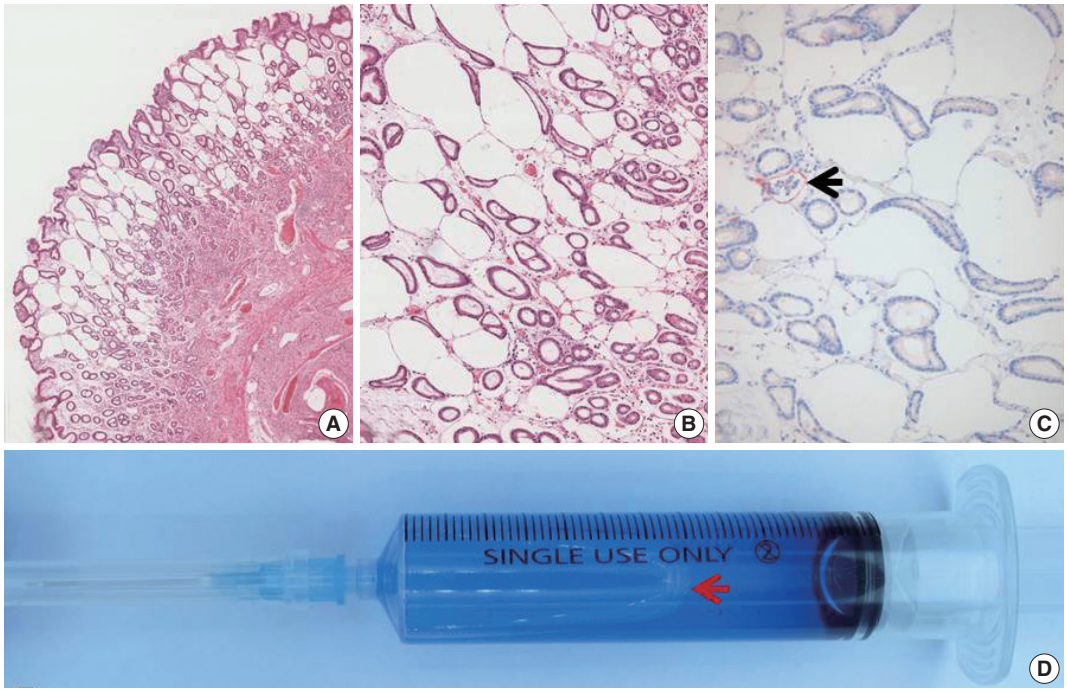

Fig. 2. Morphologic findings of the lesion. (A) Submucosal inflammatory fibroid polyp and a number of clear vacuoles overlying within the mucosa, mimicking lymphangioma or lipomatous metaplasia. (B) High resolution view of the lesion. The characteristic appearance of pseudolipomatosis shows a number of unlined empty spaces with various sizes in an otherwise intact mucosa. (C) Negative immunoreactivity for D2-40 on vacuoles. D2-40 immunostaining highlighted the preexisting lymphatic structures (arrow). (D) Presence of incompletely removed air inside the syringe (arrow).

support this notion. First, there were no apparent etiologic factors in our case. There was no mucosal lesion such as atrophy or ulcer. In addition, *H. pylori* was not identified. Hydrogen peroxide was not used either. Second, there was no inflammatory or fibroblastic reaction in the vicinity of unlined empty spaces, suggesting short duration of this lesion. Third, the endoscopist noted incompletely removed air in the syringe containing submucosal solution and observed air bubbles being released from the gastric tissue during submucosal dissection. This lesion may represent a gastric pseudolipomatosis with an undescribed unique iatrogenic artifact while performing injection of submucosal solution during ESD procedure. Recognition of this iatrogenic artifact is important to endoscopists and pathologists because it is preventable. In addition, it might mimic other lesions, such as mucosal lymphangioma or lipomatous metaplasia.

https://doi.org/10.4132/jptm.2017.04.25

Conflicts of Interest

No potential conflict of interest relevant to this article was reported.

Acknowledgments

This work was supported by the National Research Foundation of Korea (NRF) grant funded by the Korean Government (MSIP) (No. 2008-0062279).

REFERENCES

1. Stebbing J, Wyatt JI. Gastric 'pseudolipomatosis'. Histopathology 1998; 32: 283-4.
2. Snover DC, Sandstad J, Hutton S. Mucosal pseudolipomatosis of the colon. Am J Clin Pathol 1985; 84: 575-80.
3. Alper M, Akcan Y, Belenli OK, Cukur S, Aksoy KA, Suna M. Gastric pseudolipomatosis, usual or unusual? Re-evaluation of 909 endoscopic gastric biopsies. World J Gastroenterol 2003; 9: 2846-8.
4. Jonas G, Mahoney A, Murray J, Gertler S. Chemical colitis due to endoscope cleaning solutions: a mimic of pseudomembranous colitis. Gastroenterology 1988; 95: 1403-8.


JPTM
Journal of Pathology and
Translational Medicine